Small Modular Boiling Water Reactor Combined with External Superheaters

Andhika Feri Wibisono

Department of Engineering

University of Cambridge

This thesis is submitted for the degree of

Doctor of Philosophy

in Nuclear Engineering

Jesus College

September 2019

Declaration

This thesis is the result of my own work and includes nothing which is the outcome of work done in collaboration except as declared in the Preface and specified in the text. It is not substantially the same as any that I have submitted, or, is being concurrently submitted for a degree or diploma or other qualification at the University of Cambridge or any other University or similar institution except as declared in the Preface and specified in the text. I further state that no substantial part of my thesis has already been submitted, or, is being concurrently submitted for any such degree, diploma or other qualification at the University of Cambridge or any other University or similar institution except as declared in the Preface and specified in the text. It does not exceed the prescribed word limit for the relevant Degree Committee.

Andhika Feri Wibisono

September 2019

Small Modular Boiling Water Reactor Combined with External Superheaters

Andhika Feri Wibisono

Abstract

In order to transform the current energy supply to low-carbon technology, the trade-off between sustainability, energy security and affordability has to be considered. The path forward lies between two alternatives, reducing the storage costs for the intermittent renewables or developing an affordable and more flexible nuclear power. One of the possible solutions proposed in this thesis is developing a Small Modular Boiling Water Reactor (SMBWR) combined with external superheaters.

The SMBWR is a BWR-type small modular reactor. It is designed to adopt natural recirculation of coolant within its primary system. The SMBWR is also combined with the external superheater system. The system consists of 3 pieces of equipment: a superheater, reheater and economiser. The heat for the external superheaters could be supplied by a conventional gas boiler, waste heat from gas turbines or heat stored in molten salt from Concentrated Solar Power (CSP) plant. By having the external superheaters, the SMBWR power conversion cycle efficiency could be substantially improved, which means more electric power could be generated, improving the economics of the reactor. Furthermore, it offers the possibility for the SMBWR to follow the load only by adjusting the external heat provided to the superheaters, while keeping the reactor power continuously at its maximum nominal level, which would be another major economic advantage of the SMBWR. The objectives of this thesis are to demonstrate that the concept is practical and to quantify a number of hypothesised benefits of the SMBWR with external superheaters.

The investigation on the effect of SMBWR operating pressure showed that increasing the SMBWR operating pressure from 6.5 to 10 MPa has no significant effect on the neutronic performance. It is also found that increase in pressure would reduce the core pressure drop but increase the minimum chimney height required to develop natural circulation. In terms of thermodynamics, it is found that increasing the SMBWR operating pressure from 6.5 to 10.0 MPa will improve its thermal efficiency slightly by $\Delta\eta$ of about 1.2%, which is small but not negligible. In order to investigate the trade-off between neutron leakage (neutronics), chimney height requirement for natural circulation (thermal-hydraulics), and dimensions of the core, three different geometry configurations, accounting for different length to diameter ratios were studied. The investigation on the power manoeuvring capability of the SMBWR found that the combined system can reduce its load down to 65% by only reducing the external heat provided to the superheaters, while keeping the reactor operation at full rated power.

Acknowledgements

I am thankful to my God and my Saviour, Jesus Christ, for his grace, unconditional and relentless love and also his faithfulness throughout my life.

I would like to thank my supervisor, Dr. Eugene Shwageraus, who has given me so much advice, insight, and guidance on my research. I really enjoyed working with Eugene, he is very supportive and his vast knowledge and insight have helped me greatly in doing my research. I am very thankful that I could have the opportunity to work with him and learn from him these past four years. I would also like to thank Dr. Jeong Ik Lee from KAIST, who also helped me considerably with my research, especially during the time he was visiting Cambridge. I would like to thank him for his continuous support, as he was my previous supervisor during my Masters study in KAIST, and it was his support that enabled me to start my PhD here in University of Cambridge.

I would like to thank my colleagues here in nuclear engineering office for their support and company, especially Dr. Marat Margulis, with whom I have had many discussions about research and other things, and Mrs. Jo Boyle, the administrator for Nuclear Energy MPhil Course, who is always taking care of the students in the office and has helped me with some administrative organisation during my PhD study, and thus, made my student life experience more enjoyable. During my PhD study, I also had the opportunity to work on a research project with my colleagues, Alisha Kasam, Zhiyao Xing, and Dr. Dan Kotlyar, and thus, I am thankful for those experiences. I also would like to thank Dr. Ben Lindley, Tony Roulstone, and Dr. Alex White for their inputs and advice on some parts of my project.

Outside my research group, I would like to thank Jesus College Cambridge for providing me with good accommodation, student support, and a great community, I am very thankful to be a part of Jesus College Badminton Club. I would also like to thank the Indonesia Endowment Fund for Education (LPDP) for their financial support throughout my PhD study. The Indonesian Student Society in Cambridge (PPI Cambridge) and the Christian Graduate Society (CGS) are two societies that have been an important part of my life here in Cambridge. A particular thanks to my church family (City Church Cambridge), who have enriched me spiritually in the last two years.

Finally, I would like to give special thanks to some people in my life, whom I am very grateful to know and are quite important in my life journey, especially during these past four years. Firstly, my mom, for her continuous love, support and prayer for me. Secondly, my

lifelong best friends, Desty Andayani, C. D. Hanung Darpito and Sauda ‘Iin’ Fatmagustina. Thirdly, people who have been an important part of my life here in Cambridge, Xinyu Zhao, mas Arief W. Lubis, Eky V. Febrianto, Artricia Rasyid, Wulansari Ardianingsih, Aulia Syakhroza-Kuncoro, Sabrina Anjara, Gamal Crichton, Jolly Dusabe, Johan Lundberg, Leon Jonck, Prof. John & Diane Lister, Mike Frisby, Papa Gerry & Mama Tessa Hessey and other good friends whom I failed to mention here but have been an important part of my life these past four years. My life here in Cambridge would not be the same without any of them and I am very thankful for their friendship and love for me. Lastly, I am grateful for the opportunity to know Jon Ogborn during my time here in Cambridge. These past few years, I came to know Jon as a loving father, a great friend and brother in Christ, and an accountability partner. And I am very thankful for his love, support, and encouragement.

Table of Contents

List of Tables

List of Figures

Nomenclature

Acronyms

ABWR	Advanced Boiling Water Reactor
AHTR	Advanced High-Temperature Reactor
BOL	Beginning of Life
BOP	Balance of Plant
BWR	Boiling Water Reactor
CCC	Committee on Climate Change
CCGT	Combined Cycle Gas Turbine
CCS	Carbon Capture & Storage
CPR	Critical Power Ratio
CSP	Concentrated Solar Power
CVC	Coolant Void Coefficient
CVTR	Carolinas-Virginia Tube Reactor
DC	Doppler Coefficient
DMS	Double MS: Modular Simplified and Medium Small Reactor
EFPD	Effective Full Power Day
EOL	End of Life
ESBWR	Economic Simplified Boiling Water Reactor
FAs	Fuel Assemblies
FSS	Free-Surface Separation
GDCS	Gravity Driven Core Cooling System
GE	General Electric
GHG	Greenhouse Gas
IAEA	International Atomic Energy Agency
IRIS	International Reactor Innovative and Secure
JAPC	Japan Atomic Power Company
LCOE	Levelised Cost of Electricity
LWR	Light Water Reactor
MCPR	Minimum Critical Power Ratio
MOL	Middle of Life
MTC	Moderator Temperature Coefficient

NEA	Nuclear Energy Agency
NPPs	Nuclear Power Plants
OCGT	Open-Cycle Gas Turbine
PCV	Primary Containment Vessel
PHS	Pumped Hydroelectric Storage
PWR	Pressurised Water Reactor
RPV	Reactor Pressure Vessel
SMBWR	Small Modular Boiling Water Reactor
SMR	Small Modular Reactor

Romans symbols

A	flow area (m^2)
C_b'	bundle friction factor correction constant
C_f'	friction factor constant
C_v	drag coefficient
D	tube diameter (m)
D_{ei}'	effective diameter of subchannel type i (m)
D_{eb}'	bundle effective diameter (m)
D_H	hydraulic diameter (m)
f	friction factor
$F_{\Delta H}$	enthalpy rise hot channel factor
$\vec{F}_{wk}$	fluid phase drag force
g	gravitational acceleration (m/s^2)
h	specific enthalpy (kJ/kg)
K	form loss coefficient
L	length (m)
$\dot{m}$	mass flow rate (kg/s)
p	pressure (Pa), (bar)
P	electric power (MW)
Re	Reynolds number
Q	thermal power (MW)
Q_{sk}	interfacial heat transfer
s	specific entropy (kJ/kg K)

S_i	ratio of flow area of subchannels of type i to the bundle flow area
u, v	velocity (m/s)
v_{vj}	drift velocity (m/s)
W	work (MW)
x	flow quality

Greek symbols

α	void fraction
β	volumetric flow ratio
Δ	variation
$\Delta H_{Subcooling}$	subcooling enthalpy difference
ε	relative roughness (m)
η	efficiency (%)
ρ	density (kg/m^3)
$\emptyset^2_{TPL}$	two-phase flow multiplier
Γ_k	interfacial mass transfer rate per unit volume
ψ	friction factor constant

Subscripts

ACC	acceleration
c	contraction
CC	combined cycle
CHP	combined heat and power plant
E	elevation
ex	expansion
F	friction
f	saturated liquid
g	saturated vapour
GT	gas turbines
k	fluid phase (l for liquid or v for vapour)
L	local
l	subcooled liquid
NP, NPP	nuclear plant

s	spacer

Superscripts

n	exponent pertaining to the friction factor function of the Reynolds number

Chapter 1: Introduction

1.1 Background & Motivation

The concern for climate change has driven the need to decarbonise the energy sector. The most sensible pathway to reduce greenhouse gas (GHG) emissions in order to maintain the global warming level to be below 2 °C above the pre-industrial level is by reducing emissions in the power sector to almost zero, while transforming the other energy intensive sectors (transportation, heat, industrial, etc) to take advantage of clean electricity **[1]**. In order to decarbonise the electricity sector, a transition from fossil fuels to low-carbon technologies, such as nuclear, wind, and solar is necessary.

1.1.1 UK electricity projection & challenge

The United Kingdom (UK) has been among the most successful countries in the developed world in growing their economy while reducing emissions. The Climate Change Act in 2008 requires an 80% reduction in emissions by 2050 compared with 1990 levels. In order to achieve that target, the electricity sector has to play a key role, thus the Committee on Climate Change (CCC) recommends a reduction of emissions in electricity sector to 50 gCO_2eq/kWh by 2030 **[2]** and to a 'net-zero' by 2050 **[3]**. In 2017, the Department for Business, Energy & Industrial Strategy (BEIS) published projections of UK energy demand and supply **[4]**, which extend up to 2035. Table 1.1 shows the projected capacity of all power producers in the UK (in GW), while Table 1.2 shows the total generation by source for all power producers (in TWh). By considering the carbon footprint of each energy source used in the UK (as listed in Table 1.3), one can easily observe that in order to reach the emission reduction target, the UK needs to substitute more fossil fuel with low carbon sources of electricity such as nuclear power and renewables. Fig. 1.1 shows that the UK would require nuclear capacity of approximately 30 GW to reduce its emissions to below 50 gCO_2eq/kWh. A study conducted by MIT **[5]** shows that, in the UK, nuclear will provide notable cost benefits at emissions targets of 10 and 1 gCO_2eq/kWh.

Table 1.1 Capacity Projection (in GW) of all Power Producers in the UK **[4]**

Source	2017	2020	2025	2030	2035
Coal	14	7	1	0	0
Coal & natural gas CCS	0	0	0	0	1
Oil	0	1	1	2	2
Natural gas	38	39	35	32	26
Nuclear	9	9	6	8	14
Renewables	40	46	56	63	68
Interconnectors	5	6	19	19	20
Storage	3	3	3	7	11
Total capacity (GW)	**110**	**110**	**122**	**130**	**142**

Table 1.2 Projection of UK Electricity Generation by Source in TWh **[4]**

Source	2017	2020	2025	2030	2035
Coal	10	9	6	0	0
Coal & natural gas with CCS	0	0	0	0	7
Oil	0	0	0	0	0
Natural gas	155	121	74	73	49
Nuclear	58	59	39	67	113
Renewables	101	123	149	161	192
Storage	4	4	4	5	6
Total supply (gross)	**327**	**316**	**272**	**306**	**368**
Used in pumping	5	5	5	7	8
Net supply (in TWh)	**322**	**311**	**267**	**299**	**359**

Table 1.3 Estimated Range of Carbon Footprint Value for several Energy Sources **[2]**

Energy Source	**Estimated range of Carbon Footprint value (gCO_2eq/kWh)**
Coal	786 - 990
Gas (CCGT)	410 - 650
Coal fired with CCS	80 - 310
CCGT with CCS	90 - 245
Solar	30 - 85
Nuclear	3 - 10
Onshore wind	7 - 20
Offshore wind	5 - 24

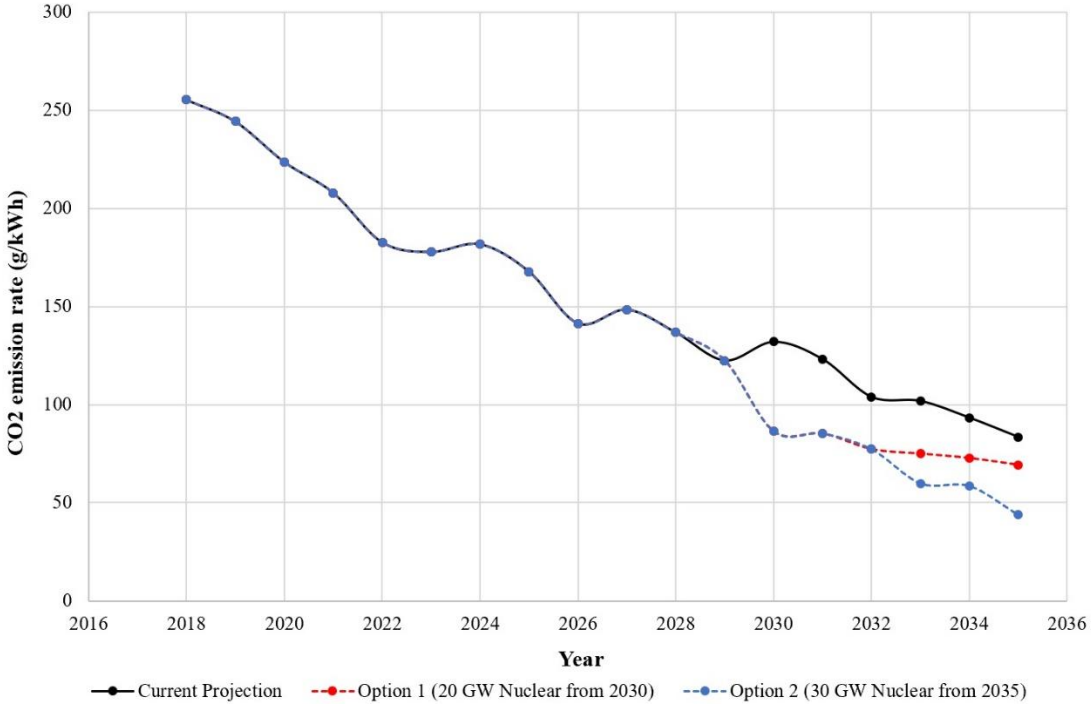

Fig. 1.1 UK average emission rate projection.

The main challenge of increasing nuclear capacity in order to meet the emissions target is the economics. Nuclear power plants (NPPs) usually have high fixed costs and low variable costs while gas fired plants usually have lower fixed costs and much higher variable costs. For this reason, it is obvious that in order to minimise costs, NPPs (even if designed with a load-following capability) should always operate at their full power, while any automatic frequency response operation and load-following should be done by the fossil fuel burning generators.

The Nuclear Energy Agency (NEA) performed an investigation on how the load-following operation would affect the Levelised Cost of Electricity (LCOE) and projected costs of generating electricity for nuclear, coal and gas **[6]**. Fig. 1.2 displays the LCOE of nuclear, coal, and gas as a function of the load factor. It is clearly observed from Fig. 1.2 that the LCOE of nuclear power is more sensitive to the variation of the load factor compared to that of gas and coal. The priorities for the task of load-following where there is a need to balance the network should be given to the power source which is the least sensitive to load variation, i.e. natural gas.

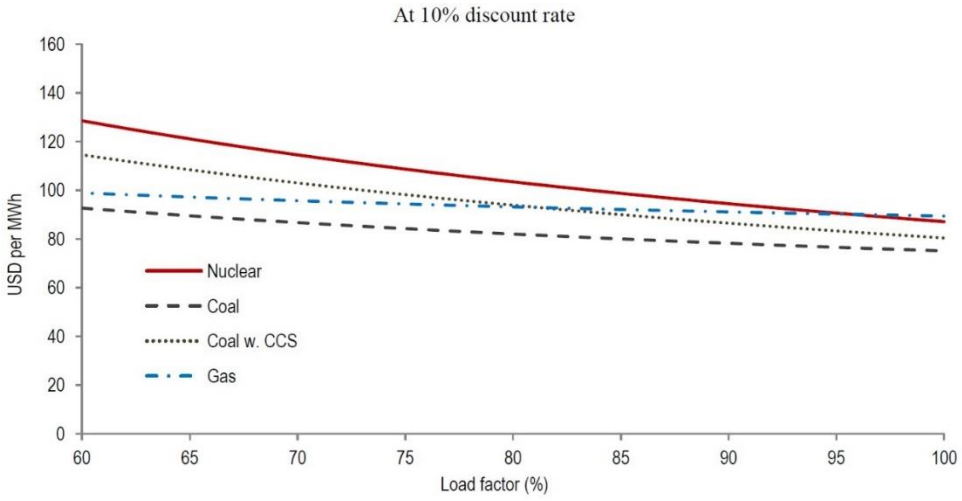

Fig. 1.2 Variation of LCOE as a function of the load factor for main power sources **[6]**.

In a low-carbon electricity grid, the reduction of fossil fuels and the increased fraction of intermittent renewables would therefore require more flexibility from the NPPs. The share of nuclear power in the energy mix is typically relatively small and usually is used as a base-load provider. The power manoeuvring capabilities of the NPPs were limited to ensure the stability of the grid (emergency load variation) and frequency regulation **[6]**. As the share of nuclear power in the energy mix increases, the manoeuvring capability (load-following) of the NPPs becomes more important in order to adapt the electrical supply to daily or seasonal variations of the power demand. In addition, the increased role of intermittent renewables can lead to more frequent occurrences of negative electricity prices during high renewable output and/or low demand, reduced overall base-load generation capacity and associated base-load generator power reductions. The growth of renewables in some deregulated markets, often with substantial government subsidies, is contributing to the premature closure of nuclear plants, as they cannot compete directly in the deregulated market. Developing an economical load-

following operation using NPPs could improve their competitiveness in the deregulated market **[7, 8]**.

1.1.2 The future grid in the low-carbon world

As mentioned above, the future electricity grid will most likely be relying on low-carbon generators such as nuclear, wind and solar technology. In order to meet the daily and seasonal variation of electricity demand, it is important for the low-carbon system to integrate with energy storage for the intermittent renewables or find solutions for making NPPs' load-following operation more economic. De Sisternes et al. **[9]** investigated the integration of low-carbon technology system into the energy mixture with respect to emissions limits and average generation costs and proposed the optimal portfolio, shown in Fig. 1.3, in the absence of energy storage. It is shown in Fig. 1.3 that the role of nuclear energy becomes more important as the emissions limit tightens. With flexible operation, NPPs provide a flexible base of zero-carbon energy supplies, providing operating reserves, and helping minimise curtailment of wind and solar resources.

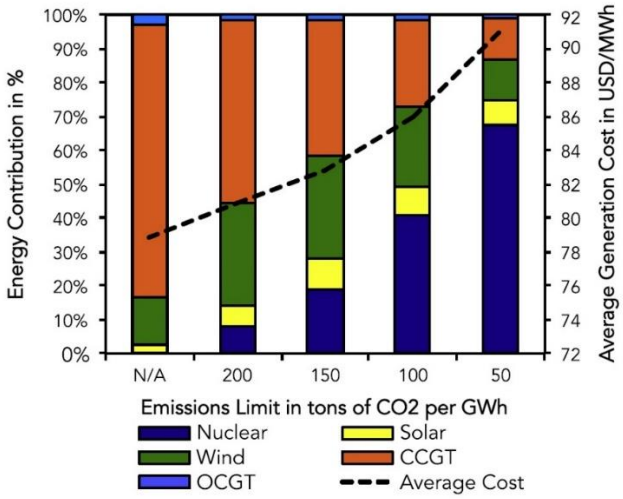

Fig. 1.3 Energy contribution and average costs of electricity generation under various carbon emissions limits, no storage cases **[9]**.

De Sisternes et al. **[9]** also found that installation of energy storage helps reduce average electricity generation costs by increasing the utilisation of wind and solar. However, under a carbon emissions limit of 100 tCO_2/GWh, average system costs (including storage costs) increase in most cases, as shown in Fig. 1.4. In their model, the 2-hour (2-h) generic storage technology can be considered broadly consistent with commercially available Lithium-ion (Li-

ion) battery systems, while the 10-hour (10-h) storage technology is broadly consistent with pumped hydroelectric storage (PHS) systems. It can be seen from Fig. 1.4 that the storage costs have to be reduced in order to make the economic case comparable to the case without storage.

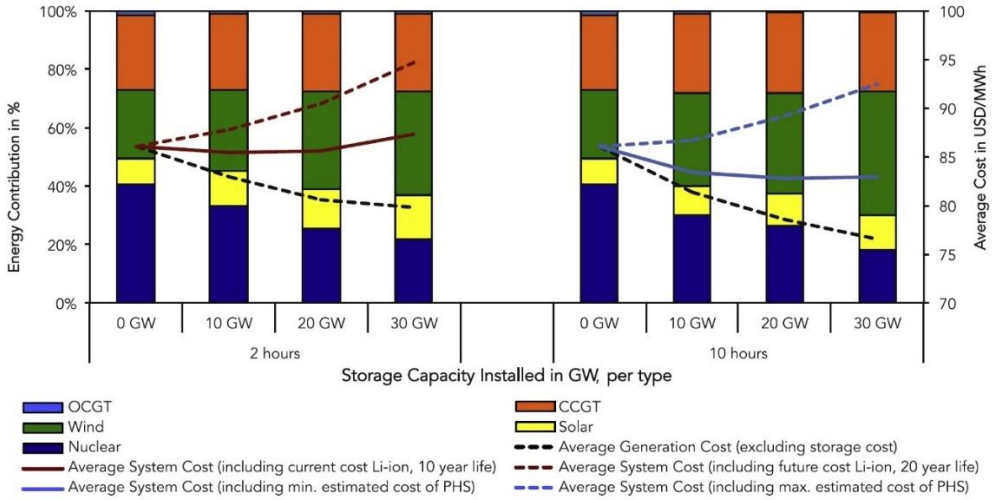

Fig. 1.4 Impact of energy storage on energy contribution and average system costs under emissions limit of 100 tCO_2/GWh **[9]**.

It can be observed that there is a trade-off between the system costs and the flexibility of the system to meet daily and seasonal variation of demand. On one hand, by having more nuclear in the grid, the stability of electricity supply is improved. Nuclear is a good base-load provider of electricity, but its electricity cost is relatively sensitive to the change in load as nuclear is highly capital intensive and tends to have low operating costs. On the other hand, having more renewables, such as wind and solar, would reduce the average generation cost of the electricity. However, the intermittency of wind and solar would be a problem for the stability of the grid and, thus, storage system is required to ensure the stability of the system, which would increase the average system costs. Thus, the options to minimise the system cost lie in how to reduce storage costs to utilise more renewables or reduce costs for building NPPs and develop more flexible power generation for the NPPs to meet daily and seasonal demand variation.

1.1.3 Nuclear with superheat for flexible power generation

One option to minimise the average system costs, which is the proposed solution in this thesis, is by combining NPP with external superheaters. The incentives for combining NPP with external superheaters are the improvement in its cycle thermal efficiency and the

possibility to follow the load to some extent while maintaining the nuclear reactor operating at 100% of its full rated power and thus maximising its economic value. According to previous studies **[10, 11, 12]**, combining LWR with a gas fired superheater will provide additional electric power output (up to 80% of its full rated power), improve the plant thermal efficiency by 2 - 5%, and its operational load variation capability can be between 100% and 65% by only adjusting the heat supplied to the external superheaters.

The amount of additional electricity generated by this hybrid concept might be more valuable if adopted by SMRs, as there is a limitation on the existing capacity of the commercial steam turbines. There is no sufficiently large single shaft steam turbine commercially available that can produce more than 2,000 MW_e at the moment. The largest operating steam turbines are ARABELLE^{TM} steam turbines designed by Alstom with capacity of 1,550 MWe each. There is also a 1,750 MWe single shaft ARABELLE^{TM} steam turbine for the Flamanville 3 **[13]**. Hence, at the moment, it is not possible to add significant amount of power to a large NPP without installing a new turbine unit. Although it is possible to use more than one unit of steam turbine in the plant, the additional costs related to the equipment siting and operation and maintenance of the additional turbine system need to be considered, which might end up increasing the cost of the electricity. Although this option might still be the most favourable one to pursue when it comes to the implementation of this hybrid system in existing operational nuclear reactors, it was not explored in this thesis.

In terms of building a new reactor with this hybrid concept, combining a superheater with an SMR is preferable. Since SMRs have a lower electric power output compared to large reactors, the implementation of the superheater concept in SMRs would be beneficial in terms of generating more power for the same reactor size or reducing the size of the reactor to produce the same amount of power. In addition, SMRs offer several benefits compared to large reactors, such as smaller financing requirements and more flexibility to fit into smaller national grids, which makes a new build SMR more economically attractive and feasible to implement in developing countries. The hybrid system of SMR with an external superheater would add significant value in the SMR development as more power could be generated or smaller sizes of the reactor vessel and other components would be required. In addition, by having the external superheater, an economical load-following operation for the SMR could be achieved.

It is important to note that by having an external superheater powered by a conventional fossil fuel such as natural gas, the NPPs will not be totally carbon emission-free even though the emissions would not be as high as stand-alone gas turbines or combined cycle gas turbines (CCGT). There is also an option to rely on cleaner heat for the superheater heat source. For

example, Concentrated Solar Power (CSP) technology is able to store thermal energy by using molten salt. Thus, there is a possibility that one could use the heat stored in the solar salt to power the superheater, which would reduce the CO_2 emissions of this hybrid energy system practically to zero.

1.1.4 Superheating in nuclear power plants

The combination of a nuclear reactor, as a steam producing boiler, and a superheater was attempted in the past by power reactor designers from the 1950s to 1970. As a result, several nuclear reactors in the past have implemented the concept to produce superheated steam. Superheating can be implemented in NPPs by using either a nuclear superheater or a fossil fuel superheater. In terms of simplicity of the system, superheating by a fossil fuel superheater is potentially more favourable compared to a nuclear superheater. Table 1.4 lists several reactors developed in the US which had a fossil fuel superheater in their design **[14, 15, 16]**. There are also several nuclear power plants developed outside the US which had secondary reheating powered by oil, such as Garigliano (Italy) and Lingen (Germany). The performance of the combined cycle was questionable due to low load factor and material failures. It is, however, reasonable to reconsider this concept as the technology of thermal power plants, nuclear and conventional, has become more reliable than it was back in 1960s **[17]**.

Forsberg and Conklin **[18]** proposed a hybrid power cycle by coupling the Advanced High-Temperature Reactor (AHTR) with the Combined Cycle Gas Turbine (CCGT). During low electricity demand, the nuclear heat from AHTR could provide an adequate supply for base-load electricity with the CCGT. When the demand is high, further heating of the air in the gas turbine could be done by a conventional combustor fuelled by natural gas. Although the AHTR is a different type of reactor from the LWR, their study shows **[18]** that nuclear power could be more competitive when it is coupled with a conventional heater, as it can produce low-cost base-load electricity and lower-cost peak power relative to the existing combination of base-load nuclear power plant and fossil-fired peak electricity production. The fact that the fossil heat is used on top of nuclear heat means that CO_2 emitting heat is used more efficiently and only occasionally. The combination of nuclear and fossil heat also helps in improving the overall thermal efficiency of the system.

Table 1.4 US Reactors with Fossil Fuel Superheater

Reactor	Year	Type	Moderator & Coolant	Thermal Power (MWth)[1]	Electric Power (MWe)	Efficiency (%)	Steam Temp. (°C)
Elk River	1962-1968	BWR	H_2O	58.2 (N) 14.8 (F)	22.5	30.8	441
Indian Point I	1962-1974	PWR	H_2O	585 (N) 215 (F)	255	32.0	538
CVTR	1963-1967	Pressure tube	D_2O	65	19	29.2	385

Darwish et al. **[11]** investigated the thermal performance of the PWR nuclear reactor AP600 combined with existing gas turbines in Kuwait. The results of their study show that this combination scheme could increase the nuclear power plant (NPP) power output from 607 MWe to 1,151.4 MWe. The electricity cost of the modified AP600 was predicted to be $49.83/MWh, which was less by 45.6% than that of Gas Steam Turbine Combine Cycle (GSTCC) power plant ($91.6/MWh). Zaryankin et al. **[12]** studied the hybrid nuclear power plant (WWER-1000) with fossil fuel superheater (gas combustor technology) and found that the hybrid nuclear power plant could increase the power generation from 1,000 MWe to 2,050 MWe with an efficiency increase of 8%. The designed external steam superheater enables an increase in steam temperature from 274 °C to 600 °C.

A similar option has also been investigated as part of this thesis **[10]**, focusing on the thermodynamic power conversion efficiency improvement of adding gas fired superheaters to the AP1000 and mPower reactors. The results of this preliminary investigation, which will be explained in detail in Chapter 3, are in good agreement with the previous studies. It is found that adding gas fired superheaters to a PWR system, either a large reactor or SMR, would increase the thermal efficiency of the power conversion cycle. Furthermore, it is also found that the PWR combined with gas fired superheaters can follow the load to some extent by adjusting the external heat provided to the superheater, keeping the reactor power at 100% of its full rated power.

[1] N refers to nuclear (thermal) power produced by the reactor while F refers to thermal power added by fossil fuel superheater.

In a Boiling Water Reactor (BWR), adding external superheaters can provide additional benefits, namely, the possibility of eliminating the steam dryer, which is located above the core increasing the BWR vessel height. A steam dryer is required for a BWR to ensure high steam quality before entering the steam turbine. Since the hybrid system operates with superheated steam, the steam dryer could be removed and, thus, the vessel size could be reduced. Furthermore, by removing the steam dryer, the total pressure drop in the coolant recirculation loop inside the BWR vessel will also be reduced, and it would also be easier to develop natural circulation coolant flow inside the vessel. In addition, by adding a superheater system to a BWR-type SMR, the system would have the potential to operate at higher steam pressure and thus further improve its cycle thermal efficiency. The optimal operating pressure for nuclear steam cycle is usually in the range of 6 - 7 MPa because it is operating with saturated steam. In contrast, the steam cycle pressure in a fossil fuelled plant can be as high as 33 MPa by using steam in the supercritical state. By generating superheated steam in the BWR, it is possible to shift the optimal operating pressure to be higher than 7 MPa with a potential of increasing the thermal efficiency of power conversion. The problem related to design and manufacture of a BWR pressure vessel that can withstand higher than 7 MPa pressure can be addressed by simply reducing the size of the reactor. In other words, boiling water SMRs could be easier to design and manufacture for operation at higher pressure than large BWRs.

1.1.5 BWR with natural circulation

After the Fukushima accident, there is a growing tendency in the nuclear industry to develop passive safety systems. Most of the passive safety systems developed for LWRs are relying on natural circulation. BWRs in particular can take advantage of having two-phase flow driving head to develop natural circulation in the coolant recirculation system. Thus, a BWR has the potential to be able to use natural circulation not only for passive decay heat removal but also during normal operation. There are several BWRs with natural circulation developed around the world, some of the examples are ESBWR (Economic Simplified Boiling Water Reactor) **[19]** and DMS (Double MS: Modular Simplified and Medium Small Reactor) **[20]**.

ESBWR is a large power BWR designed by GE Hitachi. The natural circulation conditions in ESBWR are ensured by shortening the active fuel length (approximately 3.1 m compared to 3.7 m in a conventional BWR), adding a tall chimney (approximately 6.6 m) above the core, which required an increase in the reactor vessel length. Because of this reason, the ESBWR is able to remove the recirculation pumps from its Reactor Pressure Vessel (RPV) and associated

vessel penetrations and pump shaft seals. The design of ESBWR also enables the reactor to implement the Gravity Driven Core Cooling System (GDCS) as one of its passive safety features for decay heat removal **[19]**.

DMS is a small BWR, also developed by Hitachi-GE Nuclear Energy under the sponsorship of the Japan Atomic Power Company (JAPC). DMS has a shorter primary containment vessel (PCV) height due to reduced active fuel length (2 m compared to 3.7 m in a conventional BWR). By having larger flow area and lower core power density while adopting natural circulation of the coolant, the steam evaporation rate of DMS is low, enabling the moisture to be separated simply by gravity. The concept is also known as a Free Surface Separation (FSS) system. This feature allows DMS to eliminate the need for a moisture separator, and therefore reduce the vessel height **[20]**.

The preliminary investigation, which will be presented in detail in Chapter 3, shows that by using the gas fired superheater system both ESBWR and DMS power conversion cycle efficiency could be increased, making it comparable to those of stand-alone gas turbines. It is also found that the addition of the superheater would increase the maximum electric power of ESBWR to approximately 2.8 GWe, which is higher than the largest commercially available steam turbine. Therefore, assuming that the total system power is constrained by the size of available steam turbines, a smaller reactor such as DMS would be a more plausible route for a hybrid nuclear system with added superheater.

As briefly mentioned above, SMRs could counter the economies of scale by offering a number of additional economic advantages such as modular off-site fabrication with associated productivity increase and reduced labor costs **[21]**. By increasing the coolant flow area to reduce the steam evaporation rate, DMS suffers from having a relatively large vessel diameter (approximately 5.8 m). The low loader lorries, a means of road transport for abnormally large and heavy loads, usually have a maximum width limitation of 4.3 m **[22]**. Thus, having a diameter of 5.8 m would complicate transportation of the vessel if it is not manufactured on-site.

1.1.6 The proposed solution

In summary, in order to transition from the current energy supply towards low-carbon technology, the trade-off between sustainability, energy security, and affordability has to be taken into consideration. The path forward lies between two alternatives, reducing the storage costs for the intermittent renewables or developing an affordable and more flexible nuclear

power. One of the possible solutions proposed by this thesis is by developing a Small Modular Boiling Water Reactor (SMBWR) combined with external superheaters.

One of the problems faced by the nuclear industry is the financing scheme to build new NPPs. It is known that NPPs are highly capital intensive and this is probably one of the reasons for relatively slow nuclear new-build in the recent years. A small reactor could be more attractive, especially for the developing countries, as the total financial commitment to build small reactors would be lower than large reactors. The fact that the size is smaller would also reduce the duration to build the NPP thus reducing the financial risk of the project as well, making it more attractive for the potential investors. In addition, as mentioned in the previous section, SMRs are claimed to offer several possibilities to counter the economies of scale through their standardisation, modularisation and mass production in factories.

One of the design features for SMBWR that was chosen to be adopted in this thesis is to rely on natural circulation of coolant within the reactor vessel during normal operation. This will also allow passive decay heat removal under accident conditions, although safety analyses were outside the scope of this thesis. By adopting natural circulation, the recirculation pumps could be eliminated from the vessel, thus enabling the removal of some of the RPV penetrations below the core. As mentioned previously, it is easier to develop natural circulation in BWR compared to PWR, because of the greater coolant density change (two-phase flow driving head). A smaller reactor would also mean a shorter core, and, thus, lower core pressure losses, resulting in a smaller chimney height required to provide the driving head to counter the pressure losses inside the loop.

By having the external superheaters attached to the SMBWR, the power conversion cycle efficiency of SMBWR would be improved, which means more electric power could be generated, thus improving the economics of the reactor. Furthermore, it offers the possibility for the SMBWR to reduce its load only by adjusting the external heat supplied to the superheaters, operating the reactor at full power all the time and improving its economics. For the reasons mentioned in the previous section, by adding superheaters, the SMBWR would no longer need steam dryers, further reducing the vessel height. The smaller vessel dimensions offer the possibility to increase the operating pressure of the SMBWR, which would further increase its thermodynamic performance.

1.2 Research Objectives

The main objective of this work is to explore design space of a hybrid system of a Small Modular Boiling Water Reactor combined with external superheaters. The hybrid SMBWR is postulated to operate with natural circulation of coolant within the pressure vessel and to be able to vary its power only by adjusting the external heat supplied to the superheater while maintaining reactor operation at its full rated power. Therefore, the following tasks are set as the objectives for this thesis:

1. Demonstrate that the concept is practical and achievable, which includes analysing the performance of the SMBWR in terms of its neutronics, thermal-hydraulics, and power cycle thermodynamics.
2. Quantify the hypothesised benefits of adding external superheaters to SMBWR.
3. Quantify the benefits of increasing the operating pressure in terms of the system size and power conversion efficiency of SMBWR.

1.3 Thesis Organisation

This thesis investigates the effects of several design parameters of the hybrid Small Modular Boiling Water Reactor combined with external superheaters. Chapter 2 summarises the methodology and analytical tools used in this work. Chapter 3 presents a preliminary investigation on adding gas fired superheaters to LWRs. A trade-off study for increasing the pressure of the BWR is presented in Chapter 4. The neutronic and thermal-hydraulic performance of the SMBWR is discussed in Chapter 5. Chapter 6 discusses the load-following capability of the SMBWR and its implications to economics and emission rates. Chapter 7 provides the summary and conclusions of the performed work and makes a number of recommendations for future work.

Chapter 2: Methodology

2.1 Design Parameters & Scope of the Analysis

As mentioned in the previous chapter, three initial design choices are postulated for the Small Modular Boiling Water Reactor. The first design choice postulates that the reactor power should be in the category of small or medium sized reactors. According to the IAEA **[23]**, medium sized reactors are those with electric power between 300 to 700 MWe and small sized reactors have less than 300 MWe. The second one is to adopt natural circulation for the reactor coolant within the RPV. The last postulated feature is that the SMBWR would have an external superheater system added to its balance of plant (BOP) and used to adjust the plant's power to load, while maintaining the reactor operation always at 100% of its full rated power.

One of the objectives of this work is to investigate whether there is sufficient incentive for the SMBWR to operate at high pressure. In order to fully understand the effect of the operating pressure on the SMBWR hybrid energy system, an analytical procedure that covers analyses in the neutronics, thermal-hydraulics and thermodynamics of SMBWR is needed. Fig. 2.1 displays a schematic diagram of the analytical methods used in this study. For the neutronic analysis, the cross-sections library was prepared by WIMS and the analysis was done by using PANTHER. A BWR loop model was built in MATLAB to analyse the natural circulation flow within the SMBWR vessel. The coolant flow through the core was modelled in more detail by using the channel thermal-hydraulics code COBRA-EN. A steam cycle model was also developed in MATLAB for the thermodynamic analysis.

The underlying hypothesis is that by operating at higher pressure, the steam turbine could produce more work, thus, generate more electric power and improve power conversion cycle efficiency of the SMBWR. Operation at different pressure means there would be changes in the coolant density inside the primary recirculation system and, thus, the core neutronics and thermal-hydraulics would be affected. In a system driven by natural circulation, which relies on buoyancy forces to counter the pressure losses throughout the loop, the change in coolant density would affect the requirement for the driving head to provide sufficient buoyancy forces to the system. Thus, this effect has to be accounted for when making the case for high pressure operation. The variables that are expected to have significant effects on the thermodynamics performance of the SMBWR are steam mass flow rate and steam operating conditions, while the ones that would affect the primary loop thermal-hydraulics are primary coolant flow rate

and pressure losses inside each component of the coolant circulation loop. The core pressure drop would significantly depend on the boiling length, which is the axial distance where the flow is a two-phase mixture, as the pressure drop in two-phase flow is higher than in single-phase flow. Therefore, in order to make a fair comparison of thermal-hydraulics and thermodynamics performance at various operating pressures, some boundary conditions have to be set consistently across all considered cases to limit the number of degrees of freedom. The boundary conditions set for this study are constant primary coolant mass flow rate, constant core subcooling enthalpy ($\Delta H_{Subcooling}$) and constant turbine outlet pressure. The pressure range for the comparative study on SMBWR operating pressure is 6.5 – 10.0 MPa. According to Shirvan **[24]**, 6 MPa is the minimum limit for BWR operating pressure, which is restricted by the thermodynamic performance of the steam cycle and stability limits due to the higher ratio of liquid to vapour densities. While the maximum pressure (~12 MPa) is mainly restricted by the availability of Critical Power Ratio (CPR) data correlations.

At different operating pressures, although the mass flow rate of the coolant entering the assembly and the assembly power are kept constant, the reactor steam outlet condition and recirculation rate will be changed. In order to conserve the core subcooling enthalpy, the change in the recirculation rate has to be compensated by the change in feedwater inlet temperature. Thus, the loop model would have to communicate the reactor steam outlet and feedwater inlet conditions to the steam cycle model. The loop model would also provide the core inlet temperature for the PANTHER and COBRA-EN models, while PANTHER would supply the axial power distribution to COBRA-EN and the loop models.

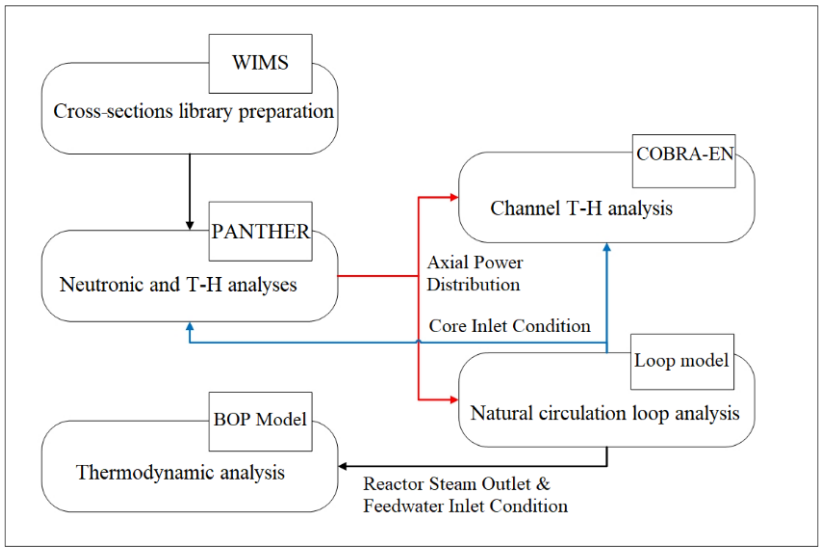

Fig. 2.1 Schematic diagram of the analytical methods in the operating pressure study.

In the SMBWR core design study, the main goal is to identify the effect of core dimensions (active fuel length and number fuel assemblies) on the performance of SMBWR. As the core dimensions for SMRs are smaller, the system becomes more sensitive to leakage. Therefore, the trade-offs between neutron leakage (neutronics), chimney height requirements for natural circulation (thermal-hydraulics), and the dimensions of the core and vessel which would limit the manufacturing and transportation complexity are interesting subjects to investigate. In terms of neutronics, a thin and tall core would have high radial leakage, while a wide and short core would have high axial leakage. In terms of loop thermal-hydraulics, a different core length means a different pressure drop across the core, thus, the requirement for the driving head to develop natural circulation would be different. Three core configurations, with variation of length to diameter ratio, are investigated in this study by keeping a constant thermal power, core power density, coolant mass flow rate and inlet conditions. The reference fuel assembly design adopted in this study was the GE14 BWR design, which is used in both Advanced Boiling Water Reactor (ABWR) **[25]** and ESBWR **[19]**.

Additional design parameters selected for the SMBWR are summarised below.

- Hydrogen to heavy metal ratio (3.5 – 4.5): the hydrogen to heavy metal ratio is related to the core average void fraction. The nominal H/HM of all GE-Hitachi designs have been around 4 for an average void fraction of 40 %.
- Subcooling temperature at the core inlet (10 – 50 °C): this limit is restricted by BWR stability. The core inlet subcooling temperature would determine the boiling length inside the core and, thus, affect the ratio of single-phase pressure drop to two-phase pressure drop. The single-phase to two-phase pressure drop ratio could affect both channel stability and core-wide stability **[26]**. In the comparative study on SMBWR operating pressure, the value of the core inlet subcooling temperature is varied depending on feedwater temperature. However, in all cases considered, the value is still inside the range of the parameter limits.
- MCPR (> 1.05): MCPR limit is commonly taken as the thermal safety margin of BWRs. Thus, it was one of the thermal-hydraulic constraints that has to be met for a feasible SMBWR design.
- Void reactivity coefficient (< 0): a negative coolant void coefficient is one of the neutronic parameters set as a constraint for the SMBWR design.
- Average fuel temperature (< 1400 °C): this limit is commonly used in previous studies to limit fission gas release and control the fuel pin internal pressure.

- Maximum fuel temperature (< 2500 °C): this limit provides minimum margin to the fuel centreline temperature before the onset of melting.

2.2 Neutronic and Thermal-hydraulic Tools

The tools used to perform the neutronic analysis in this work were WIMS and PANTHER. WIMS **[27]** is a modular software package for fuel assembly lattice neutron transport calculations. WIMS was used as a lattice code to generate homogenised constants libraries for PANTHER **[28]**, a nodal diffusion code which includes thermal-hydraulic feedback. This cross-section library includes dependence of diffusion parameters on operating conditions such as fuel temperature, moderator density, and fuel burnup.

The thermal-hydraulic tool used in the work was the COBRA-EN code **[29]**. The specific design parameters used for modelling the SMBWR coolant loop are listed in Table 2.1, while Table 2.2 lists various core and vessel dimensions investigated in this work. Fig. 2.2 displays the fuel assembly configuration. Some of these values, such as length of the upper and lower plenum, as well as the moisture separator pressure drop, are assumed by using ESBWR **[19]** data as a reference. The neutronic analysis for various system pressure values was done with axially uniform enrichment of 4.2 wt-% U^{235}. Nine of the fuel rods contained gadolinia poison (Gd_2O_3) with a concentration of 2 wt-%.

Table 2.1 Parameters Used for the Hydraulic Model

Parameter	Value
Fuel rod outside diameter (cm)	1.026
Water rod outside diameter (cm)	2.489
Rod pitch (cm)	1.295
Channel box inside width (cm)	14.0
Assembly pitch (cm)	15.5
Fuel assembly type	10×10 (GE14)
Number of fuel rods per assembly	92
Chimney flow area (m^2)	7.34
Upper plenum length (m)	2.75
Lower plenum length (m)	4.13
Moisture separator pressure drop (kPa)	11.35

Table 2.2 Core Geometry Specification

Parameter	Geometrical Variation		
	1	2	3
No. of fuel assemblies	192	256	368
Power density (kW/L)	48.2	48.2	48.2
Active fuel length (m)	3.60	2.70	1.88
Shroud diameter (m)	2.60	2.90	3.52

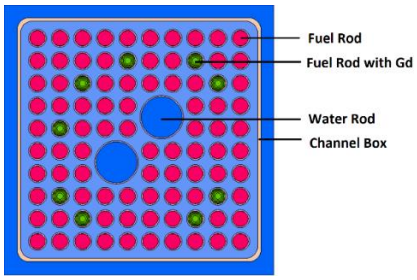

Fig. 2.2 BWR fuel assembly configuration.

The thermal-hydraulic behaviour of BWR is very different compared to a PWR because of boiling inside the core. The varying fraction of liquid and vapour phases between core inlet and outlet means there is greater variation of coolant density inside the reactor core. To analyse the neutronic performance of a PWR core, it is sufficient to generate nuclear cross-section data by depleting the fuel with one historical density and a set of instantaneous branches of the operating conditions. However, in order to accurately capture BWR core performance, multiple historical coolant densities are required, as the cross-section data generated by the lattice code has to account for the coolant density variation along the core length. Therefore, the nuclear data library at each operating pressure was generated by using 3 histories for coolant density (void fraction) and also a set of branches for fuel temperature and coolant density. The density histories used to generate the cross-section data library in WIMS are listed in Table 2.3. Several histories are typically required to recognise the fact that cross-sections depend not only on instantaneous state parameters but also on their historic values. PANTHER then retrieves the cross-section data suitable for the local thermal-hydraulic conditions for each computational node by searching through the library and interpolating first between histories and then between local state parameters.

Table 2.3 Historical Density for Lattice Code

p (bar)	Coolant density (kg/m^3)		
	1	2	3
65	780	260	120
71.7	770	290	130
80	765	300	140
100	730	372	181

2.3 Natural Circulation Loop

As mentioned above, one of the design constraints of the SMBWR is to rely on natural circulation of coolant within the pressure vessel. It is obvious that the system pressure will affect the hydraulic conditions of the flow such as pressure losses inside the recirculation loop and, thus, also affect the minimum chimney height required to maintain natural circulation in the loop. According to Quezada-Garcia et al. **[30]**, the schematic flow diagram of a natural circulation loop in a boiling water reactor could be simplified as shown in Fig. 2.3. By calculating the pressure losses in each component, the minimum height required for the chimney to maintain natural circulation inside the loop can be found. There are four types of pressure losses contributing to each component inside the primary coolant loop: friction, local, elevation, and acceleration losses. In order to accurately model the natural circulation loop in a boiling water reactor, the selection of two-phase flow model is one of the important steps that has to be considered carefully. Appendix B gives a brief review of the commonly used two-phase flow models and the governing equations which are important in modelling two-phase flow **[31, 32]**.

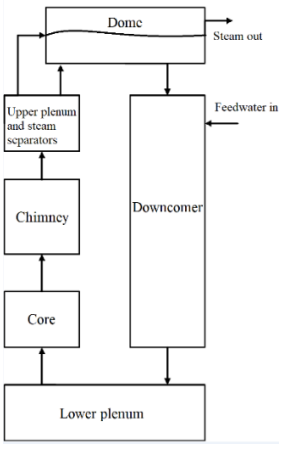

Fig. 2.3 Simplified structure of natural circulation BWR system modified from Quezada-Garcia et al. **[30]**.

The friction pressure losses in the single-phase section can be calculated from Eq. (2-1), while the respective correlation for two-phase flow is shown by Eq. (2-2), where Δp_f is frictional losses (Pa), $\dot{m}$ is the mass flow rate of the coolant (kg/s), ρ_l is the average nodal liquid density (kg/m^3), f is the friction factor, ΔL is the incremental length of the component (m), D_H is the hydraulic diameter of the component (m), A is the component flow area, and $\emptyset_{TPL}^2$ is the two-phase flow friction factor multiplier.

$$\Delta p_f = \frac{\dot{m}^2}{2\rho_l}\frac{f\Delta L}{D_H A^2} \tag{2-1}$$

$$\Delta p_f = \frac{\dot{m}^2}{2\rho_l}\frac{f\Delta L}{D_H A^2}\emptyset_{TPL}^2 \tag{2-2}$$

The friction factor for flow inside a tube can be calculated by the Colebrook equation **[33]**, which takes into account the effect of the operating flow regime and tube surface roughness. The Colebrook equation is displayed in Eq. (2-3), where Re is the Reynolds number and ε is the relative surface roughness. Asker et al. **[34]** compared several non-iterative friction factor correlations and found that the Serghides correlation **[35]**, shown in Eq. (2-4), is one of the best performing approximations of the Colebrook equation. For single-phase flow along rod bundles (flow inside fuel assemblies in the core), a correction factor needs to be applied to be more precise in calculating the friction factor. The bundle friction factor correction constant (C_b') can be estimated from Eq. (2-6) and the corrected friction factor can be estimated by Eq. (2-7). The subscript i in Eq. (2-6) defines the subchannel type (interior, edge, and corner). In terms of calculating the empirical value of the two-phase multiplier ($\emptyset_{TPL}^2$), Todreas and Kazimi **[31]** suggested that the Armand and Treschev correlation (Eq. (2-8)) **[35]** performed the best for BWR geometries. The average value of the two-phase multiplier along a heated channel is calculated from Eq. (2-9). The volumetric flow fraction (β) and void fraction (α) are given by Eq. (2-10) and Eq. (2-11) respectively. The detailed steps of the core friction losses calculation for both single-phase and two-phase flow can be found in Todreas and Kazimi **[31]**.

$$\frac{1}{\sqrt{f}} = -2log_{10}\left[\frac{(\varepsilon/D)}{3.7} + \frac{2.51}{Re\sqrt{f}}\right] \tag{2-3}$$

$$\frac{1}{\sqrt{f}} = \psi_1 - \frac{(\psi_2-\psi_1)^2}{\psi_3-2\psi_2+\psi_1} \tag{2-4}$$

where

$$\psi_1 = -2log_{10}\left[\frac{(\varepsilon/D)}{3.7} + \frac{12}{Re}\right]$$

$$\psi_2 = -2log_{10}\left[\frac{(\varepsilon/D)}{3.7} + \frac{2.51\psi_1}{Re}\right]$$

$$\psi_3 = -2log_{10}\left[\frac{(\varepsilon/D)}{3.7} + \frac{2.51\psi_2}{Re}\right] \quad (2\text{-}5)$$

$$C_b' = D_{eb}'\left[\sum_{i=1}^{3} S_i \left(\frac{D_{ei}'}{D_{eb}'}\right)^{\frac{n}{2-n}} \left(\frac{C_{fi}'}{D_{ei}'}\right)^{\frac{1}{n-2}}\right]^{n-2} \quad (2\text{-}6)$$

$$f = \frac{C_b'}{Re^n} \quad (2\text{-}7)$$

$$\emptyset_{TPL}^2 = \frac{(1-x)^{1.75}}{(1-\alpha)^{1.2}} \text{ ; for } \beta < 0.9 \,\&\, \alpha < 0.5$$

$$\emptyset_{TPL}^2 = \frac{0.48*(1-x)^{1.75}}{(1-\alpha)^n} \text{ , where } n = 1.9 + 1.48 * 10^{-2}\left(\frac{p}{10^6}\right) \text{ ; for } \beta < 0.9 \,\&\, \alpha > 0.5$$

$$\emptyset_{TPL}^2 = \frac{0.025p+0.055}{(1-\beta)^{1.75}}(1-x)^{1.75} \text{ ; for } \alpha > 0.9 \quad (2\text{-}8)$$

$$\overline{\emptyset_{TPL}^2} = \frac{1}{x}\int_{x_1}^{x_2} \emptyset_{TPL}^2 \, dx \quad (2\text{-}9)$$

$$\beta = \frac{x/\rho_g}{x/\rho_g + (1-x)/\rho_f} \quad (2\text{-}10)$$

$$\alpha = \left\{0.833 + 0.05 \ln\left(\frac{p}{10^5}\right)\right\}\beta \quad (2\text{-}11)$$

The local pressure losses are the irreversible pressure losses associated with an abrupt flow area change, such as the orifices and spacers of the fuel assembly. The calculation for single-phase local losses is given by Eq. (2-12), while the respective equation to calculate local losses in the two-phase section is given by Eq. (2-13), where Δp_L is the local pressure drop (Pa) and K is the losses coefficient for the local pressure drop. The value of K for sudden channel enlargement is given in Eq. (2-14), while Eq. (2-15) is for a sudden contraction **[37]**. The estimated average flow area and length of the main components of the SMBWR loop are listed in Table 2.4. To estimate the component flow path length in Table 2.4, both the lower plenum and upper plenum lengths are assumed to be the same value as those of ESBWR, while the core, chimney, and downcomer lengths are adjusted based on core geometries, as specified in Table 2.2, and their respective minimum chimney height required. The estimated flow areas in Table 2.4 are estimated based on the core diameter and the estimated shroud and vessel diameter. For calculating local pressure losses due to the spacers, Rehme's model is used to calculate the form losses (K_s), as shown in Eq. (2-16) **[38]**. A_v is the unrestricted flow area away from the grid or spacer, while A_s is the projected frontal area of the spacer. Rehme's data indicated that the modified drag coefficient (C_v) for square arrays is 9.5 at $Re = 10^4$ and 6.5 at $Re = 10^5$.

$$\Delta p_L = \frac{\dot{m}^2}{2\rho_l}\frac{K}{A^2} \quad (2\text{-}12)$$

$$\Delta p_L = \frac{\dot{m}^2}{2\rho_l}\frac{K}{A^2}\emptyset_{TPL}^2 \quad (2\text{-}13)$$

$$K_{ex} = \left(1 - \frac{A_1}{A_2}\right)^2 \quad (2\text{-}14)$$

$$K_c = 0.55\left(1 - \frac{A_2}{A_1}\right) \quad (2\text{-}15)$$

$$K_s = C_v\left(\frac{A_s}{A_v}\right)^2 \quad (2\text{-}16)$$

Table 2.4 SMBWR Coolant System Geometric Data

Component	Flow Path Length (m)	Average Flow Area (m^2)
Lower Plenum	4.13	7.55
Core	2.92	5.31
Chimney	TBD	7.34
Upper Plenum	2.75	10.18
Downcomer	= (L. plenum + Core + Chimney)	4.45

The elevation pressure drop is the change of pressure in the loop due to the difference in the elevation along the direction of the flow. The single-phase elevation pressure drop is given by Eq. (2-17), while the respective equation for the two-phase section is given by Eq. (2-18), where Δp_E is the elevation pressure losses (Pa), g is the specific gravity constant (m/s^2) and $\bar{\rho}$ is the average mixture density (kg/m^3) for the two-phase flow section given by Eq. (2-19). α is average void fraction, while ρ_f and ρ_g are the saturated liquid and vapour density, respectively.

$$\Delta p_E = \rho_l \Delta L g \quad (2\text{-}17)$$

$$\Delta p_E = \bar{\rho} \Delta L g \quad (2\text{-}18)$$

$$\bar{\rho} = \rho_f(1-\alpha) + \rho_g \alpha \quad (2\text{-}19)$$

The acceleration pressure drop is the change in pressure due to the density difference between the inlet and outlet in each component and the corresponding acceleration of the flow. The basic formulation for acceleration pressure drop is given in Eq. (2-20). In the two-phase

flow region, the density used in Eq. (2-20) is the momentum density (ρ_M), which can be calculated from Eq. (2-21), where x is the steam quality.

$$\Delta p_{ACC} = \frac{\dot{m}^2}{A^2}\left[\frac{1}{\rho_{M,OUT}} - \frac{1}{\rho_{M,IN}}\right] \quad (2\text{-}20)$$

$$\frac{1}{\rho_M} = \frac{x^2}{\rho_g \alpha} + \frac{(1-x)^2}{\rho_g (1-\alpha)} \quad (2\text{-}21)$$

In order to operate in natural circulation mode, it is necessary to ensure that the total pressure losses inside the loop can be compensated by the buoyancy force. By varying the system pressure, the total pressure losses inside the loop will change, and so the minimum chimney height required to provide sufficient buoyancy force would also vary depending on the system pressure. The simplest way to estimate the required chimney height for the natural circulation loop is by defining the pressure losses in each component in the loop, as defined in Fig. 2.3. The flow in the downcomer and lower plenum section are single-phase, while two-phase flow occurs in the chimney, steam separator, and partially inside the core.

A mathematical model of reactor coolant flow was built in the MATLAB programming environment. The core model is divided into multiple nodes to accurately account for the axial power profile distribution inside the core. The properties for water and steam are taken from X-Steam Table software version 2.6 **[39]**. The chimney height required for natural circulation in the hybrid SMBWR is calculated by following the flow chart shown in Fig. 2.4. As mentioned above, the boundary conditions set for comparing the operation at different operating pressure are the same core mass flow rate and core subcooling enthalpy ($\Delta H_{Subcooling}$). The main reason is because the core pressure drop strongly depends on the core mass flow rate and the boiling length. By solving the core energy balance, the core exit quality can be calculated. The height of the chimney and the feedwater temperature are initially assumed to solve the loop thermal-hydraulics. The iteration process is required to solve for the loop momentum balance and obtain the minimum height of chimney required for natural circulation. When the chimney height is adjusted to solve for the loop momentum balance (outer iteration), it results in a different exit quality. With constant feedwater temperature, this will lead to a change in the core inlet condition. Thus, to maintain the core subcooling enthalpy, the inner iteration is needed to adjust the feedwater temperature.

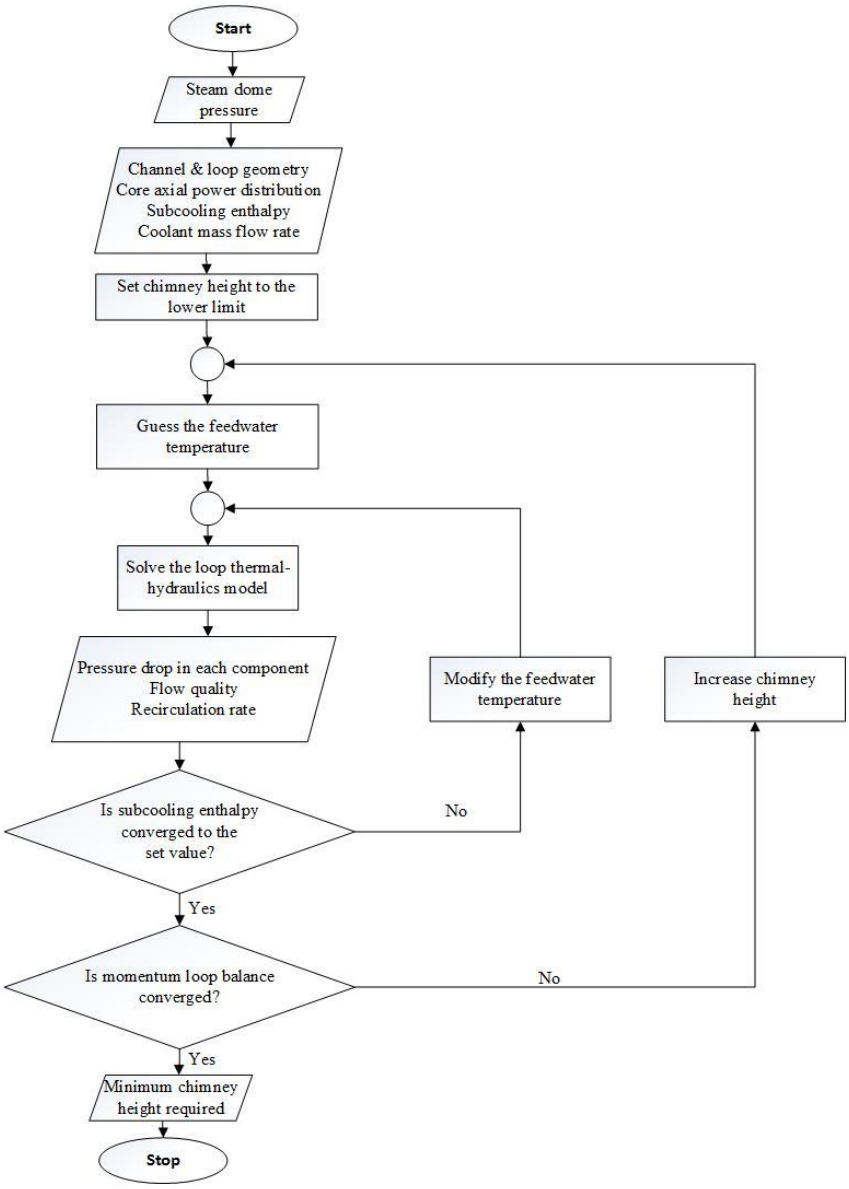

Fig. 2.4 Flow chart of the hydraulic modelling of the natural circulation BWR.

2.4 Power Conversion Cycle

A distinctive feature of the SMBWR is the addition of external superheaters to its balance of plant (BOP). Saturated steam is generated by the reactor core and heated further to superheated conditions by the external superheater before entering the high-pressure (HP) turbines. The exhaust steam from the HP turbines can then be reheated before expansion in the low-pressure (LP) turbines. The heat supplied to the superheater and reheater can either be taken from conventional fossil fuel combustion, such as hot air from a gas fired boiler or exhaust gas from gas turbines, or from a renewable heat source such as heat stored in the molten salt from a concentrated solar power (CSP) system. There are two main benefits of having an

external heat source for the superheater and reheater. These are the improvement of thermal efficiency and the ability to vary the system power to match the load demand by adjusting the external heat provided to the superheater. In most LWR steam cycles, a fraction of the steam is diverted before entering the HP turbines to supply heat to the moisture separator and reheaters (MSRs). By having a reheater which utilises an external heat source, all the steam generated by the reactor can generate useful work in the HP turbine, improving the thermal efficiency of the cycle. A small portion of steam is bled from the turbine to preheat the feedwater. The turbine outlet stream is then condensed in the condenser and directed through several stages of feedwater heaters before returning to the reactor. The last stage of the feedwater heaters cascade is an economiser which utilises the heat exhausted from both superheater and reheater to further preheat the feedwater before entering the core. The BOP for the SMBWR is displayed schematically in Fig. 2.5.

The steam expansion process inside the turbines follows Eq. (2-22) and Eq. (2-23). The heat rejection in the condenser can be calculated by Eq. (2-24). The pumping work is calculated by Eq. (2-25) and Eq. (2-26) and the feedwater heater process follows Eq. (2-27). The superheater and reheater are heat exchangers and follow Eq. (2-28). The electricity produced by the generator is calculated from Eq. (2-29). The isentropic efficiencies of the assumed turbine, pump and electric generator are based on the values reported by Ion and Codrut **[40]** and shown in Table 2.5. The energy balance calculation is performed using X-Steam Table software version 2.6 **[39],** which was developed based on the revised data from the International Association for the Properties of Water and Steam (IAPWS) Industrial formulation 1997 **[41]**.

$$\Delta h_{Turbine} = \eta_{Turbine} \Delta h_{Turbine,isentropic} \quad (2\text{-}22)$$

$$W_{Turbine} = \dot{m}_{steam} \Delta h_{Turbine} \quad (2\text{-}23)$$

$$Q_{Cond} = \dot{m}_{steam} \left(h_{Cond,in} - h_{Cond,out} \right) \quad (2\text{-}24)$$

$$\Delta h_{Pump} = \Delta h_{Pump,isentropic} / \eta_{Pump} \quad (2\text{-}25)$$

$$W_{Pump} = \dot{m}_{feedwater} \Delta h_{Pump} \quad (2\text{-}26)$$

$$\dot{m}_{feedwater} \Delta h_{feedwater} = \dot{m}_{steam} \Delta h_{steam} \quad (2\text{-}27)$$

$$\dot{m}_{sh,coolant} \Delta h_{sh,coolant} = \dot{m}_{steam} \Delta h_{steam} \quad (2\text{-}28)$$

$$P = \eta_{Generator} W_{Turbine} \quad (2\text{-}29)$$

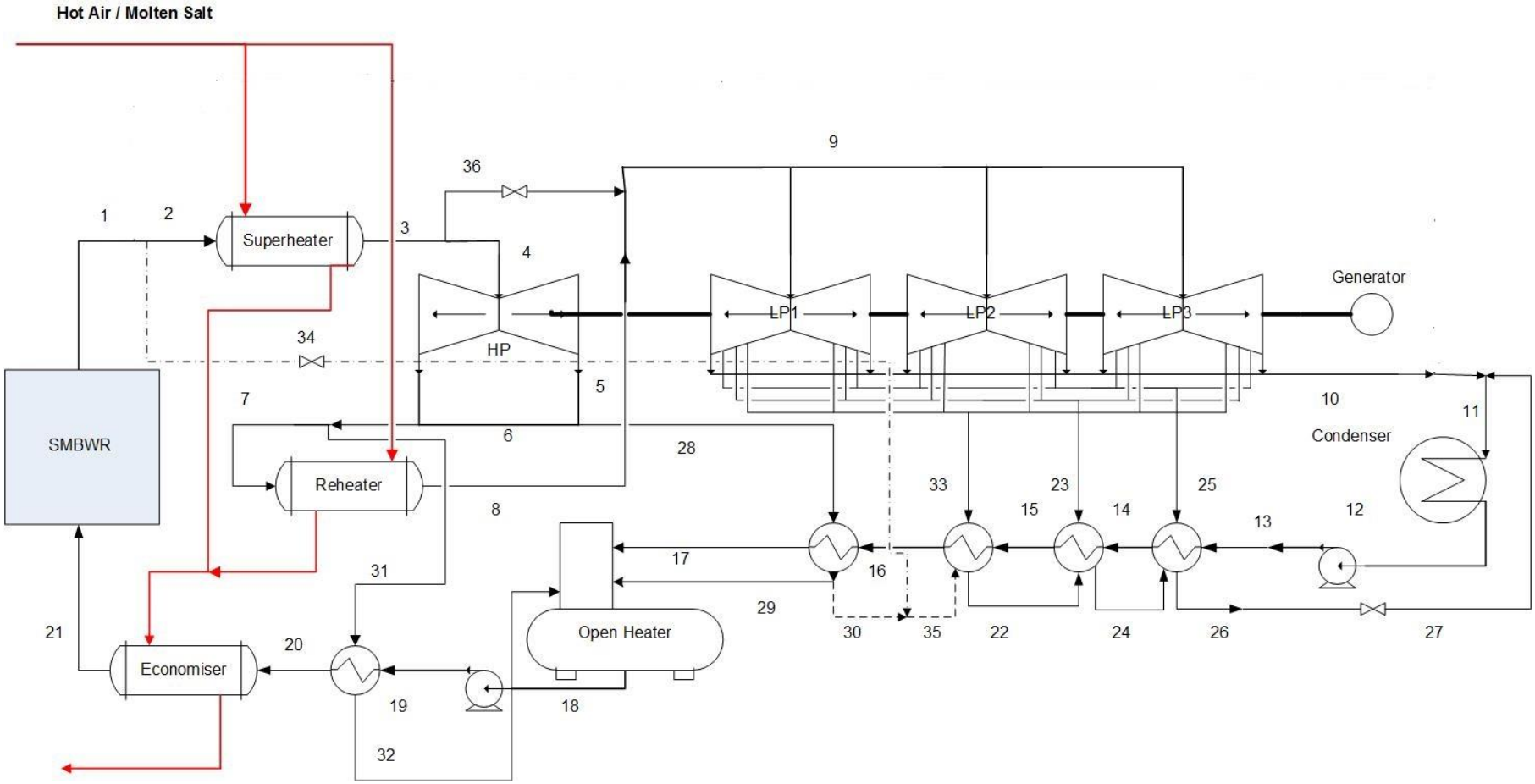

Fig. 2.5 BOP of the hybrid SMBWR.

Table 2.5 Isentropic Efficiencies used for Analysis

Variable	Value
$\eta_{HPTurbine}$	84%
$\eta_{LPTurbine}$	88%
η_{Pump}	82%
$\eta_{Generator}$	98%

The steam turbines are known to be sensitive to the steam conditions and adjusting the external heat to follow the load can result in significant variation in these conditions, which may cause thermal stress and fatigue problems in the steam turbine. In order to avoid these problems, the load-follow operation is accomplished by introducing a bypass line from the HP turbine inlet to the LP turbine inlet (point 36 in Fig. 2.5). By doing so, the work of the HP turbine and the external heat required to reheat the steam before entering the LP turbines can be varied. With this method of load-follow, the steam conditions at the entrance of both HP and LP turbines are fixed and independent of the load. The load variation is achieved by adjusting the steam flow rate through the turbines. This method of load-follow allows the reactor operation to be maintained constantly at 100% of its full rated power. However, there is a minimum limit to the extent the system power could be adjusted using this method, which will be discussed later in Chapter 5.

In designing the BOP for the SMBWR, the reactor feedwater inlet and steam outlet conditions are used as the boundary conditions. It is known that the steam cycle performance is determined by the operating parameters selected for the steam cycle, such as turbine inlet temperature, turbine outlet pressure, and the fraction of steam bled from the turbine to preheat the feedwater. The HP turbine inlet temperature for the full power case in this study is set to 540 °C. The main reason for choosing this operating temperature is to open the possibilities for various external heat sources, such as a conventional gas boiler, exhaust gas from a gas turbine in a combined cycle mode, and heat stored in molten salt from a CSP plant. The conventional gas boiler can reach temperatures as high as 1600 °C, while the gas turbine exhaust temperature varies between 500 and 700 °C. In the case of using heat from a CSP, the molten nitrate salt (60 wt-% $NANO_3$ and 40 wt-% KNO_3) is known to be a stable mixture and suitable for use as a thermal storage medium within a temperature range of 260 °C to 621 °C **[42]**.

In the steam cycle of a conventional stand-alone NPP, the HP turbine outlet pressure is usually limited by the wetness of the steam in order to protect turbine blades. However, with

the addition of a superheater, this limitation can be relaxed. According to Al Kindi **[43]**, the LWR combined with gas fired superheater system would achieve higher cycle efficiency when the HP turbine outlet pressure becomes lower. However, the combination of a low HP turbine outlet pressure and high LPT inlet temperature could result in an undesirable steam condition at the outlet of LP turbine, where the outlet stream is still superheated. This high-grade heat would then be wasted by rejecting it through the condenser system. Therefore, the HP turbine outlet pressure and LP turbine inlet temperature are selected with the following two main considerations in mind. The first consideration is to ensure a wet, or at most saturated, steam condition at the LP turbine outlet so that no heat would be wasted. The other consideration is to ensure that both HP turbine inlet stream and LP turbine inlet stream have the same enthalpy. This is important to facilitate the load-follow operation for the hybrid SMBWR which is envisaged to be done by bypassing the steam from HP turbine inlet point to LP turbine inlet point, without altering the operating condition of the steam entering the LP turbine.

2.4.1 BOP component validation

The steam cycle mostly consists of three major components: turbines, pumps, and heat exchangers. In this sub-section, the validation exercise for these components is provided. The reference used for the BOP validation exercise is the AP600, for which a schematic diagram is shown in Fig. 2.6, while the state point conditions are displayed in Table 2.6.

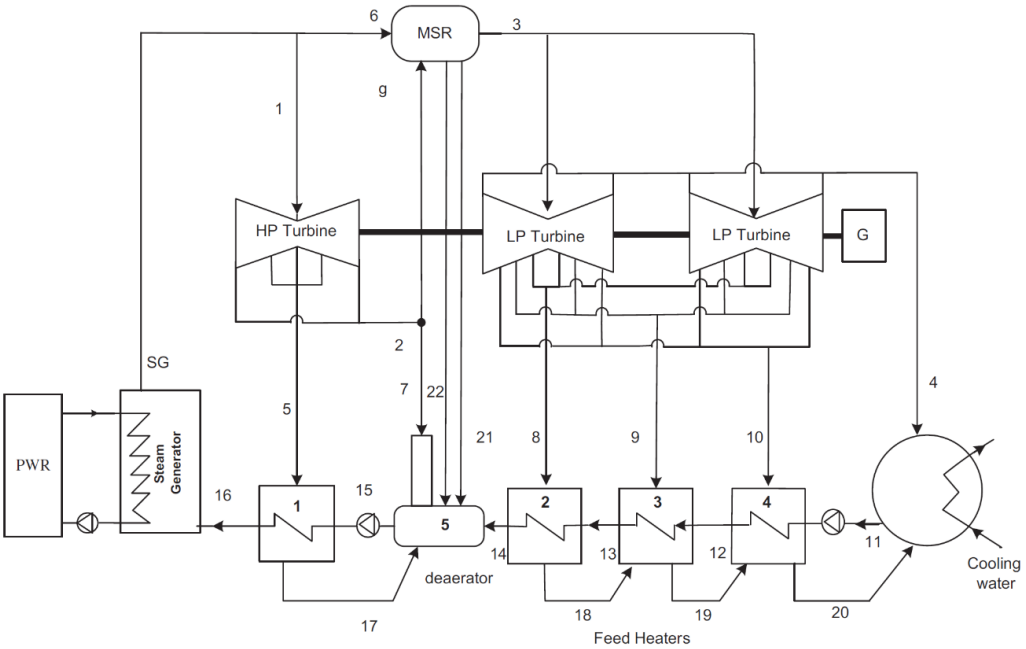

Fig. 2.6 Schematic diagram of the AP600 NPP steam cycle **[11]**.

Table 2.6 State Points of the AP600 NPP steam cycle **[11]**

Point	m (kg/s)	p (bar)	T (°C)	x	h (kJ/kg)	s (kJ/kg K)
SG	1063	57.2	272.5	1	2787.5	5.91
1	1021	57.2	272.5	1	2787.5	5.91
2	898.2	12	188	0.881	2541.4	6.01
3	746.6	11	240	Superheat	2960.4	6.83
4	609.3	0.08	41.5	0.884	2323.1	7.34
5	123.2	30	233.9	0.92	2671.2	5.91
6	41.64	57.2	272.5	1	2787.5	5.91
7	50.86	12	188	0.881	2548.7	6.01
8	48.11	3.5	138.9	0.97	2820	6.83
9	45.64	1.5	111.4	0.93	2654	6.83
10	43.47	0.5	81.3	0.882	2480	6.83
11	746.6	0.08	41.5	0	171.7	0.592
12	746.6	30	74	0	297.2	1.003
13	746.6	30	106.5	0	448.6	1.38
14	746.6	30	139	0	602.1	1.729
15	1063	62	184.1	0	718.3	2.179
16	1063	62	226.9	0	971.7	2.581
17	123.2	30	233.9	0	985.3	2.645
18	48.11	3.5	138.9	0	623.7	1.728
19	93.75	1.5	111.4	0	469.8	1.433
20	137.22	0.5	81.3	0	318.2	1.091
21	41.64	57.2	272.5	0	1197.3	2.998
22	100.8	11	184.1	0	781.4	2.178

1. Turbine model

The turbine model was used to simulate the turbine expansion process. The input parameters required are inlet pressure, inlet temperature, inlet quality, outlet pressure, and the turbine isentropic efficiency. The model is designed to produce a warning message if the outlet quality falls below 0.8, which is usually a limiting condition for wet steam in order to protect the turbine blades. In order to validate the turbine model, the parameter values from Table 2.6 state no. 1 were selected as inlet parameters, the pressure from state no. 2 was selected as the

outlet pressure, and a turbine isentropic efficiency of 0.84 was used. The comparison between parameters for state no. 2 calculated by the turbine model and the reference values is presented in Table 2.7, where the %-difference of the parameters is calculated by Eq. (2-30). It can be observed from Table 2.7 that all output parameter values calculated from the model are within 1% of the reference values. Therefore, it can be concluded that the turbine model used in the BOP model is sufficiently representative of turbines used at NPP in general.

$$\%\ difference = \frac{Ref.value - Calc.value}{Ref.value}\ x\ 100\% \qquad (2\text{-}30)$$

Table 2.7 Turbine Model Comparison

Parameter	Ref. value	Calc. value	%-difference
T (°C)	188	187.96	-0.02
h (kJ/kg)	2541.4	2548.5	0.28
x	0.881	0.882	0.06

2. Pump model

The input parameters required for the pump model are inlet pressure, inlet specific enthalpy, outlet pressure, and the pump isentropic efficiency. In order to validate the pump model, the parameter values of the deaerator outlet were taken as the inlet parameters for the pump, the pressure from state no. 15 was selected as the outlet pressure, and a pump isentropic efficiency of 0.82 was used. The comparison between parameters for state no. 15 calculated by the pump model and the reference values is presented in Table 2.8, where the %-difference of the parameters is calculated by Eq. (2-30). It can be observed from Table 2.8 that the calculated temperature is within 1% of the reference temperature, while the difference in specific enthalpy is roughly 9%. However, at the same pressure and a slightly different temperature, it is almost impossible to get a large discrepancy in the specific enthalpy. Hence, the possible reason which might cause this discrepancy, other than the possibility of a typing mistake in the reference value of the specific enthalpy for state point no. 15, is that the water properties data used to obtain the reference values are taken from a different source of steam tables compared to the one used in our model.

Table 2.8 Pump Model Comparison

Parameter	Ref. value	Calc. value	%-difference
T (°C)	184.1	184.0	-0.06
h (kJ/kg)	718.3	783.3	9.05

3. Heat exchanger model

No separate heat exchanger component model was built for the steam cycle model. In principle, the heat exchanger was modelled by solving the mathematical model of the heat exchange process between two different fluid conditions while assuming that no heat is lost during the exchange process. Since there is no external component modelled specifically for the heat exchanger, the heat exchange process will be included in the whole cycle validation in the next section.

2.4.2 BOP whole cycle validation

Two cases were considered for the BOP whole cycle validation exercise. The first case was to recreate the AP600 NPP steam cycle by following the schematic diagram shown in Fig. 2.6. The second case was to recreate the hybrid AP600 NPP combined with gas turbines, as shown in Fig. 2.7. The additional information required to recreate both cases and the reference data to compare with the calculated results can be found in the study of Darwish et al. **[11]**.

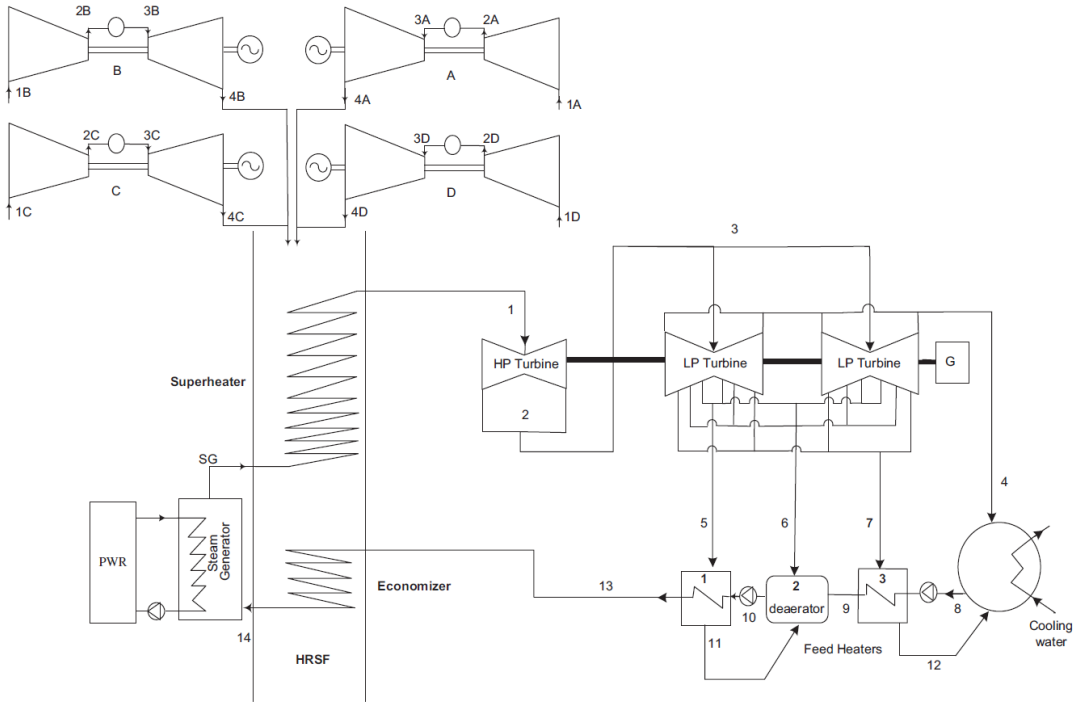

Fig. 2.7 Schematic diagram of the AP600 combined with gas turbines **[11]**.

The comparison of parameter values for the AP600 NPP steam cycle is listed in Table 2.9, while the one for the superheating case is displayed in Table 2.10. Table 2.11 and Table 2.12 show the comparison of the state points' operating conditions for the AP600 NPP steam cycle without and with superheating, respectively. These results are in good agreement with the reference and provide confidence that the NPP steam cycle and combined cycle can be modelled within reasonable accuracy by combining the major components of the steam cycle defined in the previous section.

Table 2.9 The Steam Cycle Parameter Comparison for the AP600

Parameter	Ref. value	Calc. value	%-difference
Reactor thermal power (MW)	1933	1924.1	-0.46
Net work of the turbine (MW)	619	642.75	3.84

Table 2.10 The Steam Cycle Parameter Comparison for the hybrid AP600 Combined with Gas Turbines

Parameter	Ref. value	Calc. value	%-difference
Reactor thermal power (MW)	1926	1925.2	-0.04
Net work of the turbine (MW)	1151.4	1174.5	2.01
External heat for superheater (MW)	754.1	754.02	-0.01
External heat for superheater (MW)	447.653	457.56	2.21

Table 2.11 The Comparison of the State Points' Conditions for the AP600 NPP Steam Cycle

Point	m (kg/s)			p (bar)			T (°C)			h (kJ/kg)		
	Ref.	Calc.	%-diff.	Ref.	Calc.	%-diff.	Ref.	Calc.	%-diff.	Ref.	Calc.	%-diff.
SG	1063.0	1063.0	0.00	57.2	57.2	0.00	272.5	272.5	0.00	2787.5	2787.6	0.00
1	1021.0	1021.4	0.04	57.2	57.2	0.00	272.5	272.5	0.00	2787.5	2787.6	0.00
2	898.2	898.2	0.00	12	12	0.00	188	188.0	-0.02	2541.4	2547.0	0.22
3	746.6	746.5	-0.01	11	11	0.00	240	240.0	0.00	2960.4	2916.9	-1.47
4	609.3	609.3	0.00	0.08	0.08	0.00	41.5	41.5	0.02	2323.1	2291.8	-1.35
5	123.2	123.2	0.00	30	30	0.00	233.9	233.9	-0.02	2671.2	2684.4	0.50
6	41.6	41.6	0.00	57.2	57.2	0.00	272.5	272.5	0.00	2787.5	2787.6	0.00
7	50.9	50.9	0.00	12	12	0.00	188	188.0	-0.02	2548.7	2547.0	-0.07
8	48.1	48.1	0.00	3.5	3.5	0.00	138.9	141.7	2.01	2820	2738.4	-2.89
9	45.6	45.6	0.00	1.5	1.5	0.00	111.4	111.4	-0.04	2654	2622.9	-1.17
10	43.5	43.5	0.00	0.5	0.5	0.00	81.3	81.3	0.02	2480	2487.5	0.30
11	746.6	746.5	-0.01	0.08	0.08	0.00	41.5	41.5	0.02	171.7	173.9	1.25
12	746.6	746.5	-0.01	30	30	0.00	74	75.5	2.04	297.2	318.5	7.17
13	746.6	746.5	-0.01	30	30	0.00	106.5	108.7	2.05	448.6	457.9	2.07
14	746.6	746.5	-0.01	30	30	0.00	139	141.4	1.71	602.1	596.7	-0.90
15	1063.0	1063.0	0.00	62	62	0.00	184.1	184.0	-0.06	718.3	783.3	9.05
16	1063.0	1063.0	0.00	62	62	0.00	226.9	227.1	0.09	971.7	977.5	0.60

Contd. The Comparison of the State Points' Conditions for the AP600 NPP Steam Cycle

Point	m (kg/s)			p (bar)			T (°C)			h (kJ/kg)		
	Ref.	Calc.	%-diff.	Ref.	Calc.	%-diff.	Ref.	Calc.	%-diff.	Ref.	Calc.	%-diff.
17	123.2	123.2	0.00	30	30	0.00	233.9	233.9	-0.02	985.3	1008.4	2.34
18	48.1	48.1	0.00	3.5	3.5	0.00	138.9	138.9	-0.03	623.7	584.3	-6.32
19	93.8	93.8	0.00	1.5	1.5	0.00	111.4	111.4	-0.04	469.8	467.1	-0.58
20	137.2	137.2	0.00	0.5	0.5	0.00	81.3	81.3	0.02	318.2	340.5	7.00
21	41.6	41.6	0.00	57.2	57.2	0.00	272.5	272.5	-0.01	1197.3	1197.8	0.04
22	100.8	100.8	0.00	11	11	0.00	184.1	184.1	-0.02	781.4	781.4	0.00

Table 2.12 The Comparison of the State Points' Conditions for the hybrid AP600 Combined with Gas Turbines

Point	m (kg/s)			p (bar)			T (°C)			h (kJ/kg)		
	Ref.	Calc.	%-diff.	Ref.	Calc.	%-diff.	Ref.	Calc.	%-diff.	Ref.	Calc.	%-diff.
SG	1063	1063	0.00	57.2	57.2	0.00	272.5	272.5	0.00	2787.5	2787.59	0.00
1	1063	1063	0.00	57.2	57.2	0.00	530	530.0	0.00	3496	3496.92	0.03
2	1063	1063	0.00	12	12	0.00	314.7	325.3	3.38	3077	3101.17	0.79
3	1063	1063	0.00	11	11	0.00	314.7	324.3	3.04	3080	3101.17	0.69
4	904.87	904.87	0.00	0.08	0.08	0.00	41.5	41.5	0.02	2366	2330.59	-1.50
5	40.86	40.86	0.00	3.5	3.5	0.00	176.4	199.6	13.15	2856	2862.64	0.23
6	52.62	52.62	0.00	1.5	1.5	0.00	111.4	123.2	10.58	2725	2717.99	-0.26
7	64.65	64.65	0.00	0.5	0.5	0.00	81.31	81.3	0.01	2576	2558.38	-0.68
8	969.52	969.52	0.00	0.08	0.08	0.00	41.5	41.5	0.02	173.7	173.85	0.09
9	969.52	969.52	0.00	1.5	1.5	0.00	74	76.9	3.90	309.7	321.98	3.96
10	1063	1063	0.00	1.5	1.5	0.00	111.4	107.5	-3.52	467.1	450.67	-3.52
11	40.86	40.86	0.00	3.5	3.5	0.00	138.9	138.9	-0.01	584.4	584.31	-0.02
12	64.65	64.65	0.00	0.5	0.5	0.00	81.31	81.3	0.01	340.4	340.48	0.02
13	1063	1063	0.00	62	62	0.00	131.9	129.0	-2.22	554.4	546.01	-1.51
14	1063	1063	0.00	60	60	0.00	226.9	226.9	0.00	975.5	976.45	0.10

Chapter 3: Preliminary Investigation on LWR with Gas Fired Superheaters

This chapter presents the preliminary investigation results on adding gas fired superheaters to the existing conceptual design of LWRs. The main scope of this preliminary study is to investigate how the addition of the gas fired superheaters will affect the thermodynamic performance of the reference LWRs.

3.1 PWR with Gas Fired Superheaters

The nuclear power plant used as a reference in this study is the AP1000. It is a PWR designed by Westinghouse which produces about 1100 MWe. A schematic diagram of the AP1000 steam cycle, based on its plant description **[44]**, is shown in Fig. 3.1. The heat from the primary loop is used to generate steam in the steam generator (SG). This steam then enters the turbine after some portion is extracted to provide heat for the Moisture Separator & Reheater (MSR). The AP1000 turbine consists of a double-flow, high-pressure (HP) cylinder and three double-flow, low-pressure (LP) cylinders. The steam conditions at the inlet of the HP cylinder are 55 bar and 271 ^{o}C. Some portion of the steam is extracted from the HP turbine to provide heat to the MSR and the high-pressure feedwater heater. The HP turbine outlet then goes through the MSR to reduce its wetness before entering the LP turbine. In the LP turbine, some portions of the steam are extracted from different stages of the LP turbine to provide heat to the low-pressure feedwater heaters. The outlet steam from the LP turbine is condensed before being pumped and heated as feedwater for the steam generator **[44]**. The conditions at each point in Fig. 3.1 are reported in Table 3.1.

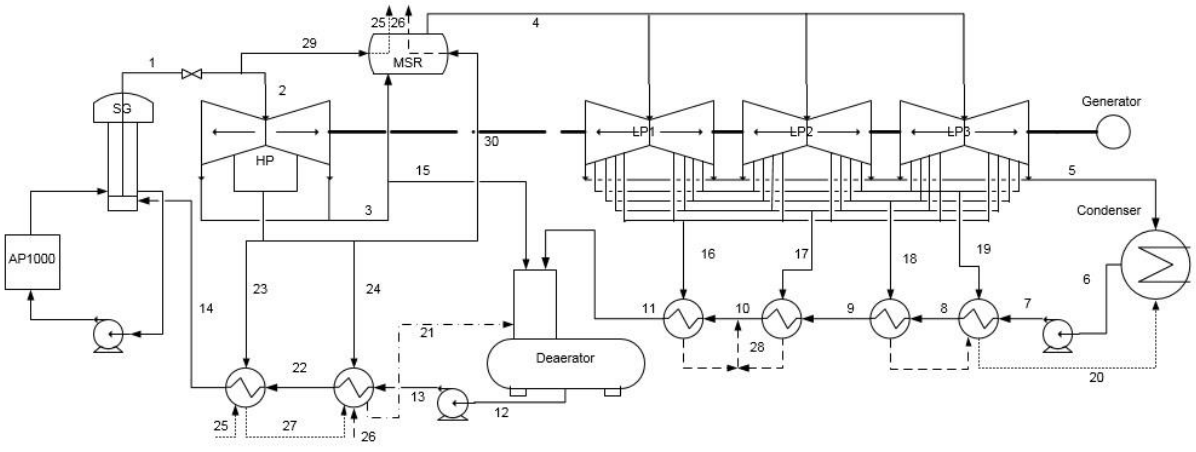

Fig. 3.1 AP1000 steam cycle flow diagram.

Table 3.1 Steam (Water) Conditions at Each Point of the AP1000 Steam Cycle

Point	m (kg/s)	p (bar)	T (°C)	x (-)	h (kJ/kg)	s (kJ/kg K)
1	1886.00	55.50	271.00	1.00	2791.3	5.93
2	1800.00	55.00	271.00	1.00	2794.5	5.94
3	1260.00	10.50	182.02	0.88	2541.1	6.05
4	1200.00	9.50	251.00	1.00	2947.3	6.96
5	1000.00	0.10	45.81	0.89	2322.7	7.33
6	1100.00	0.10	44.00	0.00	184.3	0.63
7	1100.00	30.00	44.28	0.00	188.0	0.63
8	1100.00	30.00	67.82	0.00	286.3	0.93
9	1100.00	30.00	91.48	0.00	385.5	1.21
10	1200.00	30.00	116.81	0.00	492.2	1.49
11	1200.00	30.00	138.26	0.00	583.4	1.72
12	1972.00	30.00	192.02	0.00	817.3	2.25
13	1972.00	60.00	192.64	0.00	821.4	2.25
14	1972.00	60.00	226.70	0.00	975.5	2.57
15	60.00	10.50	182.02	0.88	2541.1	6.05
16	50.00	3.50	156.97	1.00	2772.4	7.04
17	50.00	3.00	144.27	1.00	2748.7	7.05
18	50.00	1.50	111.35	0.98	2647.9	7.11
19	50.00	0.50	81.32	0.94	2504.2	7.20
20	100.00	0.10	81.32	1.00	2651.8	8.35
21	501.41	30.00	233.86	0.64	2158.9	2.65
22	1972.00	60.00	209.85	0.00	898.5	2.42
23	90.00	30.00	233.86	0.94	2696.9	5.98
24	90.00	30.00	233.86	0.94	2696.9	5.98
25	86.00	30.00	269.97	1.00	2914.7	6.40
26	360.00	30.00	233.86	0.35	1629.6	3.87
27	176.00	30.00	233.86	0.49	1885.4	2.65
28	100.00	3.00	133.53	0.01	572.9	1.70
29	86.00	55.00	271.00	1.00	2794.5	5.94
30	360.00	30.00	233.86	0.94	2696.9	5.98

There are three schemes considered in this work for such a combination. The first scheme considered was having a single superheater powered by a conventional gas boiler. This superheater was taking the steam from the SG and further heating the steam to 600 ^{o}C. The waste heat from the superheater was used to preheat the feedwater in the economiser. The second scheme was similar to the first one, but, rather than using a conventional gas boiler, waste heat from a CCGT was used to supply heat for the superheater. The exhaust temperature of this gas turbine is 577 ^{o}C and its exhaust gas flow rate is 692 kg/s at full power. Therefore, the HP turbine inlet temperature has to be reduced from 600 ^{o}C to 530 ^{o}C. The third scheme was adding an additional reheater to further utilise the waste heat from the superheater before directing it to the economiser. In this scheme, the reheated steam temperature was set to 450 ^{o}C. The properties of air needed for the thermodynamic analysis were taken from Lemmon et al. **[45]**. The schematic flow diagram for the first two schemes is displayed in Fig. 3.2, while the schematic flow diagram of the third scheme is displayed in Fig. 3.3.

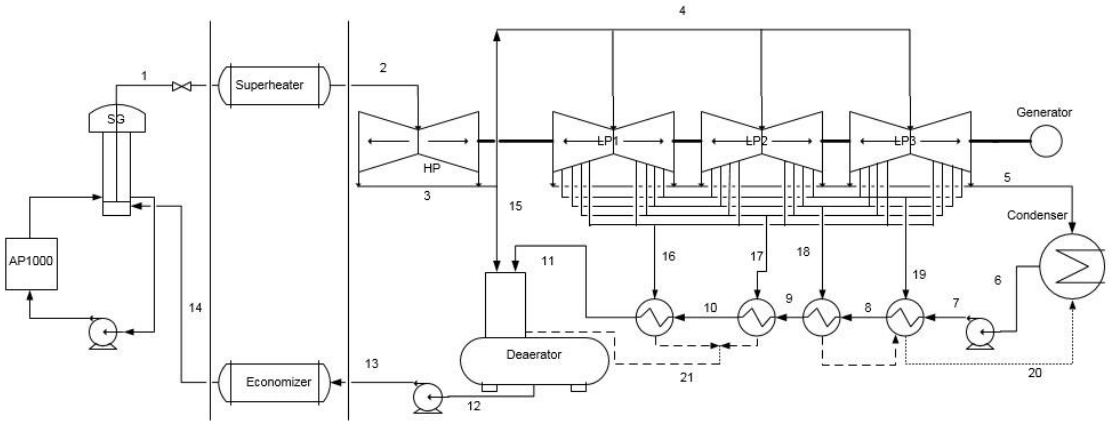

Fig. 3.2 AP1000 steam cycle with superheater flow diagram.

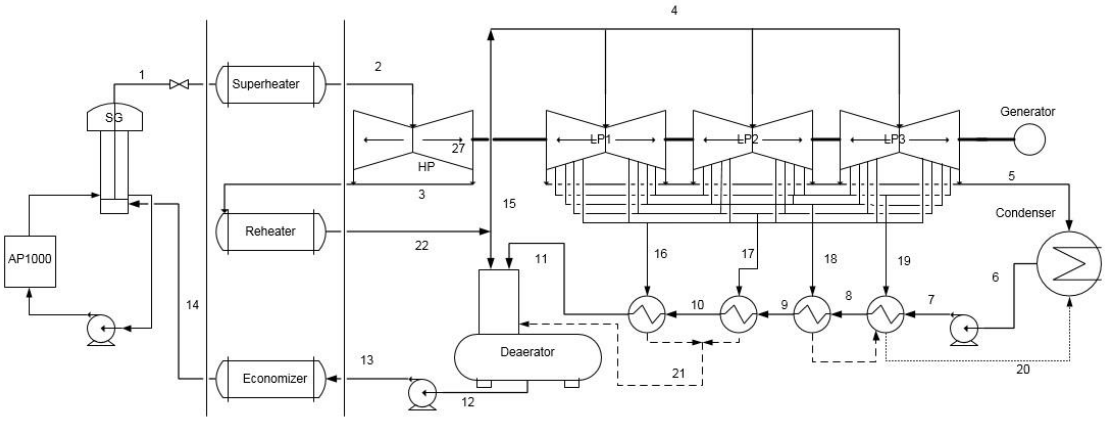

Fig. 3.3 AP1000 steam cycle with superheater and reheater flow diagram.

The thermodynamic performances of these hybrid configurations are summarised in Table 3.2. The total cycle efficiency was calculated from Eq. (3-1), while the fossil fuel cycle efficiency is calculated from Eq. (3-2). It is found that by having a superheater, the MSR and the HP feedwater heaters could be eliminated, allowing more steam to be expanded in the HP turbine, which eventually results in higher electrical power compared to a stand-alone NPP, and, thus, improves the thermal efficiency of the power conversion cycle of the system. This improvement in thermodynamic performance can be observed by comparing the T-s diagrams shown in Fig. 3.4. The reference points shown in the T-s diagrams correspond to those specified in Fig. 3.1, Fig. 3.2 and Fig. 3.3, respectively.

Table 3.2 Thermodynamic Analysis Results of AP1000 with Superheaters

Parameter	**No Superheater**	**Gas Burner Scheme**	**CCGT Scheme**	**Gas Burner with Reheating**
Number of gas turbine units	-	-	6	-
HP turbine inlet temp. (°C)	271	600	530	600
$W_{HP\ turbine}$ (MWth)	372.0	865.4	784.8	865.4
$W_{LP\ turbine}$ (MWth)	680.3	1,221.3	1,138.2	1,336.8
W_{tot} (MWth)	1,052.3	2,086.7	1,923.0	2,202.1
Total electric power (MWe)	1,031.3	2,045.0	3,900.5	2,158.1
Reactor thermal power (MWth)	3,416.6	3,416.6	3,416.6	3,416.6
Additional heat required (MWth)	-	2,318.0	5,103.8	2,481.3
Increment of power (%)	-	98.00	277.66	108.95
Fossil fuel cycle efficiency (%)	-	44.62	56.19	46.34
Total cycle efficiency (%)	30.80	36.38	45.78	37.34

$$\eta_{Total\ Cycle} = \frac{W_{net,cycle}}{Q_{Nuclear\ reactor} + Q_{Fossil\ fuel}} \quad (3\text{-}1)$$

$$\eta_{Fossil\ Cycle} = \frac{W_{net} - W_{net,w/o\ superheating}}{Q_{Fossil\ fuel}} \quad (3\text{-}2)$$

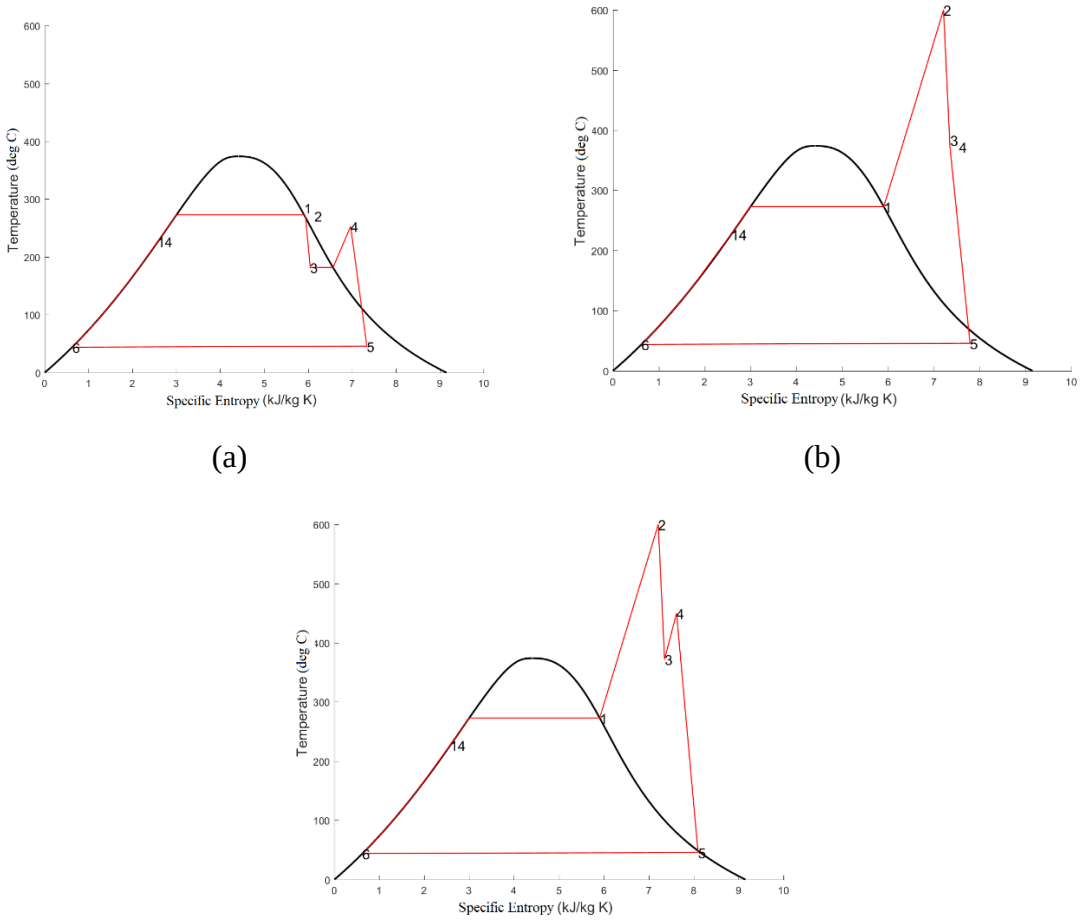

Fig. 3.4 T-s diagrams of the AP1000 steam cycle: (a) stand-alone; (b) with superheater & economiser; (c) with superheater, reheater & economiser.

The increase in total thermal efficiency by using the CCGT scheme is quite significant and is comparable to the thermal efficiency of a fossil fuelled power plant, while the total efficiency of the gas burner scheme concept is less significant. However, one can argue that, besides total thermal efficiency, the fossil fuel cycle efficiency, which is calculated by dividing the additional electric power by the additional heat supplied to the system, is also an important aspect to be considered in the performance analysis of this superheater concept. The CCGT concept can provide a fossil fuel cycle efficiency value of 56.19%, a significant increase compared to the stand-alone gas turbine thermal efficiency (approximately 40%), and it is even comparable to the existing commercial CCGT thermal efficiency, which can reach up to 60%. The fossil fuel cycle efficiency of the gas burner concept is about 44.62%. Although this value is smaller than the CCGT power conversion cycle efficiency, it is above the thermal efficiency

of existing commercial stand-alone gas turbines. Therefore, it can be concluded that the superheater concept can provide a more efficient way of using natural gas for power generation.

Although the coupling with gas turbines shows a significant improvement, the number of gas turbine units needed to achieve that performance also needs to be considered in the cost analysis. Furthermore, having both nuclear power plant and gas turbines in the same area might be difficult to justify in terms of space and safety issues. From this point of view, the conventional gas burner scheme seems to be the more favourable option due to its simplicity, and thus easier to implement. Another challenge that needs to be addressed is the existing capacity of commercial steam turbines. There is currently no single shaft steam turbine that can produce about 2,000 MWe and the cost of having more than one turbine in the plant would need to be considered in the cost estimates. Therefore, this analysis was extended to consider a smaller power nuclear unit so that the total power plant output at full capacity would be within the limits of current commercially available steam turbines. The reference reactor used for this study is a twin pack of the mPower reactor producing about 1,060 MWt and 360 MWe **[46]**. The steam cycle analysis shows that the thermal efficiency of the SMR considered in this study is 33.41%. Similar to the AP1000 analysis, both the CCGT coupling concept and the gas burner concept were studied in the context of the SMR coupling scheme and the results are shown in Table 3.3.

Table 3.3 shows that the cycle efficiency can be improved from 34% to 45% (CCGT) or 36.2% (gas burner). By using the CCGT coupling scheme, a significant improvement in the thermal efficiency can be achieved with only 2 gas turbine units instead of 6 units for the AP1000. A modification of the gas burner concept with an additional reheater to further improve the thermal efficiency is also considered. It is shown that, by installing additional reheater, the thermal efficiency of the SMR considered can increase further to 36.5%. In terms of fossil fuel cycle efficiency, it is shown that adding superheaters to a PWR-type SMR would help the hybrid plant to have a cycle efficiency comparable to the thermal efficiency of the stand-alone gas turbines (approximately 40%).

It is also found that, by having the superheaters, the NPP could develop a new method of load-following by adjusting the external heat given to the superheaters. Table 3.4 shows the hybrid plant of AP1000 combined with gas fired superheaters is able to reduce its load down to 65% only by reducing the amount of external heat given to the superheaters, keeping the nuclear reactor thermal power at 100% of its full rated power at all times. It is also shown that the hybrid plant can achieve this load reduction while maintaining its cycle efficiency above that of the stand-alone NPP.

Table 3.3 Thermodynamic Analysis Results of PWR-type SMR with Superheaters

Parameter	No Superheater	Gas Burner Scheme	CCGT Scheme	Gas Burner with Reheating
Number of gas turbine units	-	-	2	-
HP turbine inlet temp. (°C)	299.44	600	530	600
$W_{HP\ turbine}$ (MWth)	122.3	248.9	225.6	248.9
$W_{LP\ turbine}$ (MWth)	239.0	367.5	342.6	402.5
W_{tot} (MWth)	361.3	616.4	568.2	651.4
Total electric power (MWe)	354.1	604.1	1,132.9	638.3
Reactor thermal power (MWth)	1,060.0	1,060.0	1,060.0	1,060.0
Additional heat required (MWth)	-	641.9	1,458.2	722.2
Increment of power (%)	-	70.60	219.93	80.27
Fossil fuel cycle efficiency (%)	-	39.74	53.41	40.17
Total cycle efficiency (%)	34.08	36.21	44.99	36.55

Table 3.4 Load-Following Design for the AP1000 with Gas Fired Superheaters

Power Output (% of nominal)	HP Turbine Inlet Temperature (°C)	Reheated Steam Temperature (°C)	Total Power Generated (MWe)	Total Cycle Efficiency (%)
100	600	450	2,158.1	36.59
90	550	350	1,946.3	34.88
80	400	320	1,728.2	32.97
70	350	195	1,514.9	32.17
65	271	192	1,424.2	31.08

3.2 BWR with Gas Fired Superheaters

In order to investigate the effect of having gas fired superheaters with a BWR, a preliminary investigation was done by using the ESBWR **[19]** and DMS **[20]** as reference reactors. A

simplified model of a BWR steam cycle was built in MATLAB environment. In this model, some simplification of the actual NPP steam cycle was implemented, i.e. reducing the number of stages of feedheating. In the model without superheater (Fig. 3.5), about 20% of the steam entering the HP turbine is taken to provide heat to the MSRs. In the model with superheater (Fig. 3.6), a superheater is added to superheat the steam before entering the HP turbine, a reheater is used to replace the MSRs by using the waste heat exhausted from superheater, and an economiser is provided to replace the LP feedwater heater.

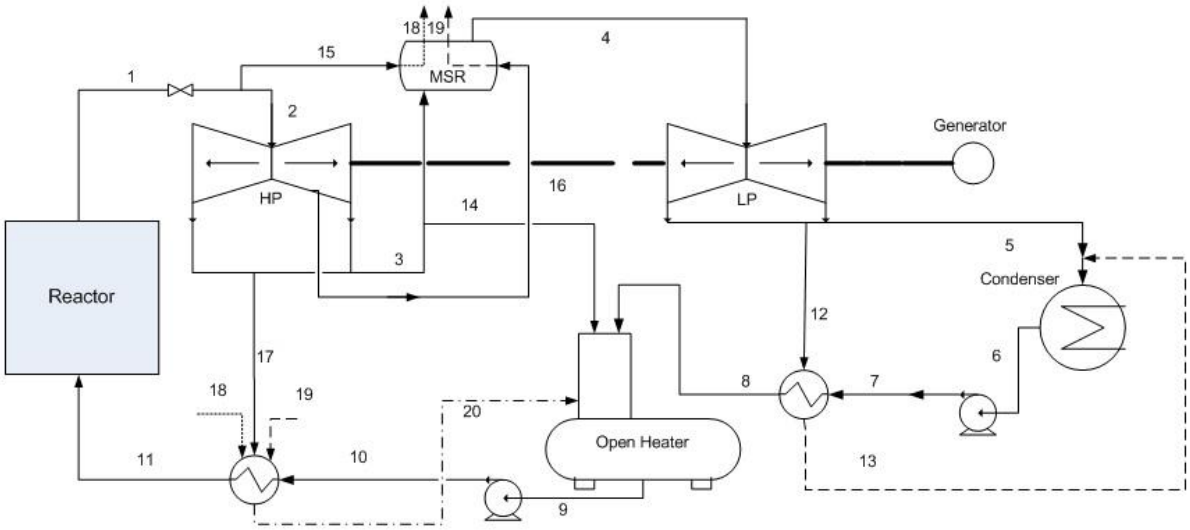

Fig. 3.5 Simplified model for DMS steam cycle.

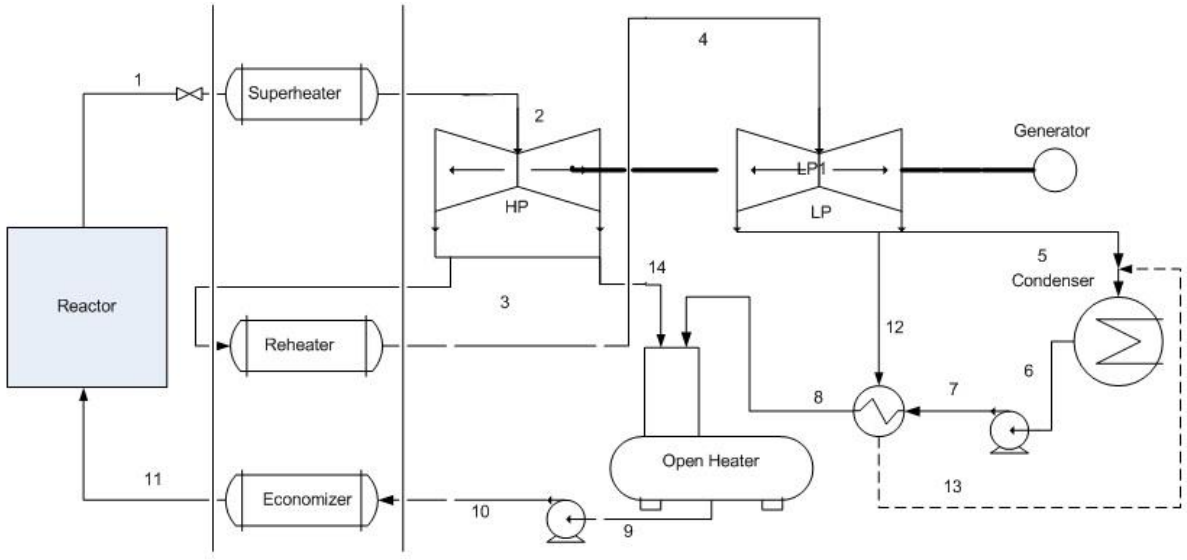

Fig. 3.6 Simplified model for DMS steam cycle with gas fired superheaters.

The thermodynamic performances of these two BWR systems, with and without gas fired superheaters, are summarised in Table 3.5. For the cases with superheaters, the HP turbine inlet

temperatures were set to be 600 ^{o}C. It is shown that, by having the gas fired superheater, both ESBWR and DMS power conversion cycle efficiency could be increased, allowing them to be comparable to those of stand-alone gas turbines. It can also be observed that the addition of the superheaters would increase the maximum electric power of the ESBWR to approximately 2.8 GWe, which is higher than the largest commercially existing steam turbine. Therefore, with an assumption that the total system power will be constrained by the size of the available steam turbines, a smaller reactor such as the DMS would be a more plausible route for a hybrid nuclear system with added superheater. This preliminary study also found that, by combining the DMS with gas fired superheaters, the NPP would be able to reduce its operational load down to 68% just by adjusting the external heat given to the superheaters. Fig. 3.7 shows the combined system specifications at various operational loads. It is shown that the HP turbine inlet temperature can be kept at its maximum value (600 ^{o}C) down to about 88% load by reducing the reheat temperature only. However, in order to reduce the load further below 88%, the HP turbine inlet temperature needs to be reduced as well, which explains the sudden change of slope in Fig. 3.7.

Table 3.5 Thermodynamic Performance of Large and Small BWRs Coupled with Gas Fired Superheater

Parameter	**ESBWR**		**DMS**	
	No Superheater	**With Superheater**	**No Superheater**	**With Superheater**
HP turbine inlet temp. (^{o}C)	284	600	287	600
$W_{HP\ turbine}$ (MWth)	579.4	1,157.4	106.9	204.6
$W_{LP\ turbine}$ (MWth)	1,046.4	1,738.5	187.6	389.9
W_{tot} (MWth)	1,625.8	2,895.9	294.5	594.5
Total electric power (MWe)	1,593.3	2,838.0	288.6	582.6
Nuclear heat (MWth)	4,503.9	4,503.9	840.0	840.0
Fossil heat required (MWth)	-	2,906.0	-	635.9
Total cycle efficiency (%)	35.38	38.30	34.58	39.99

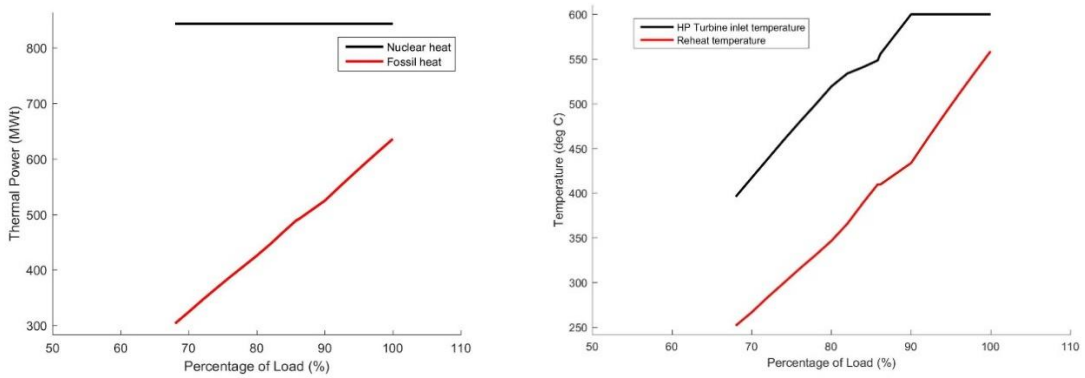

(a) (b)

Fig. 3.7 Specifications of the DMS combined with gas fired superheaters at various operational loads: (a) thermal power; (b) superheated steam temperature.

3.3 Summary of the Preliminary Investigation

This preliminary investigation is able to identify the benefit of having external superheaters installed with LWRs. The study on both PWR and BWR systems shows that the hybrid LWRs would have improvements in their power conversion cycle efficiencies regardless of the size of the reactors. In terms of the benefit to PWR systems, the thermal efficiency of the AP1000 can be improved from 31% to 37% by installing a gas fired superheater, a reheater, and an economiser. When this concept is applied to the SMR, the hybrid system would give a thermal efficiency improvement of approximately around 3%. In terms of its benefit to BWR systems, the hybrid plant would give approximately 3-5% improvement in the system's thermal efficiency. Although this might not seem to be a significant increase, it can potentially improve the competitiveness of nuclear energy compared to fossil fuelled power plants, which have thermal efficiencies of roughly 36-48%.

It is also found that, by having external superheaters, the hybrid NPPs are able to reduce their load to some extent (around 65% in PWR and 68% BWR) without perturbing the reactor power. It should be noted that, in this preliminary investigation, the load-following operation was done by changing the steam operating temperature before entering the steam turbines, keeping the mass flow rate of the steam at a constant value. However, this might not be the most ideal way for load-following in the steam cycle. The changes in turbine inlet temperature would cause thermal shock to the turbine blades to a certain degree, and, thus, the changes in steam temperature at each load condition might negatively affect the performance of the steam turbine. Therefore, the focus on load-following operation in the next stage of the study is

devoted towards finding a load-following scheme which relies on steam flow rate perturbation, keeping the steam operating condition fixed at any given point on the steam cycle.

Chapter 4: Comparative Study on Operating Pressure

This chapter provides a comparative study on the SMBWR performance operating at different pressure. This study includes neutronics, thermal-hydraulics, and steam cycle thermodynamic analysis of the SMBWR at the selected operating pressure values. As mentioned previously in Chapter 1, the purpose of this study is to quantify the extent of potential benefits from increasing the operating pressure of the SMBWR. The selected values of operating pressure considered in this study range between 6.5 and 10.0 MPa. The feedwater inlet temperature is varied in order to maintain a constant core subcooling enthalpy ($\Delta H_{Subcooling}$) as discussed earlier.

4.1 Neutronic Performance

4.1.1 Benchmark of the neutronic tools

It is mentioned in the previous chapter that the neutronic tools used for the neutronic analysis are the WIMS-PANTHER package. WIMS is a lattice code which has been proven to accurately model the neutronic behaviour of PWR cores and PANTHER was originally developed to model the whole core performance of PWR and Advanced Gas-cooled Reactor (AGR) plant in the UK. Since the capability of modelling a BWR has been recently added to the codes, a benchmark study of the WIMS package with the continuous energy Monte Carlo reactor physics code Serpent **[47]** was carried out to gain confidence in the model. A 2-dimensional assembly benchmarking of WIMS and Serpent was done using the fuel assembly configuration shown in Fig. 2.2 for 3 different historical coolant densities. The assembly power for the 2D-assembly configuration is approximately 11,574 W. The resonance self-shielding calculation in WIMS uses the equivalence theory approach, with subgroup treatment for U^{235} and U^{238}, and the Method of Characteristics (MOC) is used to obtain the neutron transport equation solution. The Serpent model for the 2D-geometry was created with 3 million neutron histories (5,000 source neutrons per cycle, 600 active cycles, and 100 inactive cycles). The 2D-benchmark result is displayed in Fig. 4.1. The reactivity differences shown in Fig. 4.1 are calculated from Eq. (4-1). By comparing the depletion behaviour of the WIMS and Serpent simulations for the 2-dimensional assembly, it is shown that there are some discrepancies between WIMS and Serpent especially in the beginning of life which become smaller with the

burnup. This behaviour suggests that the main cause of this discrepancy is related to a difference between WIMS and Serpent in modelling the depletion of Gadolinium poison.

$$\Delta\rho\ (pcm) = \frac{(k_{inf,WIMS} - k_{inf,Serpent})}{k_{inf,WIMS} * k_{inf,Serpent}} * 10^5 \qquad (4\text{-}1)$$

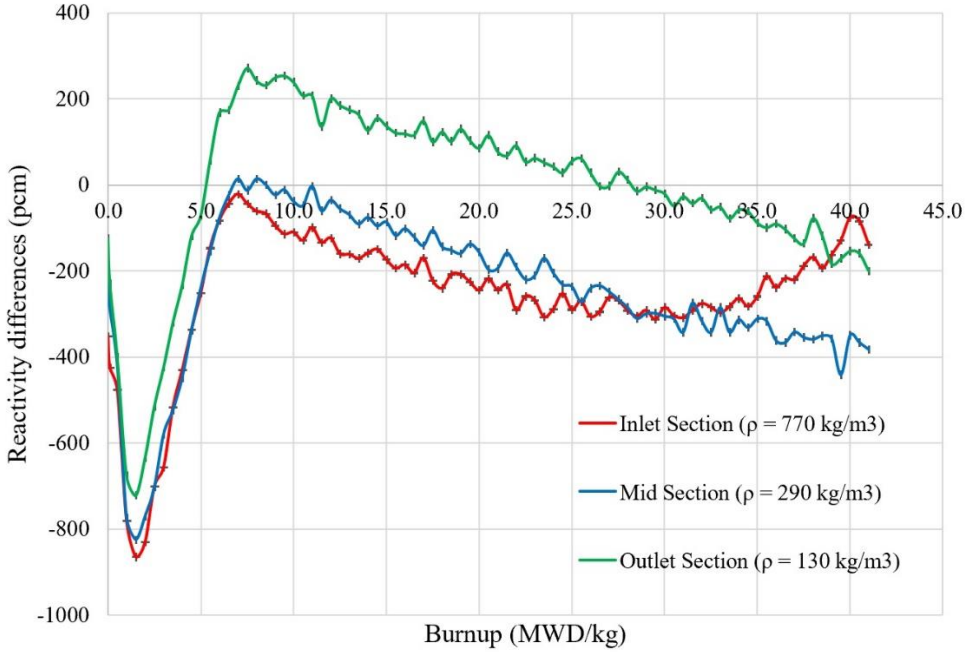

Fig. 4.1 Benchmark 2D-assembly level of WIMS vs Serpent.

In a 3D-assembly benchmark, it is important to note that the fuel burnup in a specific node location in the core is accumulated under operating conditions that could be significantly different from the core averaged value. This is especially important for BWRs since the coolant density changes drastically as it flows through the reactor core channels. It is therefore important to account for the local spectral history effect in modelling a BWR assembly. As mentioned in Chapter 2, the cross-section data library is generated in WIMS by depleting the fuel with 3 historical coolant densities and a set of instantaneous branches, in order to account for the local spectral history effect. The perturbed cases for the cross-section data library branches include 3 different fuel temperatures, 5 different coolant densities, and 2 coolant temperatures. Another method which could be used for better capturing the spectral history effect is the microscopic depletion method. The method accounts for the spectral history effect by calculating the actual concentrations of important nuclides in each node and explicitly adding their contributions to the homogenised macroscopic absorption and fission cross-sections **[48]**. Fig. 4.2 shows the difference between depletion behaviour of the 2×2 cluster of

3-dimensional SMBWR fuel assemblies modelled with Serpent and PANTHER. In this 3D-benchmark, the length of the fuel assembly is set to 2.7 m and the assembly power is set to 3.125 MW. In both Serpent and PANTHER, 10 axial nodes are defined, a reflective boundary condition is set for the radial direction and a void boundary condition in the axial direction. No thermal-hydraulics calculation is done in PANTHER and the coolant densities defined in the Serpent input are set to mimic PANTHER coolant densities. The Serpent model was created with 16 million neutron histories (20,000 source neutrons per cycle, 800 active cycles, and 100 inactive cycles). It can be observed from Fig. 4.2 that the combination of multiple historical densities and microscopic depletion helps in reducing the discrepancies between the 3D-model simulation in Serpent and PANTHER.

By comparing the axial power distribution and axial burnup distribution, as shown in Fig. 4.3 and Fig. 4.4 respectively, it can be concluded that PANTHER could model BWR cores with accuracy sufficient for the purposes of this study. Both Fig. 4.3 and Fig. 4.4 display selected burnup points which represent the beginning of life (BOL), middle of life (MOL), and end of life (EOL). Although the discrepancy in reactivity increases with the depletion towards the end of life, the resulting reactivity differences are still within tolerable limits. This is another indication that the SMBWR could be representatively modelled by the selected tools.

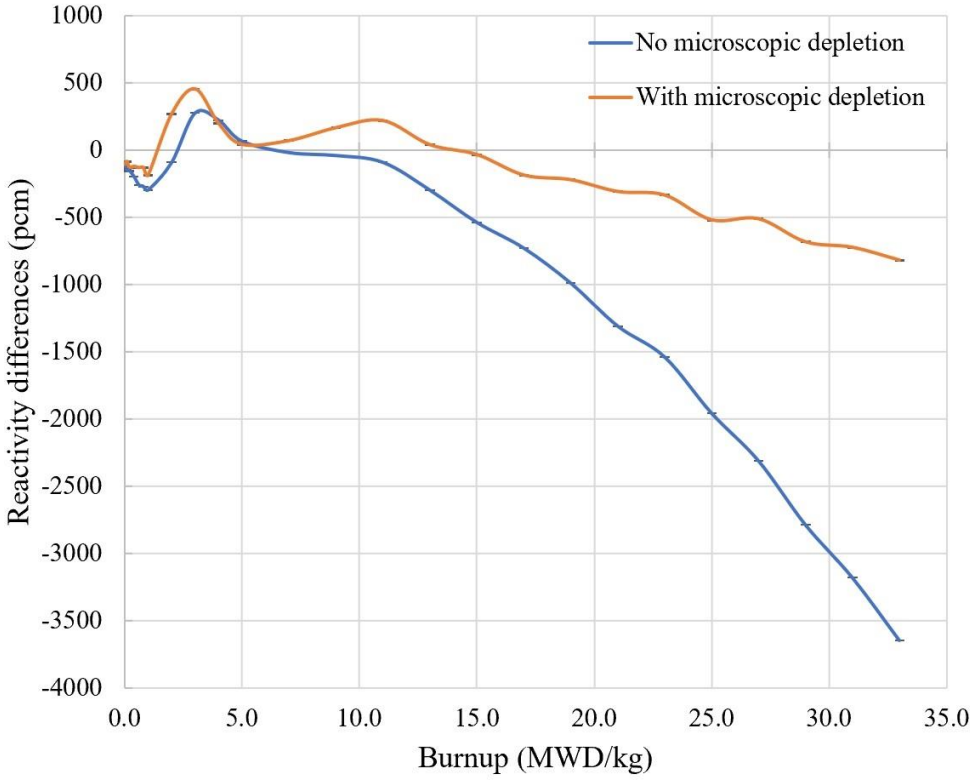

Fig. 4.2 Benchmark 3D-assembly level of PANTHER vs Serpent.

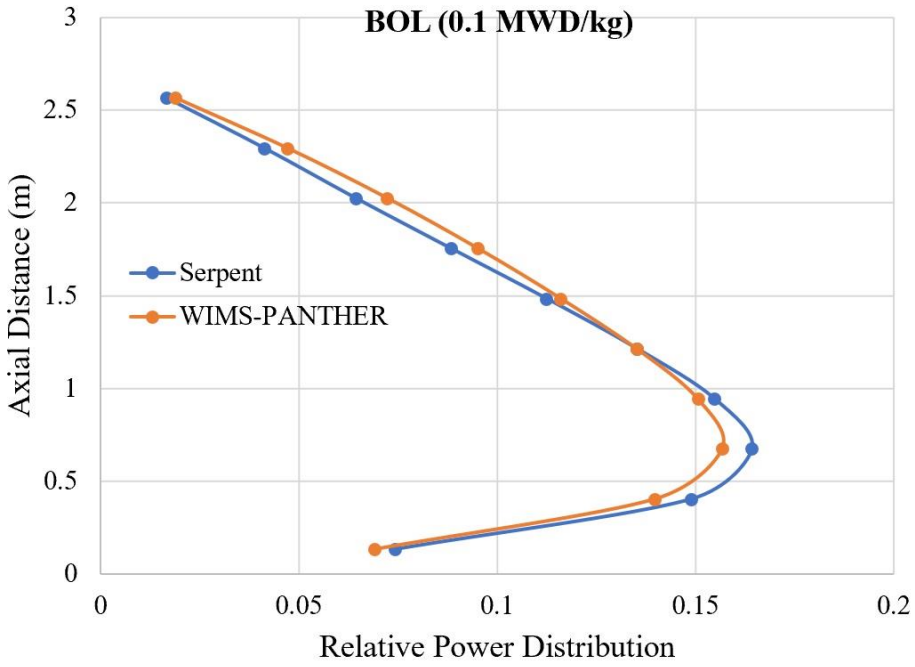
BOL (0.1 MWD/kg)
Axial Distance (m)
Relative Power Distribution
Serpent
WIMS-PANTHER
0
0.5
1
1.5
2
2.5
3
0
0.05
0.1
0.15
0.2

(a)

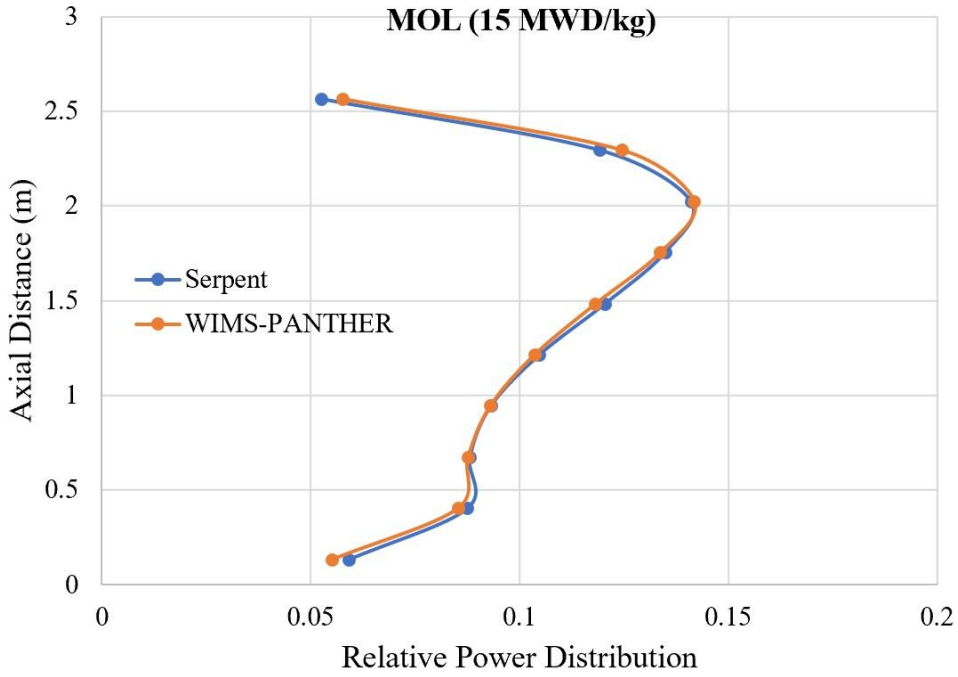
MOL (15 MWD/kg)
Axial Distance (m)
Relative Power Distribution
Serpent
WIMS-PANTHER
0
0.5
1
1.5
2
2.5
3
0
0.05
0.1
0.15
0.2

(b)

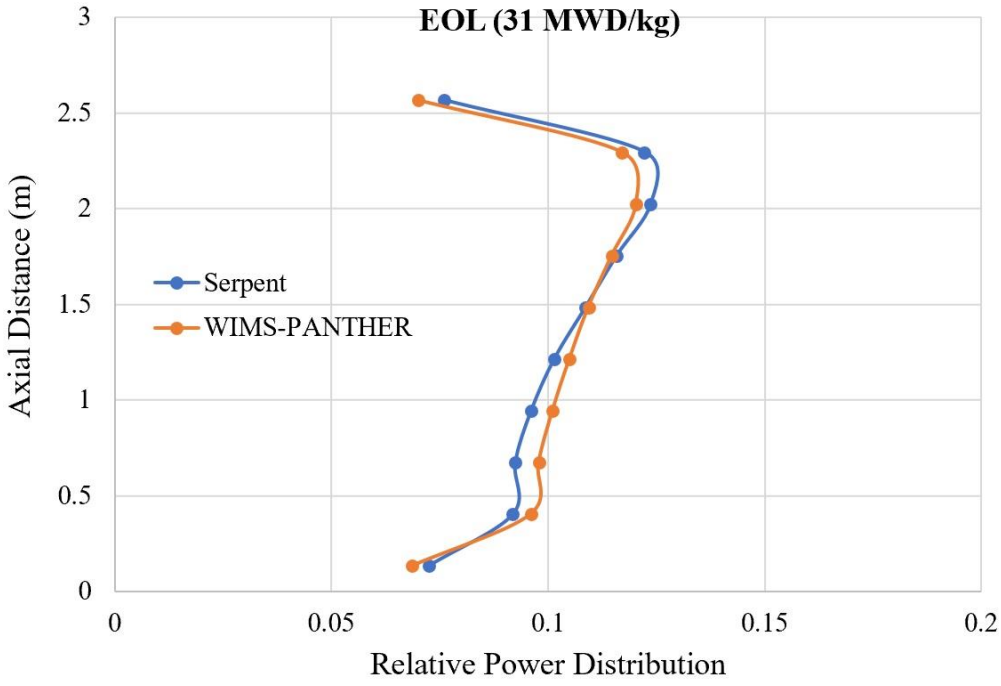

(c)

Fig. 4.3 Relative power distribution of 2×2 SMBWR assemblies at the: (a) BOL; (b) MOL; (c) EOL.

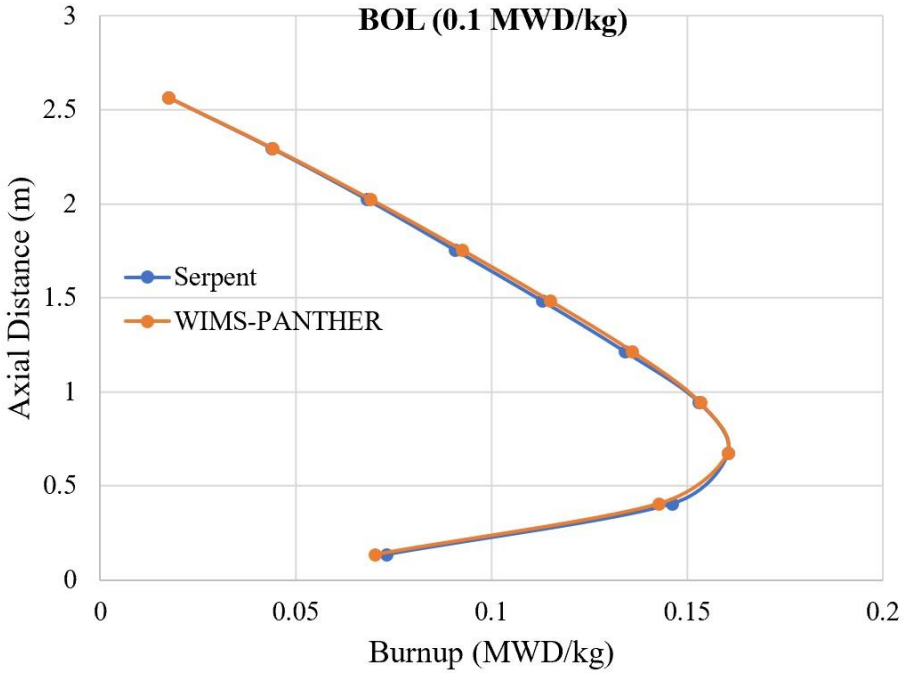

(a)

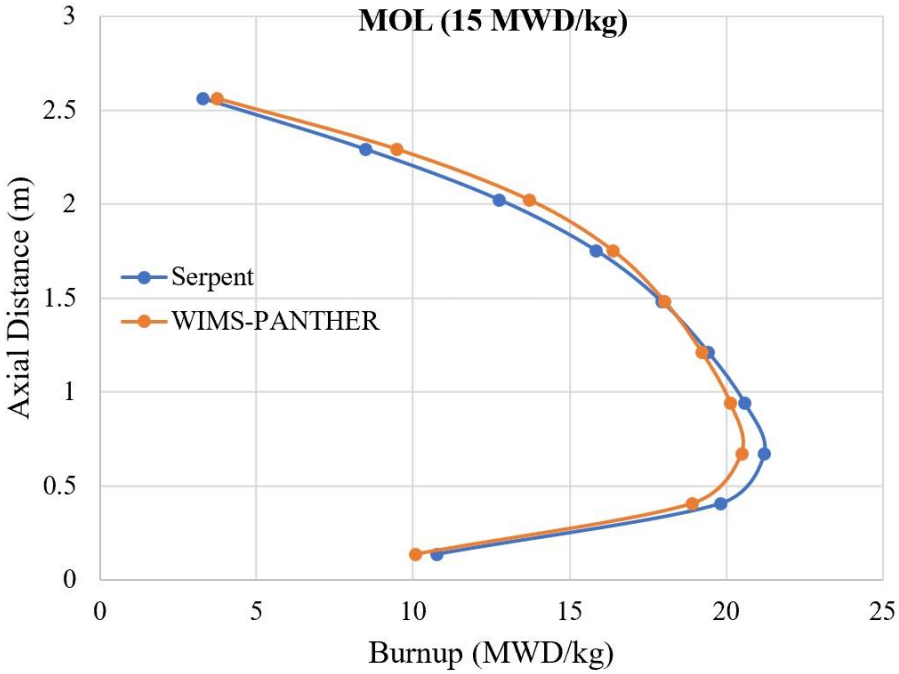

(b)

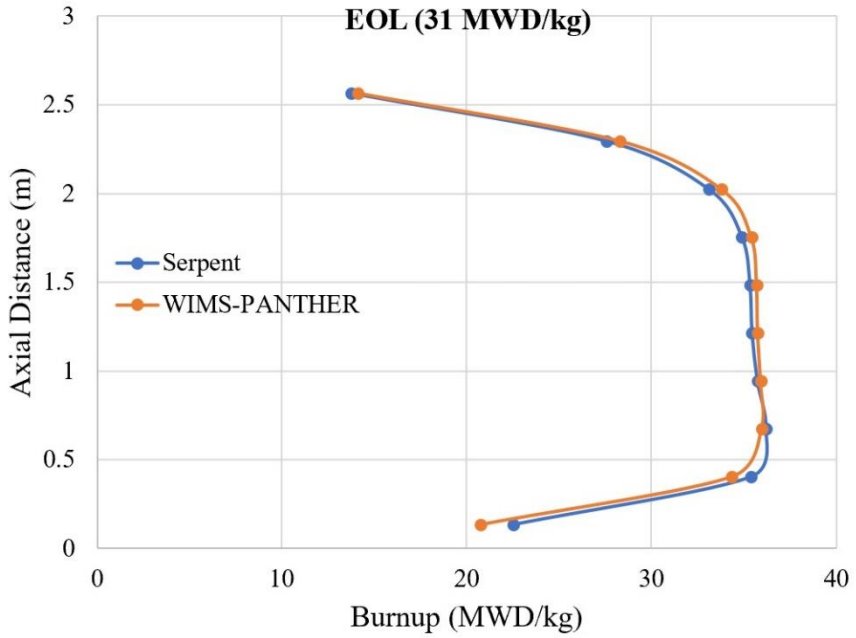

(c)

Fig. 4.4 Axial burnup distribution of 2×2 SMBWR assemblies at the: (a) BOL; (b) MOL; (c) EOL.

4.1.2 Neutronic results for SMBWR at various operating pressures

The neutronic performance of 2×2 SMBWR fuel assemblies with reflective radial and vacuum axial boundary conditions at four different system pressure values (65, 71.7, 80, and 100 bar) were modelled in PANTHER. The reactivity differences of each case to the reference

case of 71.7 bar (standard BWR operating pressure) are shown in Fig. 4.5, while the reactivity feedback coefficients are displayed in Fig. 4.6. The Doppler Coefficient (DC) was calculated by a slight perturbation in assembly power. The Moderator Temperature Coefficient (MTC) was calculated using a temperature perturbation with constant density, while the Coolant Void Coefficient (CVC) was calculated with a density perturbation. From Fig. 4.5, it can be concluded that the depletion behaviour is not affected significantly by the change in the system pressure as the reactivity differences of each case to the reference case are negligible, within 200 pcm of each other. Fig. 4.6 shows that the value of MTC changes from slightly negative at BOL to slightly positive at EOL. However, this should not be a problem because CVC is an order of magnitude higher and always negative throughout the depletion, and, thus, their combined effect will always be negative. In a BWR, throughout the length of the fuel assembly, the coolant is most likely be either in the liquid phase near the saturated condition or at the two-phase equilibrium. This means that a change in coolant temperature or enthalpy would always be immediately followed by a change in the coolant void condition, and, thus, the effects of the MTC and the CVC are inseparable. The MTC increases over the burnup due to plutonium build-up during the fuel depletion. One of the effects caused by an increase in moderator temperature and lower density is higher neutron leakage due to reduced moderation and therefore generally smaller cross-sections. The presence of higher quantities of plutonium causes MTC to be slightly positive as the spectrum becomes slightly harder. In terms of DC and CVC, the presence of Gd_2O_3 causes both DC and CVC to be more negative. Generally, as both fissile material and the poison deplete, the neutron spectrum softens and the reactivity feedbacks become more negative. Since the poison depletes faster than the fuel, the reactivity feedbacks start to rise due to the reduction in the ratio of poison compared to fuel. When the poison is fully depleted, the reactivity feedbacks start to decrease again due to the change in fuel composition, mainly the depletion of fissile material.

By comparing the reactivity feedbacks at various system pressure values, as shown in Fig. 4.6, it can be observed that the change in system pressure does not cause significant changes in the reactivity feedbacks throughout the cycle. A noteworthy phenomenon is shown in the void reactivity feedback behaviour. In the presence of gadolinium poison, the coolant void feedback is less negative at higher pressure. However, when the poison is fully depleted, the coolant void coefficient at higher pressure becomes more negative. The presence of gadolinium altered this tendency, as it competes with the fissile material in absorbing thermal neutrons. Although the reactivity feedbacks change slightly depending on the system pressure, the changes are not significant and the reactivity feedbacks remain negative, which is required to

ensure reactor safety and stability. Therefore, it can be concluded that operating SMBWR between 6.5 and 10 MPa will not have significant effect on its neutronic performance.

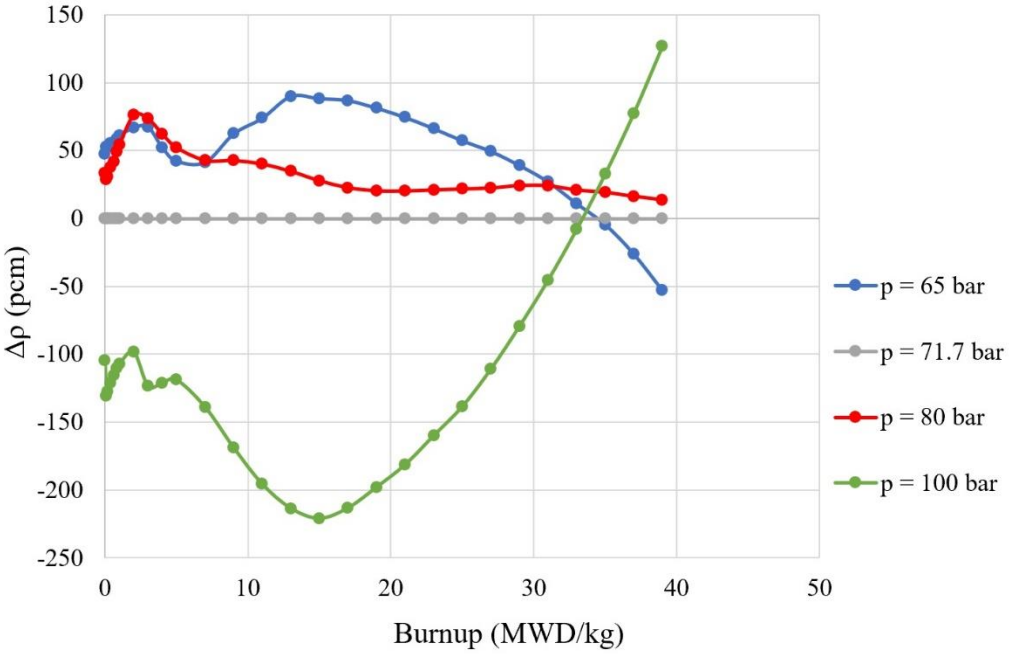

Fig. 4.5 Reactivity differences to the reference case (p = 71.7 bar).

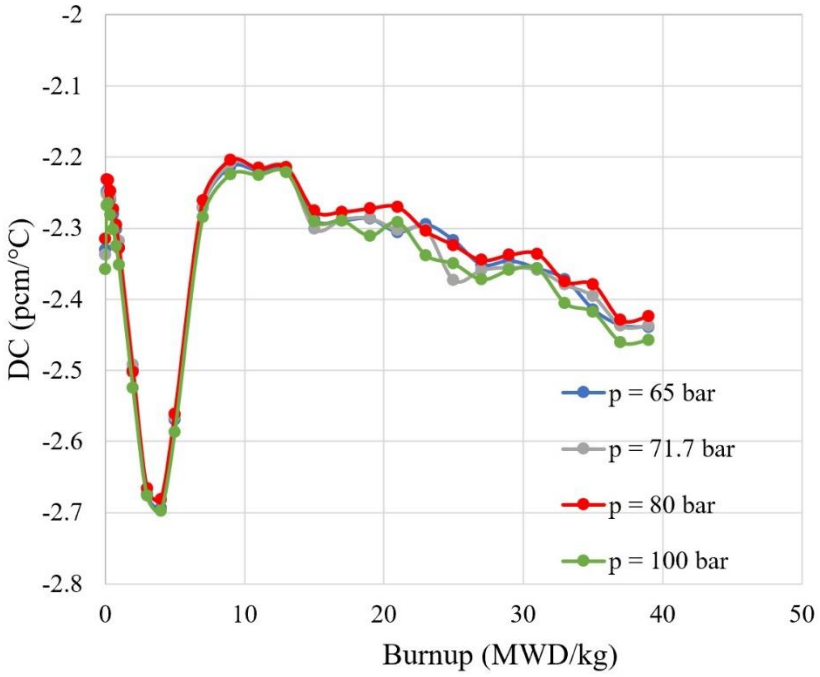

(a)

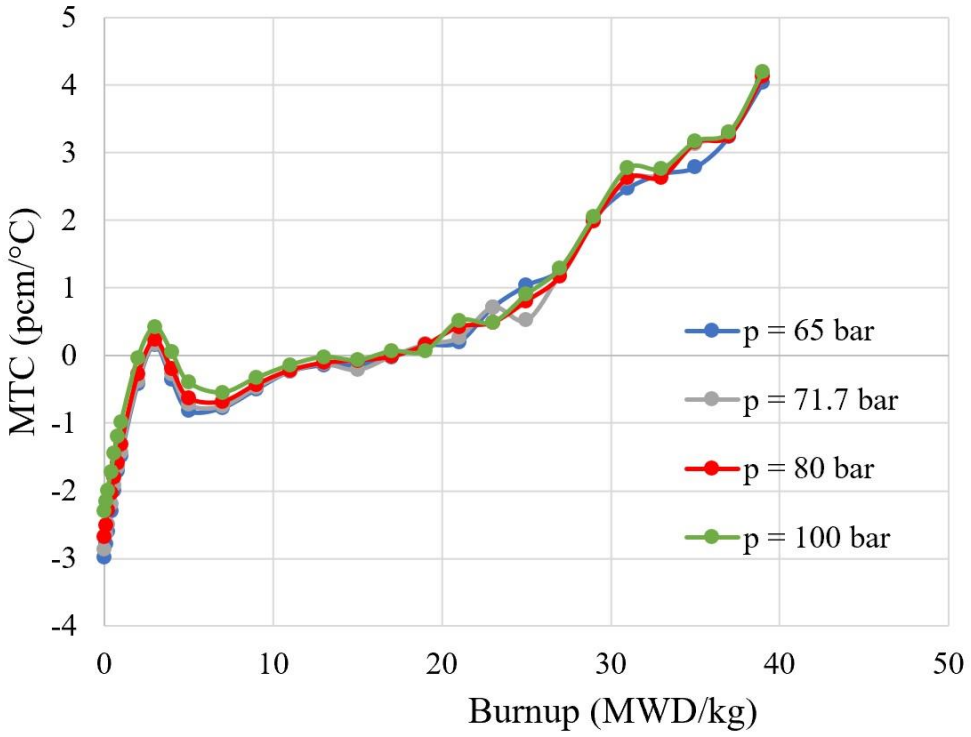

(b)

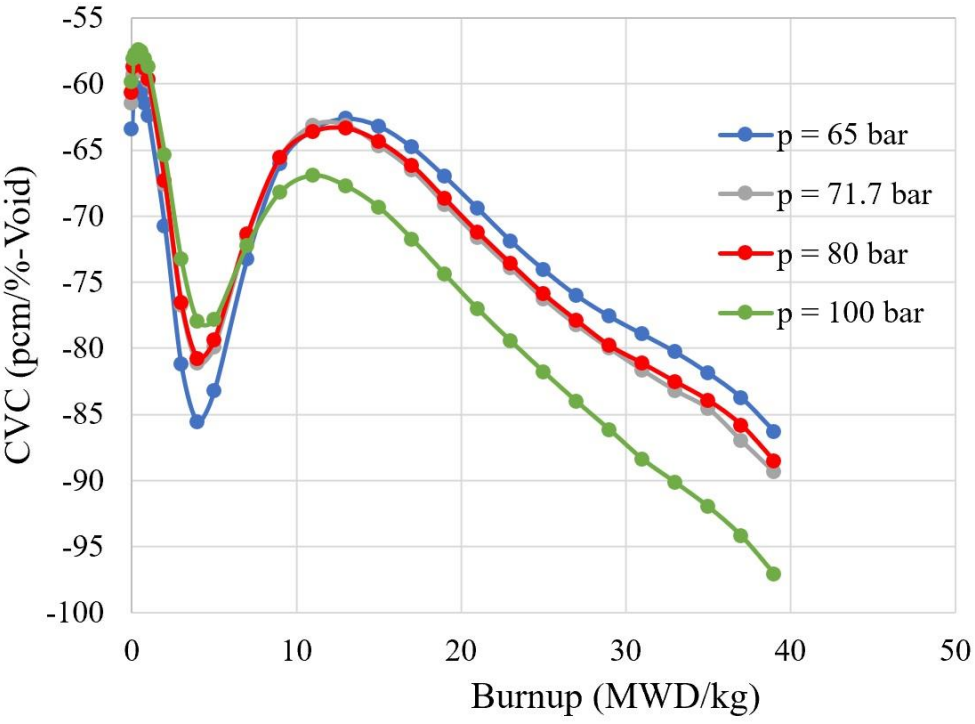

(c)

Fig. 4.6 Reactivity feedbacks for 2×2 SMBWR assemblies at selected system pressures: (a) Doppler Coefficient; (b) Moderator Temperature Coefficient; (c) Coolant Void Coefficient.

4.2 Thermal-hydraulic Performance

In order to investigate the thermal-hydraulic performance of the SMBWR core, the fuel assembly is modelled in COBRA-EN, while the recirculation loop inside the reactor vessel is modelled in MATLAB. The loop model is a tool to calculate the pressure drop in all components inside the BWR recirculation loop and solves the momentum balance analytically to find the minimum required height for the system to be able to sustain natural circulation. The core thermal-hydraulic performance was modelled with COBRA-EN, which is a sub-channel analysis code developed specifically for this purpose. Fig. 4.7 shows the core axial void distribution for the ESBWR calculated by both the loop model and COBRA-EN compared to the reference value **[49]**. As mentioned in Chapter 2, the two-phase flow model implemented in the loop analysis is based on a drift flux model, where the void fraction is calculated by the Armand-Treschev correlation **[36]**. In contrast, the correlation that was set to model the void-quality relation in COBRA-EN was the Zuber-Findlay correlation. This correlation was used in combination with the Levy subcooled boiling model correlation as suggested by the user guide **[29]**. The reference ESBWR value was obtained by using TRACG, which implements a multi-dimensional two-fluid model **[49]**. It is demonstrated in Fig. 4.7 that the core void distribution of the ESBWR modelled by COBRA-EN reasonably closely agrees with the reference value, while the loop model shows a small discrepancy compared to the reference value. The difference in the predicted core pressure drop between COBRA-EN and the loop model is approximately 1.7 kPa which is small and quite negligible. This is another reason why COBRA-EN is used to perform the channel analysis inside the core. Although the core void distribution from the loop model shows small discrepancies with the reference value, it predicts a similar trend and the core exit void fraction predicted by the loop model is close to the reference value. It is obvious that the observed discrepancies are most likely due to the different correlations used to model the void-quality relation. The facts that the pressure drop calculation does not show significant difference to the COBRA-EN result and that the core is only one component of the circulation loop where the heat source is provided, provide confidence that the loop model for solving the momentum balance in the SMBWR vessel has sufficient accuracy for the purposes of this study.

In modelling the SMBWR, both COBRA-EN and the loop model were provided with the axial power distribution calculated by PANTHER. It is important to capture the realistic power distribution effect because both single-phase and two-phase flow regimes occur inside the reactor core. As discussed previously, the two-phase flow has a higher pressure drop than

single-phase flow, and thus failing to represent the power distribution inside the core with reasonable accuracy will affect the thermal-hydraulics performance of the model as the boiling length will be affected. A schematic diagram representing the interactions of all the used models is shown in Fig. 2.1. As has also been mentioned in Chapter 2, the thermal-hydraulic boundary conditions set for the operating pressure comparative study are constant primary coolant flow rate and constant core subcooling enthalpy ($\Delta H_{Subcooling}$).

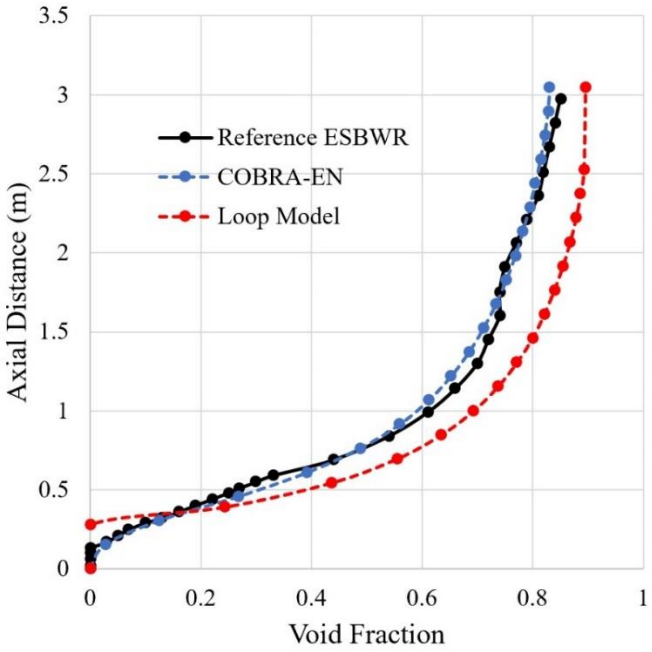

Fig. 4.7 Comparison of the T-H models in capturing the ESBWR core void distribution.

4.2.1 Core two-phase flow characteristic and thermal safety limit

The effect of operating pressure on axial void fraction and flow quality at the beginning of life, middle of life, and the end of life are displayed in Fig. 4.8 and Fig. 4.9 respectively. The results obtained in Fig. 4.8 and Fig. 4.9 show that, as the operating pressure is increased, the flow quality is increased, which is expected as the difference between saturated liquid and saturated vapour enthalpy becomes smaller with pressure. Thus, for the same channel power, a larger fraction of coolant will be converted to steam at higher pressure. However, the axial distribution of void decreases with the increasing operating pressure. This is also expected because void fraction represents the relative volume of steam in the mixture rather than mass fraction. As the system pressure is increased, the saturated liquid density is decreased but the saturated vapour density is increased and hence the void fraction profile exhibits the exact

opposite trend to that of the flow quality profile. The density behaviour can be clearly observed in Fig. 4.10.

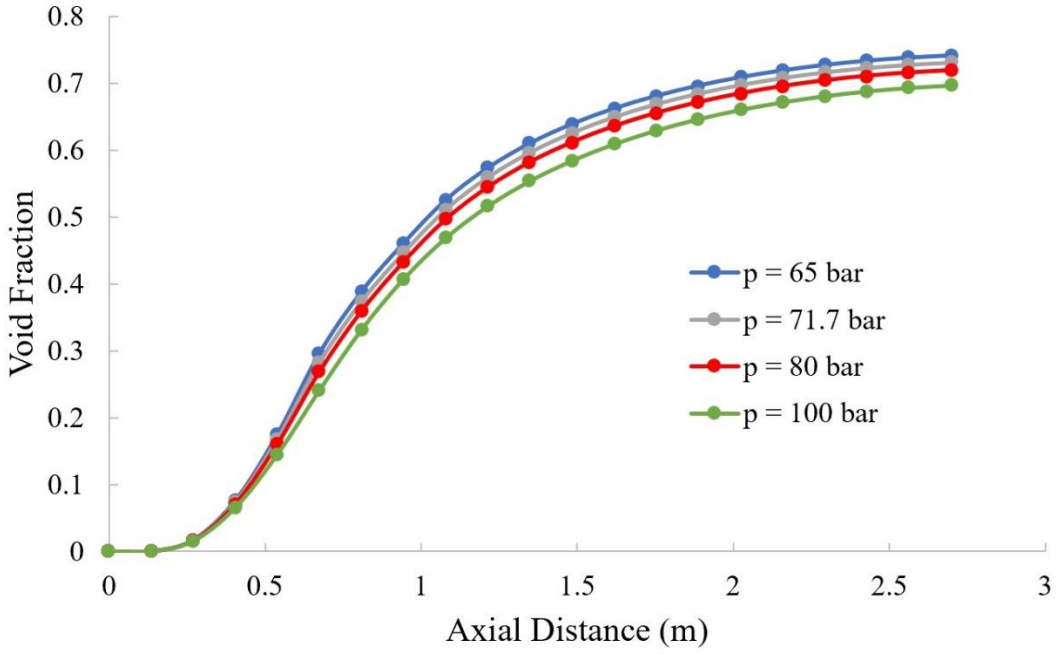

(a)

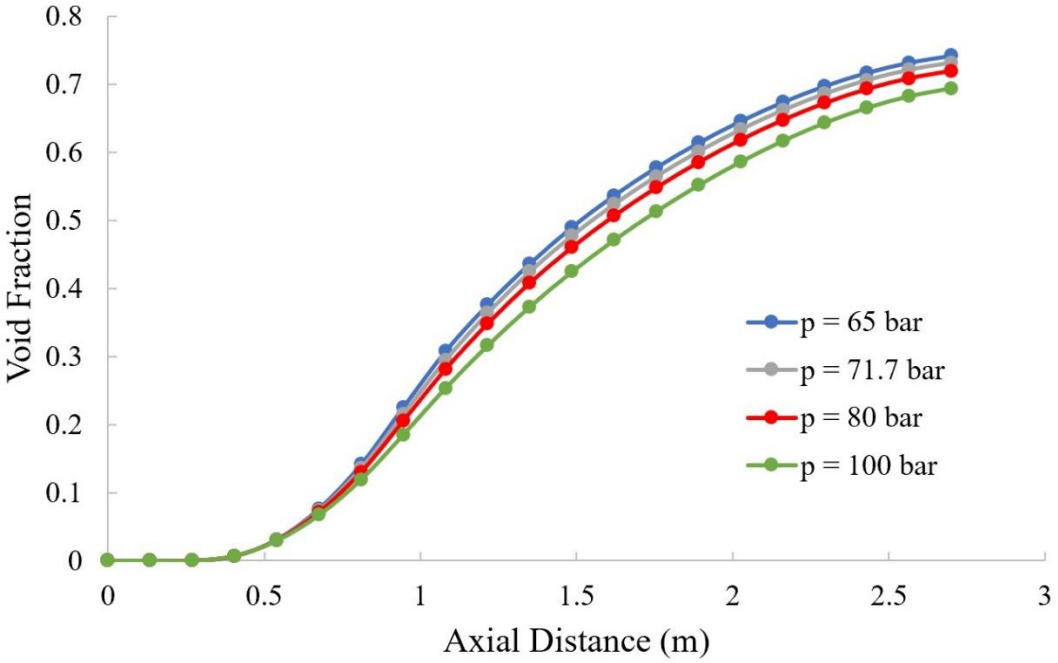

(b)

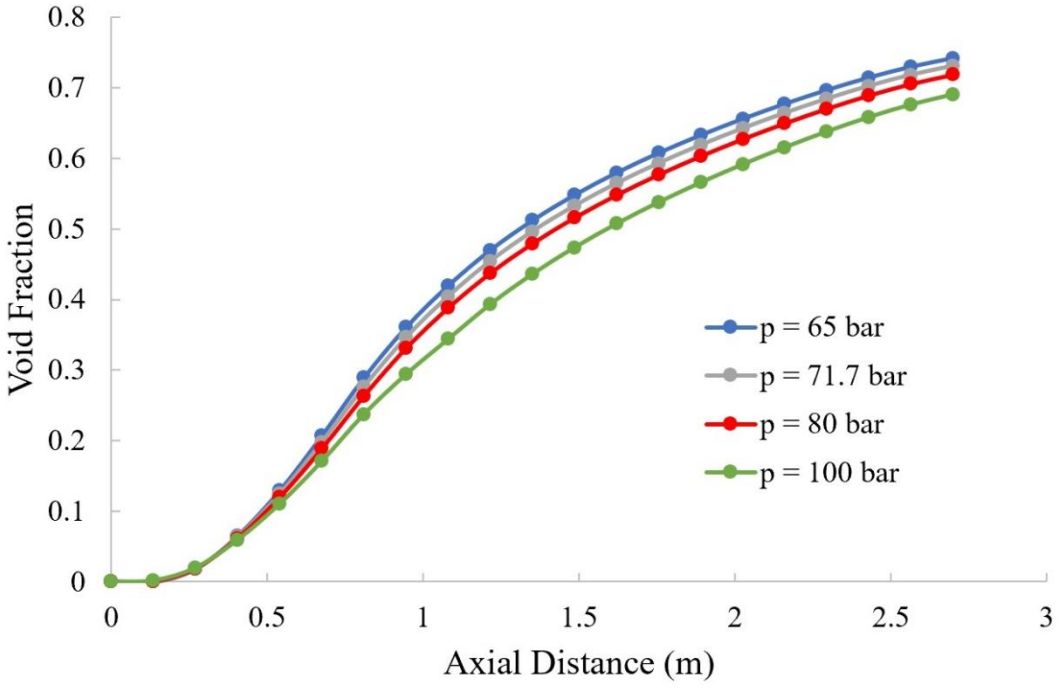

(c)

Fig. 4.8 Axial void distribution of a SMBWR fuel assembly at selected system pressures at the: (a) BOL; (b) MOL; (c) EOL.

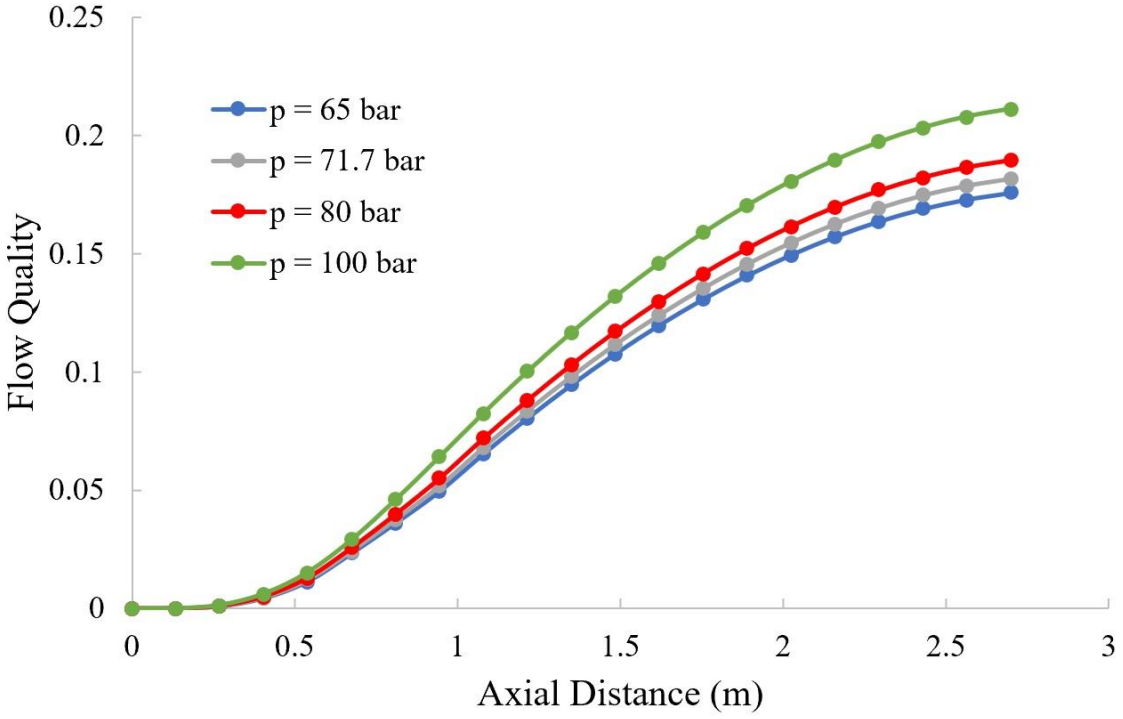

(a)

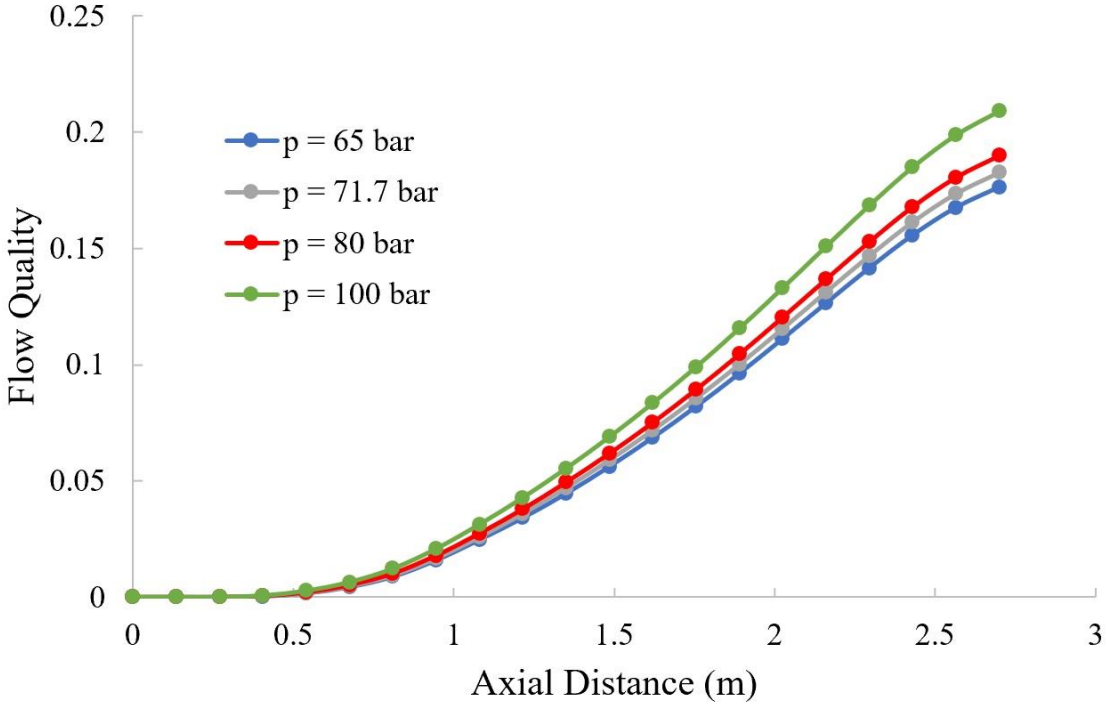

(b)

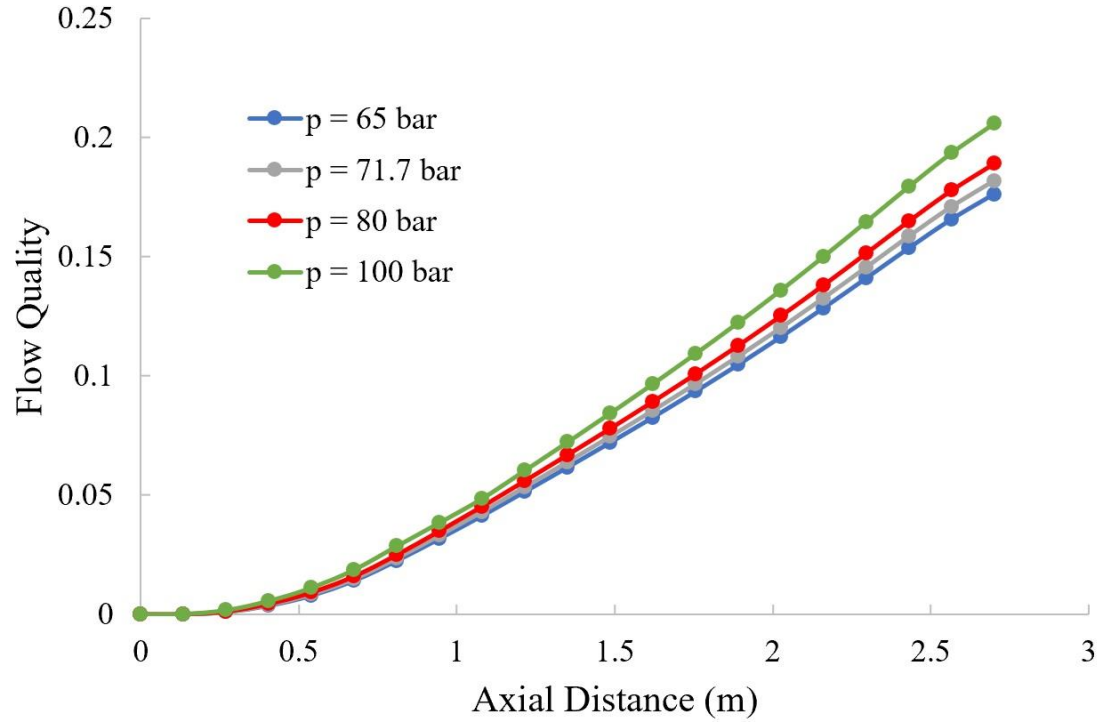

(c)

Fig. 4.9 Flow quality distribution of SMBWR fuel assembly at selected system pressures at the: (a) BOL; (b) MOL; (c) EOL.

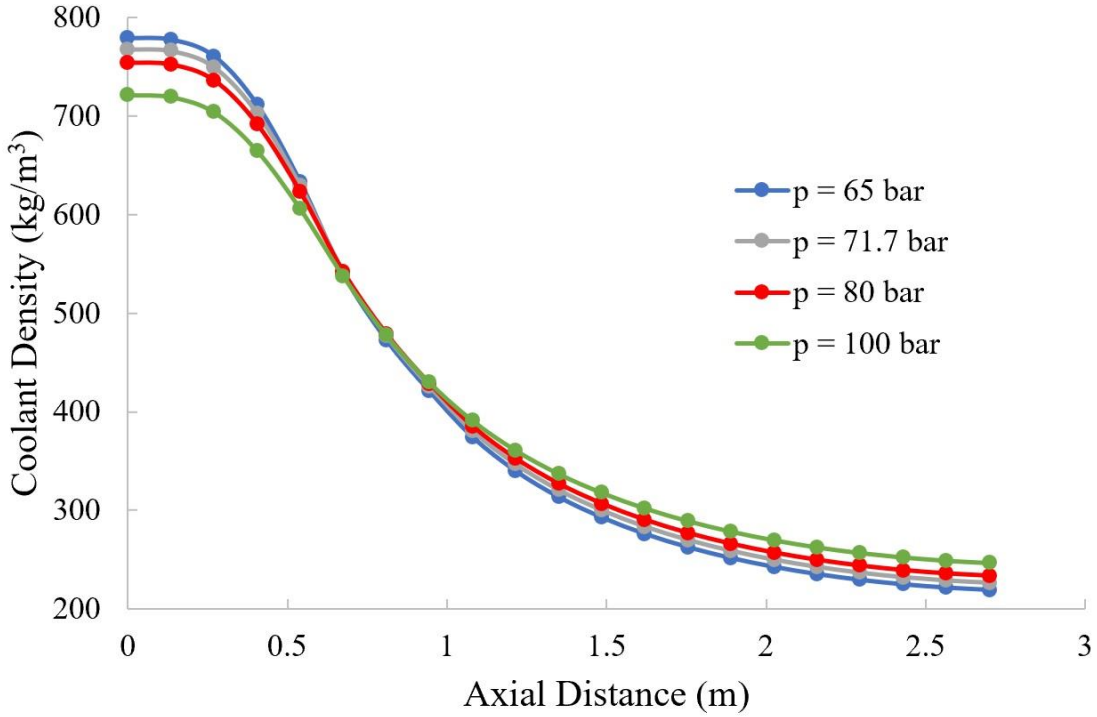
Coolant Density (kg/m3)
800
700
600
500
400
300
200
0
0.5
1
1.5
2
2.5
3
Axial Distance (m)
p = 65 bar
p = 71.7 bar
p = 80 bar
p = 100 bar

(a)

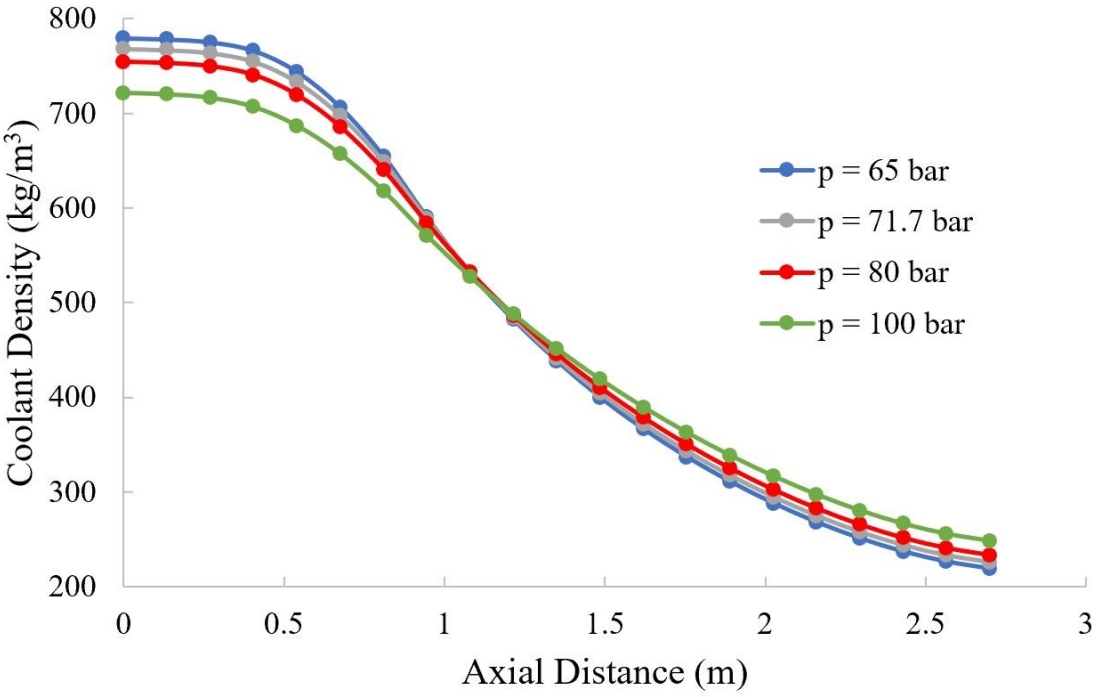
Coolant Density (kg/m3)
800
700
600
500
400
300
200
0
0.5
1
1.5
2
2.5
3
Axial Distance (m)
p = 65 bar
p = 71.7 bar
p = 80 bar
p = 100 bar

(b)

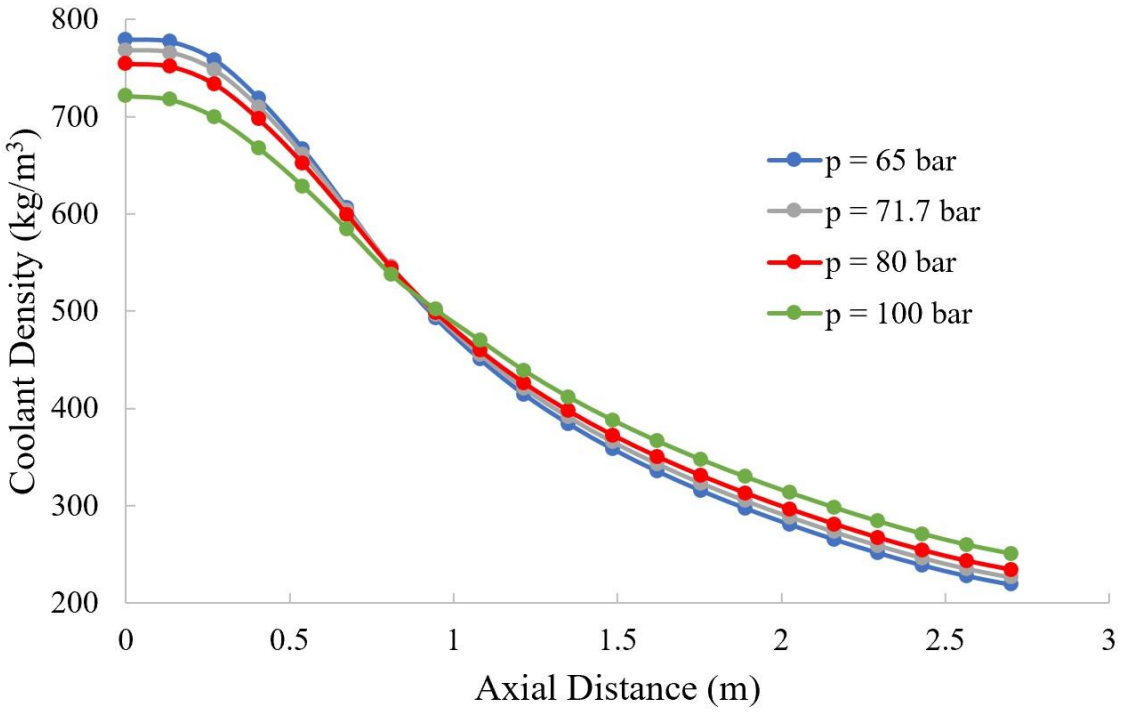

(c)

Fig. 4.10 Axial density profile of SMBWR fuel assembly at selected system pressures at the: (a) BOL; (b) MOL; (c) EOL.

Another key parameter for core thermal-hydraulics and reactor safety is the minimum critical power ratio (MCPR). Critical power ratio is defined as the ratio of the power at which the bundle channel dryout occurs, to the bundle power at the reactor condition of interest. The MCPR is known to be the most important BWR thermal limit. COBRA-EN has a number of methods of calculating critical power. The one selected for this study is proposed by General Electric **[50]** and known as the GEXL correlation. The GEXL correlation is a variation of the critical quality vs boiling length correlation and is based on experimental data obtained for the pressure range of 55 – 100 bar **[50]**. Since the GEXL correlation is developed and recommended by GE for their standard fuel geometry, it is appropriate to be used in this analysis which also uses a GE standard assembly design as a reference.

Fig. 4.11 shows the MCPR value for the reference SMBWR at various system pressure values, which is taken at the average channel power of 3.125 MW and assuming a fuel pin power peaking factor of 1.4. It can be observed from Fig. 4.11 that the MCPR has a slight dependency on axial power distribution as the distribution changes from BOL to MOL and to EOL. It is also shown that as the system pressure is increased, the MCPR is reduced, which is expected as the smaller difference between saturated liquid and saturated vapour enthalpy

would require less power to reach the boiling transition point. The lowest allowable MCPR for cases analysed with the GEXL correlation is 1.05 **[50]**, which provides 95% confidence that boiling transition will not occur. However, the thermal safety limit is usually set at a higher value (~1.2) to accommodate plant transient behaviour. At 100 bar, the MCPR value is slightly above 1.2, which is still within the safety margin although very close to the limit. However, it should be noted that these values are the results obtained with the average channel power. Thus, there is a possibility that these values would be reduced in a hot channel. Therefore, we could conclude that CPR is one of the parameters that would limit high-pressure operation in a BWR.

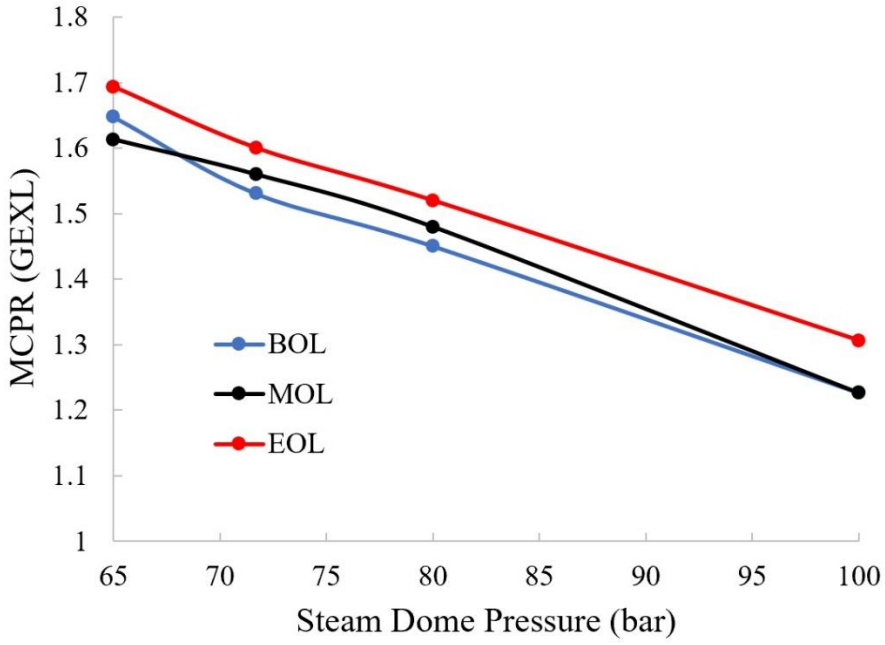

Fig. 4.11 MCPR value of the SMBWR at selected system pressures (channel power = 3.125 MW).

Another important safety characteristic of BWR systems is stability. It is known that both channel stability (thermal-hydraulic stability of a single channel) and core-wide stability (reactivity feedback stability) are affected by the ratio of pressure drop in single-phase and two-phase flow. Although the boiling length of all cases considered in this study remains approximately the same, changes in the operating pressure would change the density in both single-phase and two-phase flow regimes, thus altering the ratio of pressure drop in single-phase and two-phase flow. Therefore, the stability performance is another parameter that might limit the operating pressure. Understanding and quantifying this potential limitation is outside the scope of this thesis. However, it will need to be addressed in the future, in case higher pressure operation is found to be favourable in this study.

4.2.2 Natural circulation loop requirement

In order to rely on natural circulation of the coolant within the pressure vessel, the SMBWR has to be designed in such a way that the system buoyancy force is strong enough to counter its pressure losses. By modelling each component of the SMBWR vessel in the MATLAB programming environment, the total pressure losses in the recirculation loop can be calculated and, thus, the minimum chimney height required to produce enough buoyancy force for the system to operate with natural circulation can be found. Fig. 4.12 and Fig. 4.13 display the characteristic of the coolant flow (mass flow rate and temperature) inside the SMBWR vessel as the pressure is increased from 65 to 100 bar, which is modelled using the power distribution at the middle of life condition. Fig. 4.14 shows the core pressure drop of the SMBWR at various system pressures, while Fig. 4.15 shows the minimum chimney height required for the respective system to rely on natural circulation.

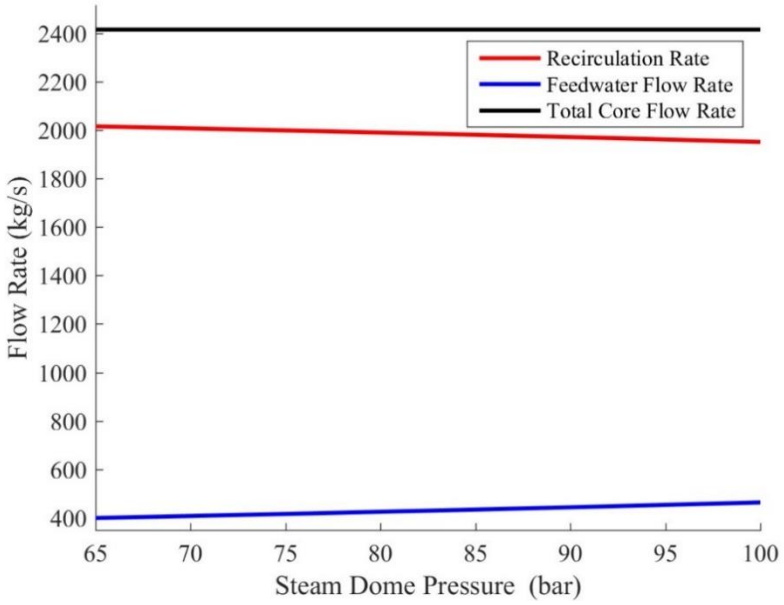

Fig. 4.12 SMBWR flow rate behaviour at various system pressures.

Fig. 4.12 and Fig. 4.13 show that the model of the recirculation loop meets the constraints set to make fair comparison of the pressure effect, which are keeping the core mass flow rate and boiling length constant in the core. As the pressure increases with a constant mass flow rate, the quality is increased because the enthalpy difference between saturated liquid and saturated vapour is getting smaller, as reported in the previous section. Thus, the recirculation rate is reduced, and more steam is taken from the SMBWR vessel to the steam turbines. The constant boiling length is achieved by keeping the inlet subcooling constant. As the saturation

temperature increases when the pressure is increased, a higher core inlet temperature is required to maintain constant inlet subcooling, and thus a higher feedwater temperature is required.

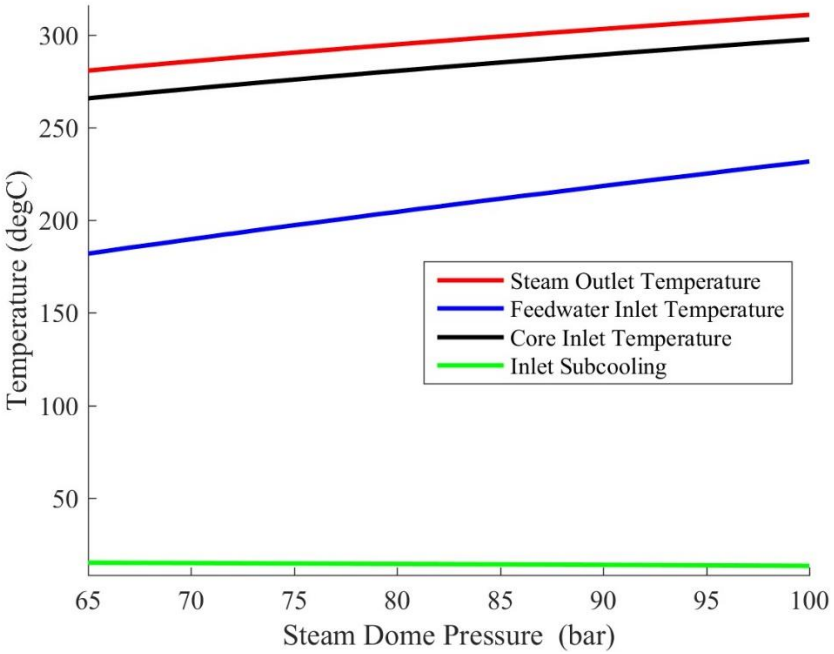

Fig. 4.13 Coolant temperature profile of the SMBWR at various system pressures.

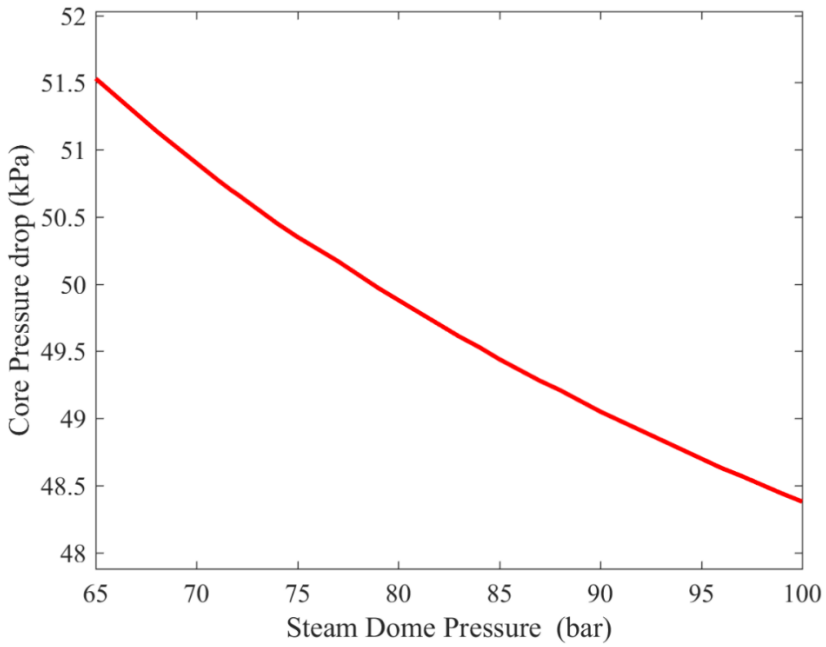

Fig. 4.14 Core pressure drop of the SMBWR at various system pressures.

It can be seen from Fig. 4.14 that, as the system pressure increases, the core pressure drop reduces. There are several phenomena that contribute to this result. In terms of single-phase

flow, the elevation pressure drop, which is the dominant factor, is proportional to the liquid density. As the operating pressure increases, in order to maintain the same flow rate and subcooled length in the core, the core inlet temperature needs to be increased at higher pressure. The higher pressure and temperature result in lower coolant density and thus the single-phase pressure drop is reduced. In terms of two-phase flow, the two-phase friction factor multiplier is inversely related to flow quality, as shown from Eq. (2-8) and, thus, it might contribute to the reduction in the two-phase flow pressure losses.

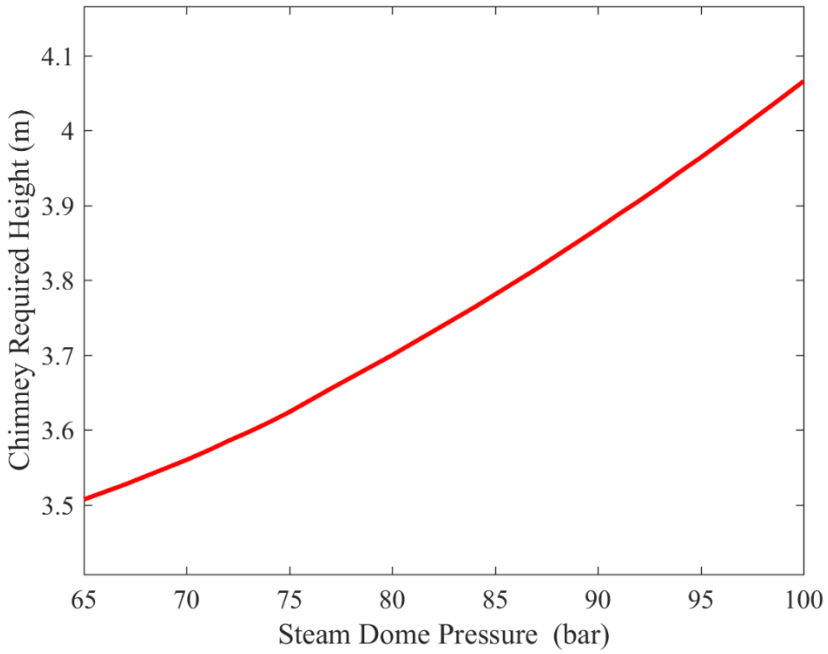

Fig. 4.15 Minimum chimney height required for the SMBWR at various system pressures.

In order to operate in a natural circulation mode, the total pressure losses within the loop must be compensated by the buoyancy force. By varying the system pressure, the total pressure losses within the loop will change, and so the minimum chimney height required to provide sufficient buoyancy force would also vary depending on the system pressure. Fig. 4.15 shows that, at higher pressure, the reactor requires a taller chimney in order to maintain natural circulation. This result is expected because, at higher system pressure, the difference between saturated liquid and vapour density is smaller. Thus, in order to fully depend on the buoyancy force to overcome the total pressure drop in the loop, a taller chimney is required.

4.3 Thermodynamic Performance

In order to investigate the thermodynamic performance of the SMBWR steam cycle, each component of the steam cycle is modelled in MATLAB and the loop model is designed following the steam cycle configuration displayed in Fig. 2.5. The assumptions used to provide consistent comparison of the steam cycle at various reactor operating pressures are constant turbine inlet temperature and constant turbine outlet pressure for both HP and LP turbines. By varying the steam dome pressure while keeping the turbine inlet temperature constant, the amount of external heat needed to reach the selected turbine inlet temperature will be varied. In addition, by having constant turbine outlet pressure, the turbine work will vary depending on the inlet condition, and, thus, the electric power produced and the cycle efficiency. The steam conditions assumed in this study are listed in Table 4.1. As mentioned in Chapter 2, these operating conditions are selected by considering two main criteria. The first consideration is to ensure saturated steam conditions at the LP turbine outlet so that no heat would be wasted. The second consideration is to ensure that both the HP turbine inlet stream and LP turbine inlet stream have the same enthalpy. Fig. 4.16 shows the *T-s* diagram (temperature versus entropy) of the selected 4 representative cases. The points displayed in Fig. 4.16 correspond to the state points specified in Fig. 2.5. Fig. 4.17 and Fig. 4.18 display the main effect of reactor operating pressure on the SMBWR steam cycle.

Table 4.1 Parameters Used for SMBWR Balance of Plant (BOP) Comparison

Parameter	Value	Unit
HP turbine inlet temperature	540	^{o}C
LP turbine inlet temperature	500	^{o}C
HP turbine outlet pressure	10	bar
Condenser pressure	0.08	bar

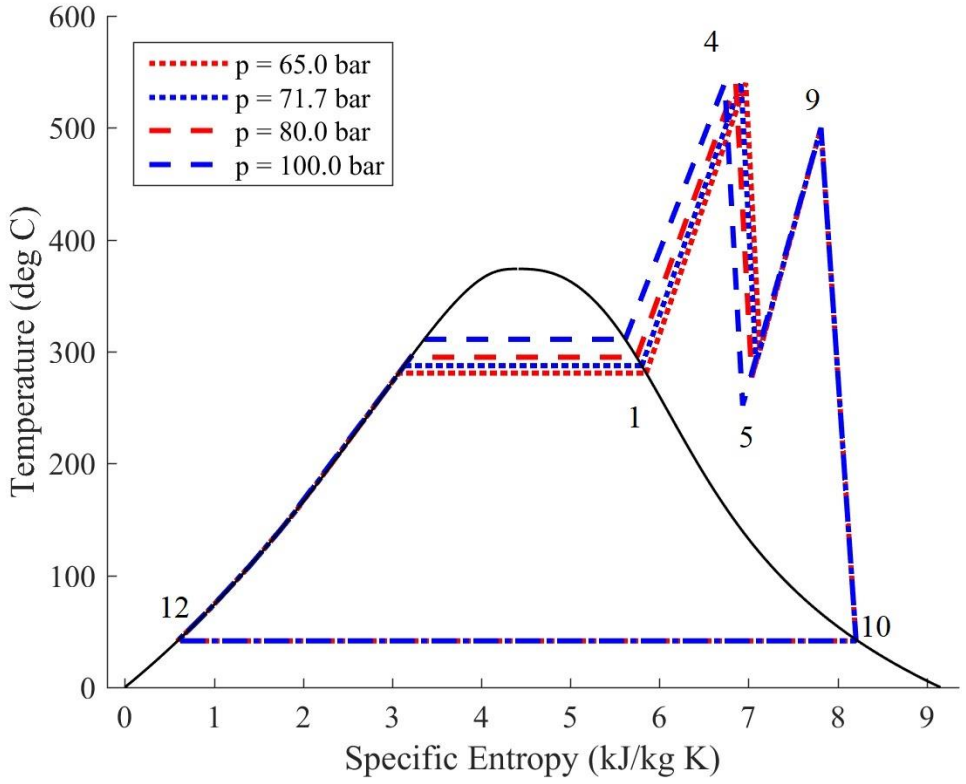

Fig. 4.16 *T-s* diagram of the SMBWR steam cycle at selected system pressures.

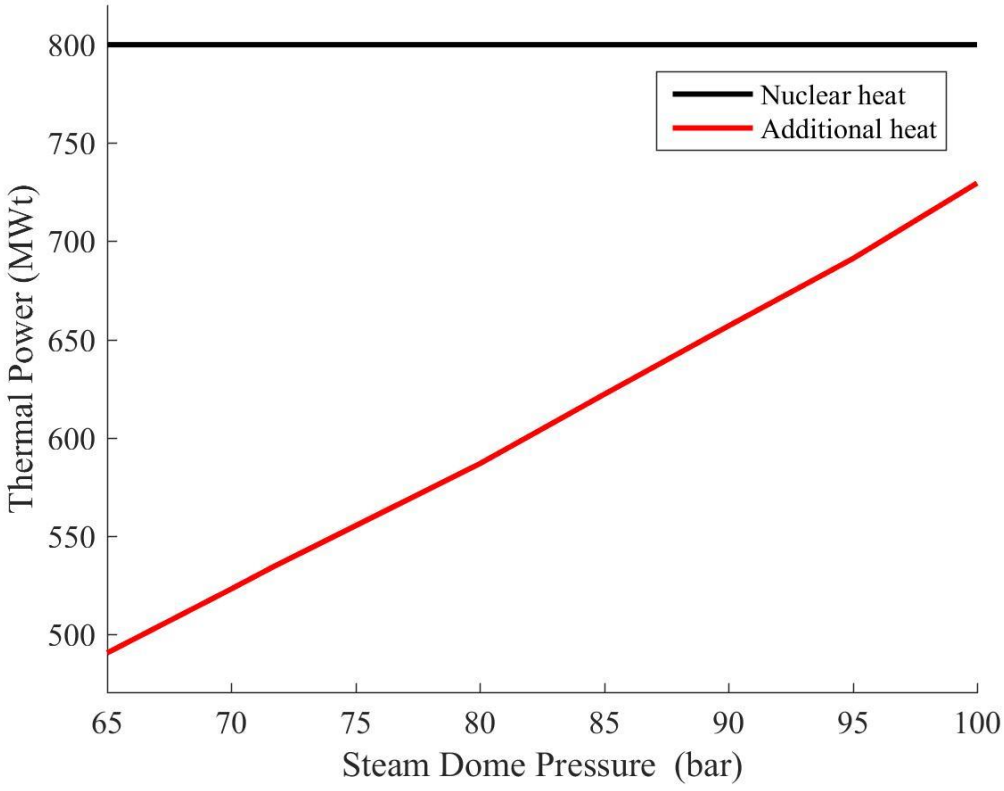

Fig. 4.17 SMBWR thermal power at various system pressures.

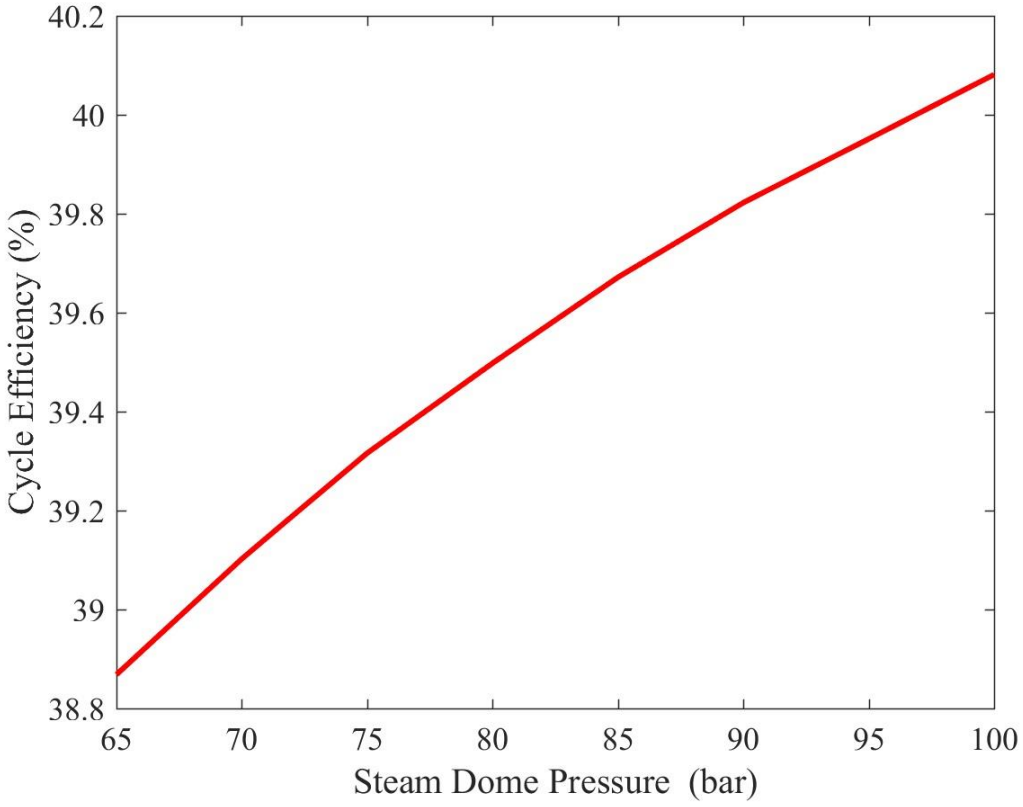

Fig. 4.18 SMBWR steam cycle efficiency at various system pressures.

Fig. 4.17 shows that as the steam pressure in the reactor increases, the amount of external heat required to reach a given turbine inlet temperature is higher. This is expected as the enthalpy of steam is a function of both its pressure and temperature and the value is higher at higher pressure. The cycle efficiency, shown in Fig. 4.18, is defined as the ratio between the net of work (produced by both turbines less the work consumed by feedwater pumps) to the total amount of heat supplied to the cycle as stated in the following equation (Eq. (4-2)). As the steam dome pressure increases, the external heat required and the work produced by the turbines increase. The increased work from turbines is higher than the additional heat required by the system at the higher pressure resulting in higher cycle efficiency. It is shown in Fig. 4.18 that increasing steam dome pressure from 65 bar to 100 bar would result in an increase in thermal cycle efficiency by approximately $\Delta\eta$ = 1.2%. It is also shown that regardless of the steam dome pressure, the thermal cycle efficiency of the SMBWR is reaching 40%, which is comparable to those of stand-alone gas turbines in general. It is obvious that the reason for the higher SMBWR cycle efficiency than the stand-alone LWR, which is normally 33 – 35%, is due to the introduction of an external superheater.

$$\eta_{Cycle}= \frac{W_{Turbine}-W_{Pump}}{Q_{Nuclear\ reactor}+Q_{Superheater}+Q_{Reheater}+Q_{Economizer}} \quad (4\text{-}2)$$

There are several other ways of defining efficiency that could be potentially interesting to examine. The first one is superheater efficiency, which is defined as ratio of the additional electric power produced by generator to external heat supplied to the superheaters, as shown in Eq. (4-3). By assuming that the external heat from the superheater and reheater comes directly from a gas burner, the superheater efficiency can be used to show how efficient the hybrid SMBWR is compared to the conventional gas fired power plant. The other efficiency value that is interesting to consider is the combined cycle efficiency, in which we assume that external heat for the superheaters is taken from the waste heat of a gas turbine system. The combined cycle efficiency is calculated using Eq. (4-4). In this method, the reference gas turbine used is the SIEMENS design SGT5-4000F, with specifications listed in Table 4.2 **[51]**. It is assumed that the gas turbine's power is a function of the superheater's coolant flow rate and will be proportional to the reference design. Fig. 4.19 displays the effect of reactor pressure on both superheater efficiency and combined cycle efficiency.

$$\eta_{Superheater}= \frac{Additional\ Electric\ Power\ produced\ by\ Generator}{Q_{Superheater}+Q_{Reheater}+Q_{Economizer}} \quad (4\text{-}3)$$

$$\eta_{CC}= \frac{Electric\ Power_{GT}+Electric\ Power_{NP}}{Q_{GT}+Q_{Nuclear\ reactor}} \quad (4\text{-}4)$$

Table 4.2 The Specification of SGT5-4000F **[51]**

Parameter	Value
Power output	329 MW
Gross efficiency	41.0%
Exhaust gas mass flow	724 kg/s
Exhaust gas temperature	599 °C

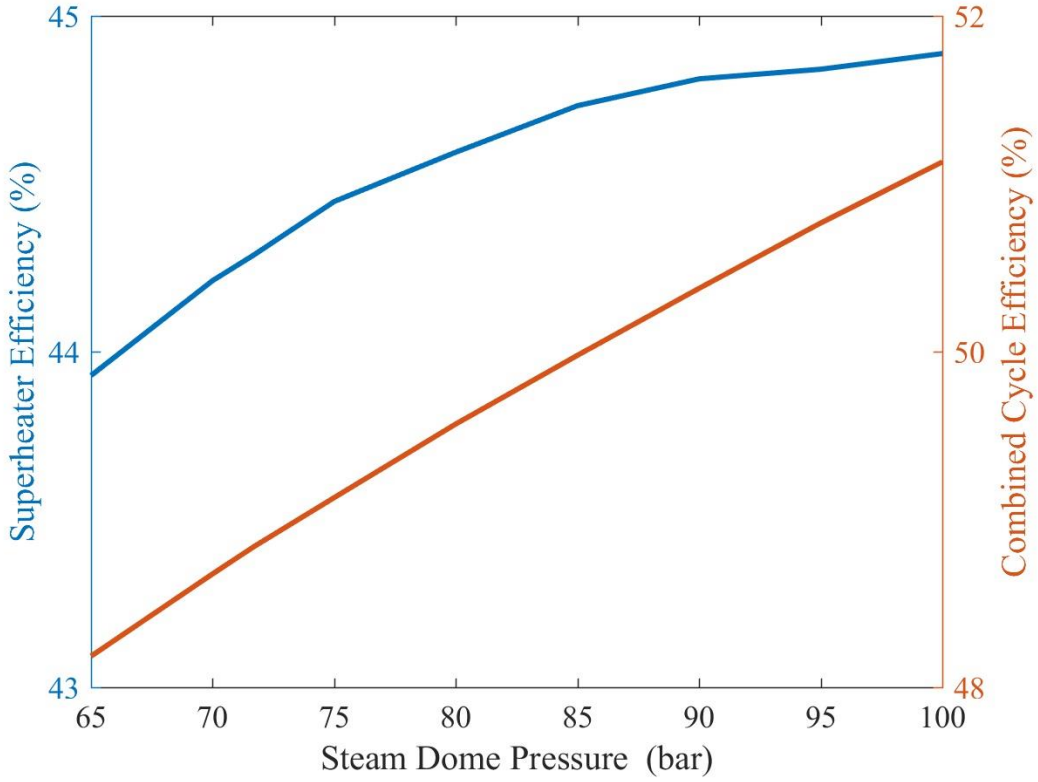

Fig. 4.19 SMBWR alternative efficiencies at various system pressures.

Fig. 4.19 shows that by using a conventional gas burner as the heat source for the superheater and reheater of the SMBWR steam cycle, the superheater efficiency is comparable to the stand-alone gas turbine, and it improves as the operating pressure increases. It also shows that, if waste heat from gas turbines is used instead of a direct gas fired boiler, the resulting combined cycle efficiency could improve by approximately $\Delta\eta$ = 3% as the pressure increases from 65 bar to 100 bar. Therefore, it can be concluded that operating the SMBWR at higher reactor pressure would provide notable improvement to its thermodynamic performance.

4.4 Summary of the Study on Operating Pressure

The study on the operating pressure of the SMBWR was conducted to determine whether there is an incentive to increase the operating pressure of the SMBWR compared to the standard BWR operating pressure, which is generally between 6 and 8 MPa. In terms of the neutronics, the results suggest that there is no significant effect of varying the operating pressure of the SMBWR from 6.5 to 10 MPa. In terms of thermal-hydraulics, the higher operating pressure and temperature would result in a higher steam flow rate to the turbine, smaller recirculation rate, smaller core pressure drop, and a slightly taller chimney will be required to develop natural

circulation. In terms of thermal-hydraulics, the results show that the limiting criterion for high-pressure operation in the SMBWR is the MCPR. The higher the operating pressure of the SMBWR, the closer the MCPR approaches the safety limit. In terms of thermodynamics, it is found that increasing the SMBWR operating pressure from 6.5 to 10 MPa would improve its thermal efficiency by $\Delta\eta$ of about 1.2%, which is relatively small but still not negligible. The improvement in efficiency would be more substantial if the external heat supplied to the superheaters is taken from the exhaust of conventional gas turbines. By comparing the neutronics, thermal-hydraulics, and thermodynamics, it is shown that there is a modest but non-negligible improvement in favour of high-pressure operation. However, further studies are required, such as the implications to safety margin reduction degradation, stability and economic performance, to confirm whether the benefits of high-pressure operation could outweigh the drawbacks that arise from having a larger pressure vessel.

Chapter 5: Core Design Options for the SMBWR

This chapter provides a comparative study on the core design options for the SMBWR. The scope of analysis provided in this chapter falls within three main categories: comparison of three different core geometries, study of the axial distribution of fuel enrichment and its effect on the core neutronics and thermal-hydraulics, and finally study of fuel management options to supress the excess reactivity throughout depletion.

5.1 Comparative Study on Core Geometry

One of the objectives of the study is to quantify how the dimensions of the core would affect the performance of the SMBWR. As mentioned in Chapter 2, SMRs core are more sensitive to leakage. Thus, it is interesting to investigate the trade-off between neutron leakage (neutronics), the chimney height requirement for natural circulation (thermal-hydraulics), and dimensions of the core and vessel which would limit the manufacturing and transportation difficulties. For this purpose, three different geometry configurations, accounting for different length to diameter ratios are selected for the study. The scope of analysis in this section is to compare the neutronic and thermal-hydraulic performance of three different core geometries, as specified in Table 2.2. Case 1 is designed to have a thin and tall shape (192 fuel assemblies with a fuel active length of 3.6 m), while Case 3 is designed to have a wide and short shape (368 fuel assemblies with a fuel active length of 1.88 m). Thus, it is expected that Case 3, which is wider and shorter than the other design, will have more neutron leakage from the top and bottom of the core, while Case 1 will have more neutron leakage in the radial direction. It is also important to note that all three geometries considered have the same power density. The neutronic study on core geometry is performed with axially uniform enrichment of 4.2 wt-% U^{235}, nine of the fuel pins contain gadolinia poison (Gd_2O_3) with a concentration of 2 wt-%. Table 5.1 shows a summary of the 3 designs compared in terms of their geometry and performance. In order to estimate the dimensions of the reactor vessel as shown in Table 5.1, the height of other components in the vessel (lower plenum, upper plenum, and dome) are conservatively assumed to be the same as those of the ESBWR. Fig. 5.1 displays the multiplication factor of the full core model using a 3-batch fuel arrangement. Fig. 5.2 shows the depletion behaviour of the core reactivity feedbacks, while Fig. 5.3 shows what the core reactivity feedbacks would look like over the cycle length in a 3-batch fuel arrangement.

Table 5.1 Thermal-hydraulic Performance Comparison for the Studied Geometries

Parameter	Geometrical Variation		
	1	2	3
No. of fuel assemblies	192	256	368
Power density (kW/L)	48.2	48.2	48.2
Active fuel length (m)	3.60	2.70	1.88
Shroud inlet diameter (m)	2.60	2.90	3.52
Core length to diameter ratio	1.47	1.01	0.60
Estimated vessel diameter (m)	3.71	3.94	4.44
Operating pressure (MPa)	7.17	7.17	7.17
Feedwater inlet temperature (°C)	192	192	192
Core inlet temperature (°C)	273	273	273
Core average void	0.32	0.36	0.40
Core mass flow rate (kg/s)	2414.3	2414.3	2414.3
Core pressure drop (kPa)	63.58	50.70	42.33
Minimum required height of chimney (m)	4. 84	3.58	3.09
Estimated vessel height (m)	18.5	16.3	15.2
MCPR	1.47	1.56	1.65

Fig. 5.1 shows that in 3-batch arrangement, the neutron economy of Case 3 is slightly more inferior due to leakage compared to the other two configurations. Fig. 5.2 shows that the shape of the core has a notable effect on the core reactivity feedbacks. In terms of Doppler Coefficient, the presence of gadolinium poison causes the DC to be more negative. Since the three core configuration cases have the same thermal power and power density, it is expected that the core with the larger number of fuel assemblies will have shorter fuel active length and, thus, higher axial neutron leakage. It is shown from Fig. 5.2 that at BOL, Case 3 has slightly less negative DC. The increase in leakage means fewer neutrons are slowed down to thermal energy, making the spectrum harder. This phenomenon increases the resonance absorption, thus increasing DC. In addition, by having higher leakage, the plutonium build-up in Case 3 is higher than in the other 2 cases, which is the reason why the DC in Case 3 shifts to become slightly more negative at EOL compared to the other cases. It is shown from Fig. 5.3 that, by having a 3-batch configuration, the DC becomes less dependent on burnup and no significant differences are observed between the studied geometries over the cycle. The loading pattern

arrangements used in cases presented in Fig. 5.3 are shown in Fig. 5.4, while the shuffling arrangements are shown in Fig. 5.5. The assembly type denoted “0” in Fig. 5.4 and Fig. 5.5 represents a fresh fuel assembly, while types 1, 2, and 3 represent once, twice, and thrice burnt fuel, respectively, and R represents the reflector.

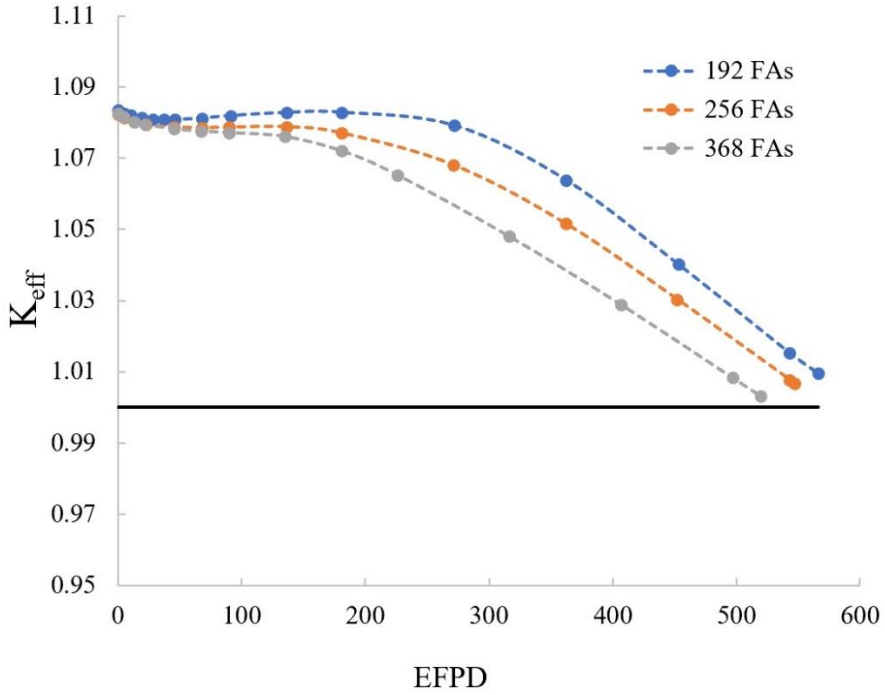

Fig. 5.1 Comparison of the effective multiplication factor for the studied geometries.

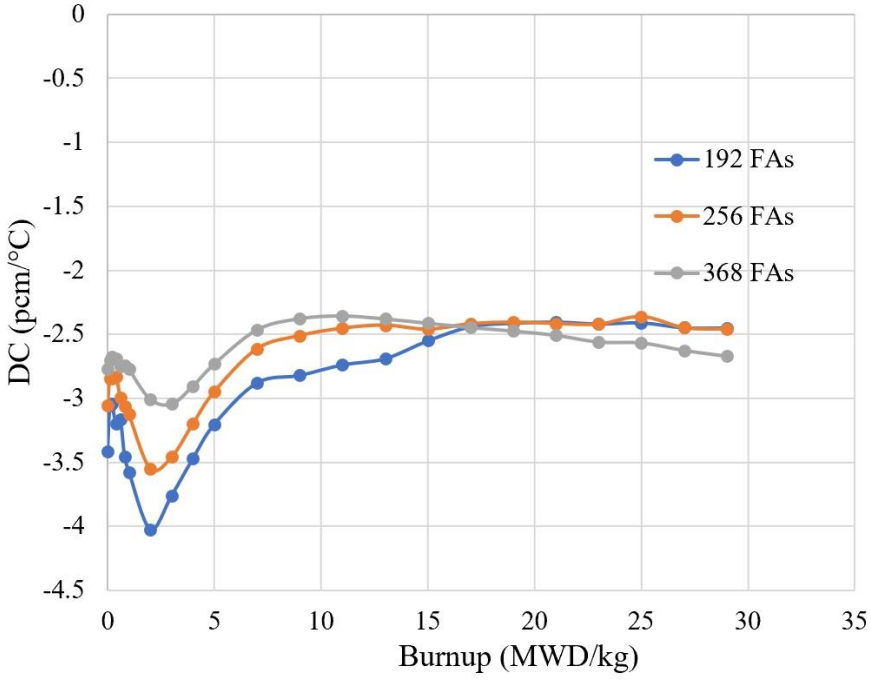

(a)

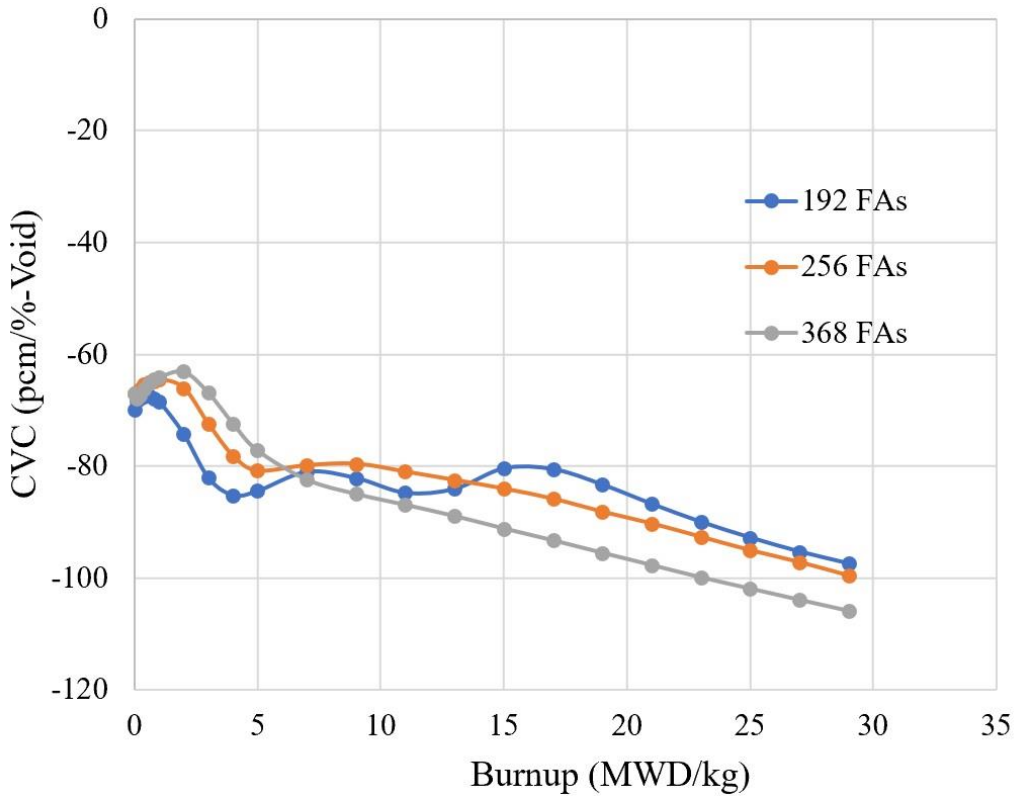

(b)

Fig. 5.2 Depletion behaviour of reactivity feedbacks for the studied geometries: (a) Doppler Coefficient; (b) Coolant Void Coefficient.

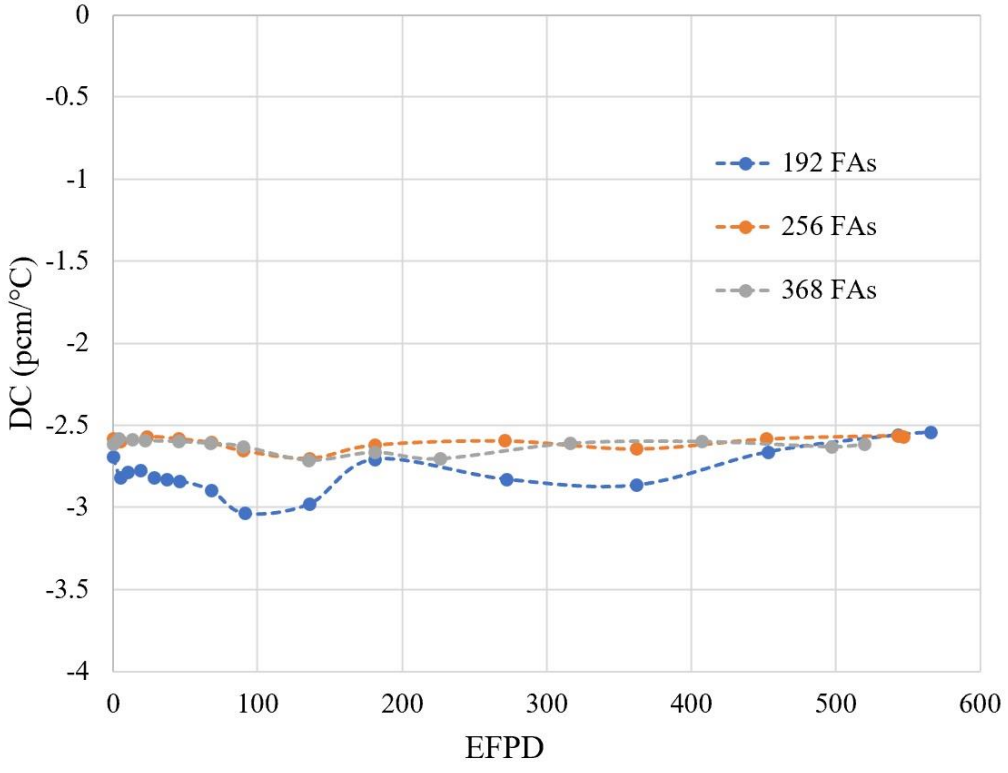

(a)

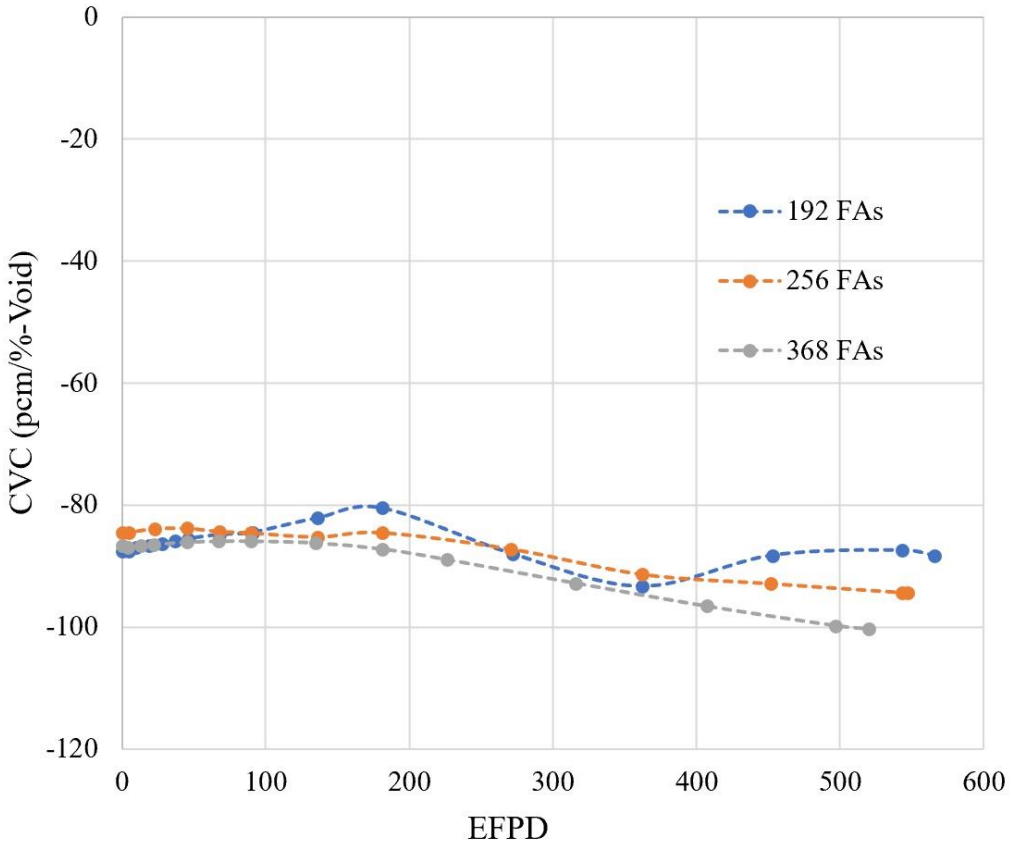

(b)

Fig. 5.3 Reactivity feedbacks comparison for the studied geometries in 3-batch arrangement: (a) Doppler Coefficient; (b) Coolant Void Coefficient.

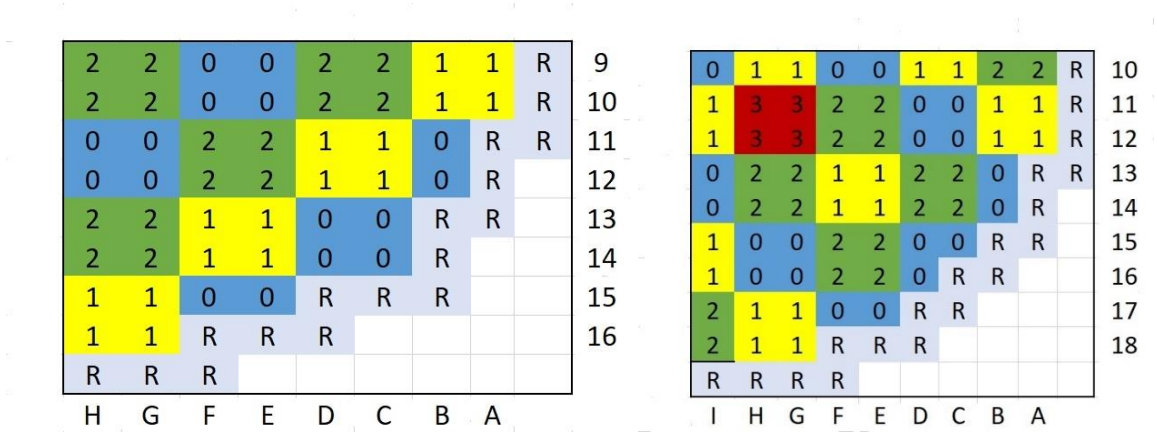

(a) (b)

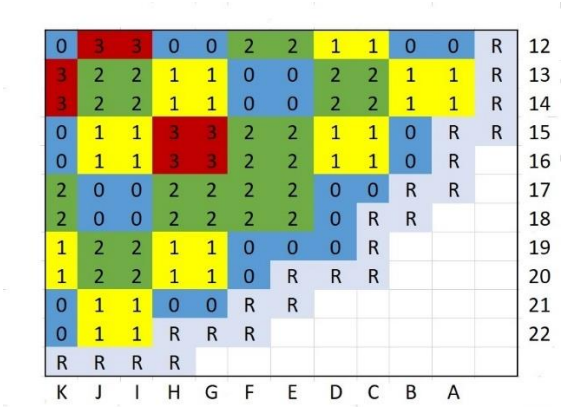

(c)

Fig. 5.4 Loading pattern configuration for 3-batch arrangement: (a) 192 FAs; (b) 256 FAs; (c) 368 FAs.

0	1	2
G5	G1	G3
E7	A7	C7
E9	A9	C9
G11	G15	G13
K9	O9	M9
K7	O7	M7
I11	I15	I13
I5	I1	I3
E15	E3	G7
C3	C5	E5
O11	C11	G9
C13	E13	E11
K15	K13	I9
M13	M11	K11
O5	M5	I7
M3	K3	K5

0	1	2
G6	G2	G4
E8	A8	C8
E10	A10	C10
G12	G16	G14
K10	O10	M10
K8	O8	M8
I12	I16	I14
I6	I2	I4
E2	E4	G8
C4	C6	E6
O12	C12	G10
C14	E14	E12
K2	K14	I10
M14	M12	K12
O6	M6	I8
M4	K4	K6

0	1	2
H6	H2	H4
F8	B8	D8
F10	B10	D10
H12	H16	H14
L10	P10	N10
L8	P8	N8
J12	J16	J14
J6	J2	J4
F2	F4	H8
D4	D6	F6
B12	D12	H10
D14	F14	F12
L2	L14	J10
N14	N12	L12
B6	N6	J8
N4	L4	L6

0	1	2
H5	H1	H3
F7	B7	D7
F9	B9	D9
H11	H15	H13
L9	P9	N9
L7	P7	N7
J11	J15	J13
J5	J1	J3
F15	F3	H7
D3	D5	F5
B11	D11	H9
D13	F13	F11
L15	L13	J9
N13	N11	L11
B5	N5	J7
N3	L3	L5

(a)

0	1	2	3
C7	A7	E7	
C11	A11	E11	
C15	E13	C13	
E9	G9	A9	
E17	C9	C5	G7
G3	G1	G5	
G15	G17	G13	
I5	I7	I1	
I13	I11	I17	
K3	K1	K5	
K15	K17	K13	
M9	K9	Q9	
M17	O9	O13	K11
O3	M5	O5	
O7	Q7	M7	
O11	Q11	M11	
O15	M13	M15	
Q5	I3	M3	K7
Q13	I15	E15	G11
I9	E5	E3	

0	1	2	3
C4	E6	E4	
C8	A8	E8	
C12	A12	E12	
E2	C10	C6	G8
E10	G10	A10	
G4	G2	G6	
G16	G18	G14	
I6	I8	I2	
I14	I12	I18	
K4	K2	K6	
K16	K18	K14	
M2	O10	O14	K12
M10	K10	O10	
O4	M6	O6	
O8	Q8	M8	
O12	Q12	M12	
O16	M14	M16	
Q6	I4	M4	K8
Q14	I16	E16	G12
I10	E14	C14	

0	1	2	3
B6	J4	N4	L8
B14	J16	F16	H12
D4	F6	F4	
D8	B8	F8	
D12	B12	F12	
D16	F14	D14	
F2	D10	D6	H8
F10	H10	B10	
H4	H2	H6	
H16	H18	H14	
J6	J8	J2	
J14	J12	J18	
L4	L2	L6	
L16	L18	L14	
N2	P10	P14	L12
N10	L10	R10	
P4	N6	P6	
P8	R8	N8	
P12	R12	N12	
J10	N14	N16	

0	1	2	3
B5	J3	N3	L7
B13	J15	F15	H11
D3	F5	F3	
D7	B7	F7	
D11	B11	F11	
D15	F13	D13	
F9	H9	B9	
F17	D9	D5	H7
H3	H1	H5	
H15	H17	H13	
J5	J7	J1	
J13	J11	J17	
L3	L1	L5	
L15	L17	L13	
N9	L9	R9	
N17	P9	P13	L11
P7	R7	N7	
P11	R11	N11	
P15	N13	N15	
J9	N5	P5	

(b)

0	1	2	3
A11	C11	E11	I11
C17	G13	C13	
E9	A9	E5	G7
E13	A13	I13	
E19	I15	I19	
G11	G3	G5	
G21	G19	G17	
I5	I1	I9	
I17	I21	E17	G15
K1	K3	K5	K9
K7	C7	E7	
K11	I7	I3	
K15	C15	E15	
K21	K19	K17	K13
M5	M1	Q5	O7
M17	M21	M13	
O11	O3	O5	
O21	O19	O17	
Q3	M7	M3	
Q9	U9	M9	
Q13	U13	Q17	O15
Q19	M15	M19	
S5	O9	S9	
S17	O13	S13	
S19	G9	C9	
U7	S7	Q7	
U11	S11	Q11	M11
U15	S15	Q15	

0	1	2	3
A12	C12	E12	I12
C6	G10	C10	
E4	I8	I4	
E10	A10	E6	G8
E14	A14	I14	
G2	G4	G6	
G12	G20	G18	
I6	I2	I10	
I18	I22	E18	G16
K2	K4	K6	K10
K8	C8	E8	
K12	G14	C14	
K16	C16	E16	
K22	K20	K18	K14
M6	M2	Q6	O8
M18	M22	M14	
O2	O4	O6	
O12	O20	O18	
Q4	M8	M4	
Q10	U10	M10	
Q14	U14	Q18	O16
Q20	M16	M20	
S4	I16	I20	
S6	O10	S10	
S18	O14	S14	
U8	S8	Q8	
U12	S12	Q12	M12
U16	S16	Q16	

0	1	2	3
B8	D8	F8	
B12	D12	F12	J12
B16	D16	F16	
D4	P14	T14	
D6	H10	D10	
D18	H14	D14	
F4	J8	J4	
F10	B10	F6	H8
F14	B14	J14	
F20	J16	J20	
H2	H4	H6	
H12	H20	H18	
J6	J2	J10	
J18	J22	F18	H16
L2	L4	L6	L10
L8	T8	R8	
L12	N16	N20	
L16	T16	R16	
L22	L20	L18	L14
N6	N2	R6	P8
N18	N22	N14	
P2	P4	P6	
P12	P20	P18	
R4	N8	N4	
R10	V10	N10	
R14	V14	R18	P16
T6	P10	T10	
V12	T12	R12	N12

0	1	2	3
B7	D7	F7	
B11	D11	F11	J11
B15	D15	F15	
D5	H9	D9	
D17	H13	D13	
D19	N7	N3	
F3	J7	J3	
F9	B9	F5	H7
F13	B13	J13	
F19	J15	J19	
H11	H3	H5	
H21	H19	H17	
J5	J1	J9	
J17	J21	F17	H15
L1	L3	L5	L9
L7	T7	R7	
L11	P9	T9	
L15	T15	R15	
L21	L19	L17	L13
N5	N1	R5	P7
N17	N21	N13	
P11	P3	P5	
P21	P19	P17	
R9	V9	N9	
R13	V13	R17	P15
R19	N15	N19	
T17	P13	T13	
V11	T11	R11	N11

(c)

Fig. 5.5 The 3-batch shuffling arrangement for: (a) 192 FAs; (b) 256 FAs; (c) 368 FAs.

In terms of CVC, it is known that the reactivity feedbacks tend to be more negative at the EOL due to plutonium build-up and overall depletion of fissile material. However, the presence of gadolinium poison alters this behaviour at the BOL. It can be observed that a 3-batch configuration helps reducing the variation in the CVC throughout the cycle in all studied geometries. In a core with a smaller number of fuel assemblies, the mass flow rate per assembly is higher compared to a core with a larger number of fuel assemblies. With higher flow rate per assembly, the effect of coolant density and void perturbation to reactivity feedback is more significant. Therefore, this phenomenon is likely to be the reason for the observed behaviour of CVC in the core with more fuel assemblies.

As natural circulation was chosen to be an integral part of the SMBWR design, a fair comparison of the core geometries would have to include a study on core pressure losses and the required height for the chimney to develop natural circulation. It is expected that a taller core would have higher core pressure losses and, thus, would require a taller chimney to develop natural circulation. In terms of thermal-hydraulics, another important parameter is the MCPR as the main indicator of safety in a BWR. It is shown that Case 1, which is the tallest option of all three geometries studied, has the lowest MCPR value at any given reactor operating pressure. This result is expected because taller core would result in higher core pressure drop, and thus, lower local operating pressure. At lower pressure, the steam saturation temperature is reduced, thus reducing the ratio between critical power and bundle operating power.

By comparing all the results above, it can be concluded that the least favourably performing core design out of the three design options is Case 1, which is the tallest and with fewest number of assemblies (192 fuel assemblies and fuel length of 3.60 m). It is shown that the thin and tall core configuration requires a taller chimney to ensure natural circulation. In addition, this core configuration will have the lowest MCPR, which means the lowest margin to the thermal safety limit. Furthermore, this configuration also has the most variation in the behaviour of the reactivity feedbacks throughout the fuel depletion. Case 3 (368 fuel assemblies and a fuel length of 1.88 m) has the lowest pressure drop, highest safety margin, and the most stable behaviour of the reactivity feedbacks throughout the fuel depletion compared to the other core designs. However, having a wider core would also mean having a larger reactor vessel diameter, which might not be the most economic option when considering the manufacturing and construction costs of the NPP.

The development strategy for SMRs relies on the assumption that their components could be produced in a factory, then transported and assembled on site. Having a large diameter vessel would complicate manufacturing and transportation of the vessel, which may affect the capital costs of the NPPs. The low loader lorries, a means of road transport for abnormally large and heavy loads, have a maximum width limitation of 4.3 m **[22]**. This indicates that the Case 3 estimated vessel diameter has surpassed the specification limit for road transport. In addition, it is also found that in terms of neutronics, Case 3 is not the most efficient design as it has larger surface area to volume ratio with high neutron leakage through the top and bottom boundaries of the core. Therefore, the next section of this study will focus on Case 2 of the core designs (256 fuel assemblies and a fuel length of 2.70 m), as it offers a compromise between the neutronics, thermal-hydraulics and RPV manufacturing and transport considerations.

5.2 Comparison of the SMBWR with Other SMRs

This section discusses additional potential benefits of the SMBWR as compared to other relevant small power LWRs. Table 5.2 shows a comparison of SMBWR power and estimated vessel dimension with a number of other SMR designs **[23]**. DMS is another BWR-type SMR, while both IRIS and the Westinghouse SMR are integral PWRs (IPWRs). In this section the value of reactor vessel size for the SMBWR (vessel diameter and height) have been estimated. The vessel diameter can be inferred from the circumferential diameter of the core (Case 2), which can be calculated from the number of rows of the FAs and the assembly pitch. Once the circumferential diameter of the core is found, the shroud and vessel diameter can be estimated,

by taking into account the component flow area as listed in Table 2.4. The vessel height can be estimated by summing up the length of the vessel components (lower & upper plenum, core, chimney, and dome). It should be noted that the thermal power of the SMBWR shown in Table 5.2 is the reactor power only. In order to produce the amount of electric power shown in Table 5.2, the SMBWR requires approximately 529 MW of additional thermal power for the superheating system.

Table 5.2 Comparison of SMBWR with Other SMRs

Parameter	**Reactor**			
	SMBWR	**DMS**	**IRIS**	**Westinghouse SMR**
Type	SMR - BWR	SMR - BWR	IPWR	IPWR
Thermal power (MWth)	800	840	1000	800
Electric power (MWe)	515	300	335	225
Cycle efficiency (%)	39.5	36.4	34.2	28.7
Fuel active length (m)	2.70	2.00	4.26	2.40
Vessel diameter (m)	3.94	5.80	6.20	3.70
Vessel height (m)	16.3	15.5	21.3	28.0
Power to volume ratio ($MWth/m^3$)	4.03	2.05	1.56	2.66

By comparing both the thermal power and electric power of the SMBWR with other LWRs, as shown in Table 5.2, it is clear that the SMBWR has the highest power conversion cycle efficiency, even after taking into account the amount of additional heat needed to be supplied for the superheaters. Table 5.2 also shows that, although these SMRs have similar thermal power, both the SMBWR and DMS (BWR-type SMR) have a shorter vessel compared to those of the IPWRs. The reason is obviously because in the IPWR design concept, the steam generators are designed to be located inside the RPV. By examining the power to volume ratio, which is calculated by dividing the thermal power by the vessel volume, it is shown that the SMBWR could achieve the highest power to volume ratio compared to some other SMRs in the market. As mentioned in Chapter 2, the DMS relies on having a large flow area to reduce the steam velocity and implement a free surface moisture separation system. This FSS allows the DMS to eliminate the steam separator and thus reduce the height of its vessel. In contrast

to the DMS, the SMBWR has a standard flow area, and thus still requires a steam separator. However, the fact that the SMBWR is combined with external superheaters means that the steam dryer could be eliminated as the superheaters will ensure that steam is going to enter turbines in a dry condition. Therefore, the SMBWR is able to achieve nearly the same vessel height as the DMS with a smaller vessel diameter, which could be more important for enabling less complex and costly manufacturing and transportation.

5.3 Axial Fuel Loading Configuration

BWR fuel assemblies are normally designed with enrichment zoning to maximise uranium utilisation and control the power shape. For example, a typical ABWR fuel assembly would have several enrichment and burnable poison zones in a single assembly. It is usually designed to have natural uranium at the top and bottom, high enrichment in the middle, low enrichment in the periphery, and higher poison concentration in the lower part **[52]**. The axial fuel loading distribution in the fuel assembly is an important parameter as it affects the core axial power distribution, and thus, local power peaking. This section focuses on analysing the effect of several axial fuel loading configurations on the neutronic performance and power distribution of the SMBWR. Once again, it is important to note that the aim of this analysis is not finding the optimal configuration for the axial fuel loading in the SMBWR, but instead examining the sensitivity of the SMBWR performance to the enrichment distribution as a design parameter. Five design options for SMBWR fuel assemblies are investigated, which include three designs with uniform enrichment (U1, U2, and U3) and two designs with axial variation of fuel enrichment (M1 and M2). The M2 design has 12 partial length fuel rods, which are only two thirds of the fuel active length of the standard rods. Table 5.3 lists the design specifications of the five design options and Fig. 5.6 displays the fuel assembly configuration for the design options with axial variation of fuel enrichment. Both the M1 and M2 assemblies have natural uranium placed at the top and bottom of the fuel assembly. This configuration minimises the axial leakage of fast neutrons. As BWRs have better moderation in the lower part of the core compared to the upper part, in order to control the axial power shape, the highest fuel enrichment is located in the middle part of the core and higher poison concentration is placed in the lower part of the core. It should be noted that a thorough optimisation procedure for finding the axial zoning for the SMBWR has not been performed in the current work. The configuration shown in Fig. 5.6 was selected by choosing the best performing configuration among a few configurations, which were investigated in the initial phase. However, at the

current phase of SMBWR development, this should be sufficient, and a thorough investigation of the axial zoning should be the subject of the next phase of SMBWR development.

Table 5.3 Design Specification for SMBWR Fuel Assemblies

Design Specification	U1	U2	U3	M1	M2
Fuel enrichment	4.2 wt-% U^{235}	3.9 wt-% U^{235}	4.2 wt-% U^{235}	varied	varied
Poison concentration	2 wt-% Gd	2 wt-% Gd	5 wt-% Gd	varied	varied
No. of FAs in the core	256	256	256	256	256
Fuel active length (m)	2.70	2.70	2.70	2.70	2.70
No. partial length rods	N/A	N/A	N/A	N/A	12
Assembly loading (kgU)	141.33	141.33	140.91	141.08	135.54
U^{235} content (kg)	5.94	5.51	5.92	5.22	5.13
Gd content (kg)	0.27	0.27	0.68	0.51	0.51

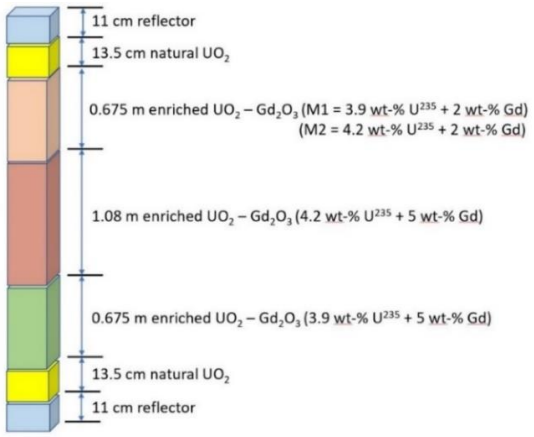

Fig. 5.6 Axial fuel configuration for M1 and M2

The neutronic performance of the five assembly designs in a 2x2 SMBWR assembly cluster were investigated in PANTHER, and the results are shown in Fig. 5.7 and Fig. 5.8. Fig. 5.7 shows the k-infinity values, while Fig. 5.8 show the axial power distribution at BOL, MOL, and EOL. It is observed from Fig. 5.7 that U1 has a higher reactivity and longer cycle length compared to U2, which is expected as U1 has higher fuel HM loading and initial fissile material compared to U2. U3 has lower excess reactivity compared to U1 but it has the same cycle length. This result is expected as the U3 design has more poison loading compared to U1, and thus it is more effective in suppressing the excess reactivity. Once the poison is fully depleted,

the reactivity of U3 assemblies becomes very similar to U1 assemblies as both have the same fuel enrichment.

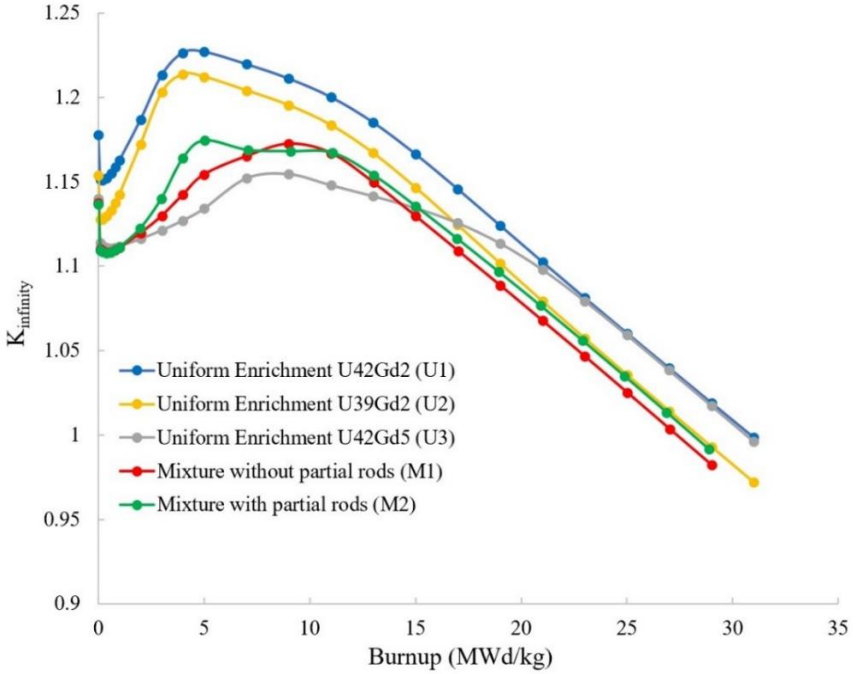

Fig. 5.7 Infinite multiplication factor of 2×2 SMBWR assemblies with several fuel loading configurations.

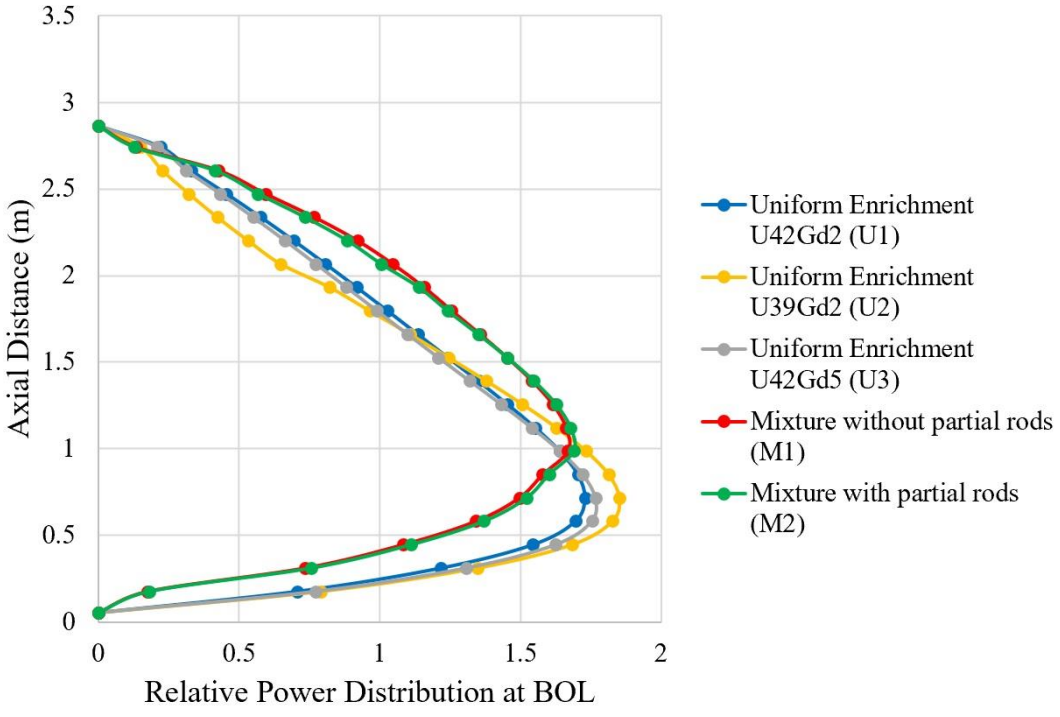

(a)

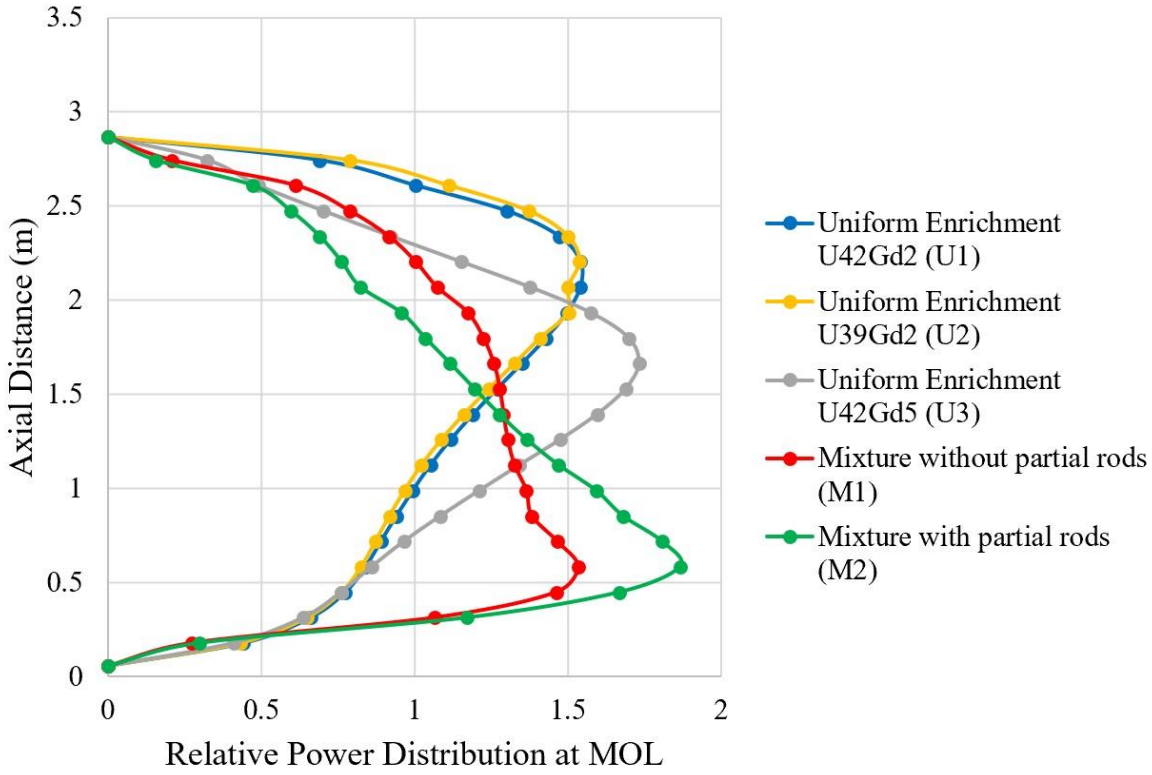

(b)

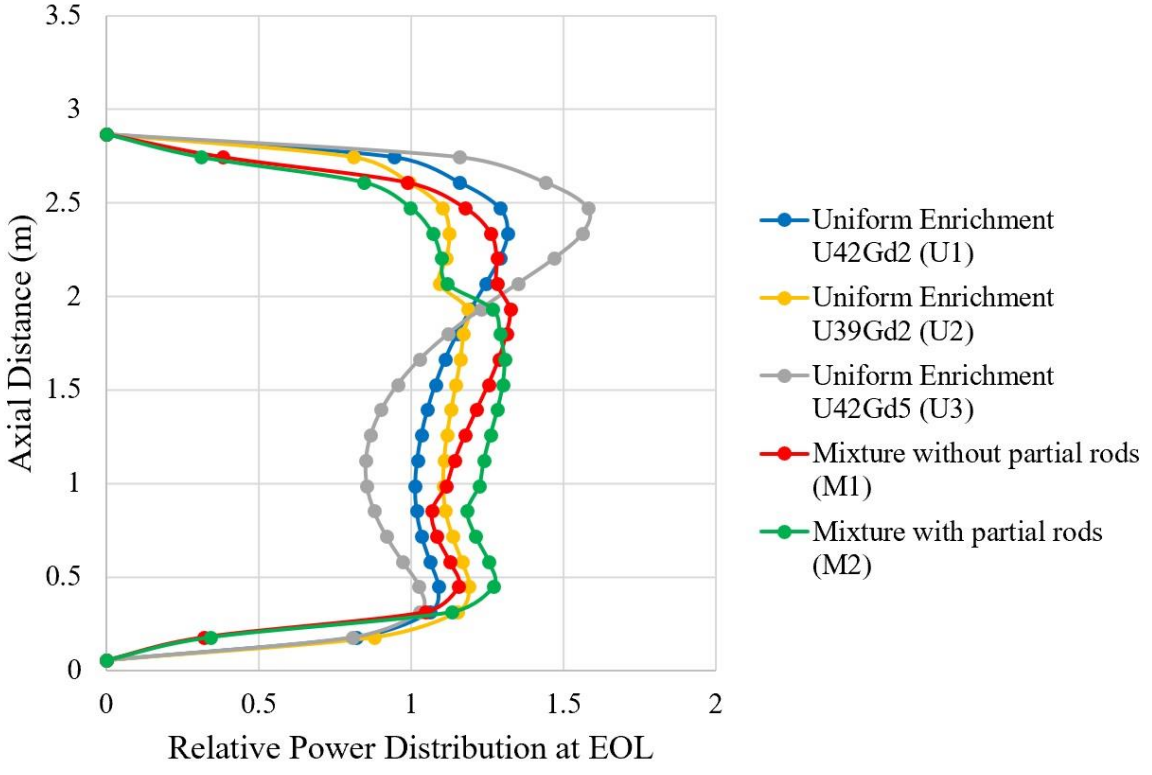

(c)

Fig. 5.8 Relative power distribution of 2×2 SMBWR assemblies with several fuel loading configurations at the: (a) BOL; (b) MOL; (c) EOL.

There are a number of reasons for introducing partial length fuel rods into BWR assemblies. In terms of neutronics, it is generally known that the occurrence of boiling in a BWR makes the lower part of the core better moderated compared to the upper part. Using partial rods to reduce the fuel content in the upper part of the core is one way to improve the fuel utilisation in a BWR core. In terms of thermal-hydraulics, two-phase flow is known to have higher friction losses compared to single-phase flow and, thus, partial rods are used to reduce the core pressure drop. It is important to note that the fact that the SMBWR has shorter fuel active length and less flow rate through its core compared to a large BWR means that the core pressure drop in the SMBWR is lower compared to an ABWR or even ESBWR. Therefore, the SMBWR might avoid having partial rods in its fuel assemblies.

By examining the power distribution of the studied assembly types, it is shown that without having axial variation of fuel enrichment, the peak of the power distribution shifts from the lower part of the core at BOL to the upper part as the fuel is depleted. At BOL, the peak of the power distribution is in the lower part of reactor because water has better moderation compared to steam. Since the fissile material at the bottom depletes faster compared to the top, at some point the peak is shifted towards the upper part of the core. This behaviour could be altered by having higher poison concentration at the bottom of the core. It is shown in Fig. 5.8 that by having more poison at the bottom of the core, the peak of the power distribution is reduced and shifted to the centre of the core. However, after the poison is fully depleted, the peak starts moving back to the bottom of the core. This tendency results in a higher impact on M2 power peaking compared to M1 because the M2 assembly has lower fuel content in the upper part of the core compared to M1 due to the partial-length fuel rods. It can be observed that for a BWR type SMR, reducing the fuel enrichment at the top of the core would give better assembly performance than having partial rods.

It is important to note that the results shown in this section are produced only for 2x2 assemblies with reflective radial boundary conditions, which is representative for the assemblies located near the core centre. Generally, the peripheral assemblies would have different power shape due to radial leakage, which would affect the core power distribution. Furthermore, a standard BWR typically operates with multiple fuel batches and uses control rods to manage the radial power distribution and compensate for fuel depletion and reactivity loss of the core. However, if the fuel management strategy is able to achieve a close to uniform power distribution, which does not change significantly throughout the burnup, and the core excess reactivity is small due to use of burnable poisons, the reliance on control rods could be reduced, increasing the relevance of the presented results.

5.4 Fuel Management & Reactivity Control

Reactivity control is an important part of reactor operation. In PWRs, it is normally achieved by a combination of soluble boron, control rods and burnable poison, while BWRs usually rely on burnable poison, control rods and the speed of the recirculation pump. In a natural circulation BWR system, the removal of the recirculation pump means that the system needs to rely exclusively on control rods for managing the excess reactivity and facilitating start-up and shut-down operations. As mentioned earlier, the use of burnable poisons can reduce this reliance. This section of the study focuses on options for managing the excess reactivity of the SMBWR. A full core model of the SMBWR with 256 fuel assemblies, 2.70 m active fuel length, and axial variation of assembly type M1 is modelled with the nodal diffusion code PANTHER. The two methods of reactivity control investigated in this study are multi-batch fuel management and feedwater coolant temperature variation.

5.4.1 Multi-batch fuel management

In terms of multi-batch management options, both 3- and 4-batch arrangements were considered and their depletion behaviour was compared in terms of excess reactivity and channel power peaking factors ($F_{\Delta H}$), as shown in Fig. 5.9 and Fig. 5.10 respectively. Channel $F_{\Delta H}$, also known as enthalpy rise hot channel factor, is defined as the ratio of maximum individual assembly channel enthalpy rise to core average enthalpy rise. A typical limit for Channel $F_{\Delta H}$ is 1.5 at the reactor full power **[53]**. The loading pattern and shuffling scheme for the 3-batch arrangement were defined to follow the configuration defined in Fig. 5.4 (b) and Fig. 5.5 (b) respectively. While the loading pattern and shuffling scheme for the 4-batch arrangement are shown in Fig. 5.11 and Fig. 5.12 respectively. The assembly type denoted “0” in Fig. 5.11 and Fig. 5.12 represents a fresh fuel assembly, while types 1, 2, and 3 represent once, twice, and thrice burnt fuel, respectively, and R represents the reflector.

Fig. 5.9 shows that the greater the number of batches used, the lower the core excess reactivity throughout the irradiation cycle. In the once-through cycle, the core reactivity increases as the gadolinium poison depletes, and once it is fully burned, the core reactivity starts decreasing. As expected, this behaviour is altered in the multi-batch configuration as the average core reactivity is an average of the reactivity of the pins from different stages of the irradiation cycle. It is shown that in the multi-batch configurations, the initial excess reactivity has the highest value throughout the cycle. Considering the maximum value of core reactivity in each scheme, it is shown that using a 4-batch scheme would result in an excess reactivity

reduction of approximately 1051 pcm compared to a 3-batch scheme. In PWRs, soluble boron is used to reduce the excess reactivity and maintain criticality throughout the cycle. However, BWRs with natural circulation do not use borated water, and thus, all excess reactivity has to be reduced by means of utilising the control rods. Having less excess reactivity is preferable as it would mean fewer CRs are required.

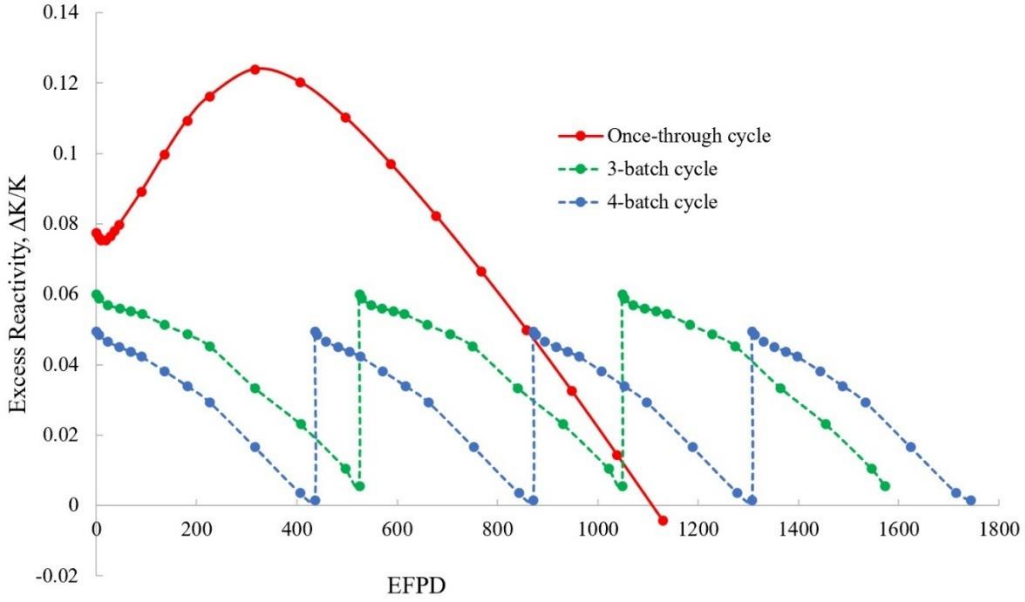

Fig. 5.9 Excess reactivity of the SMBWR with various fuel management schemes.

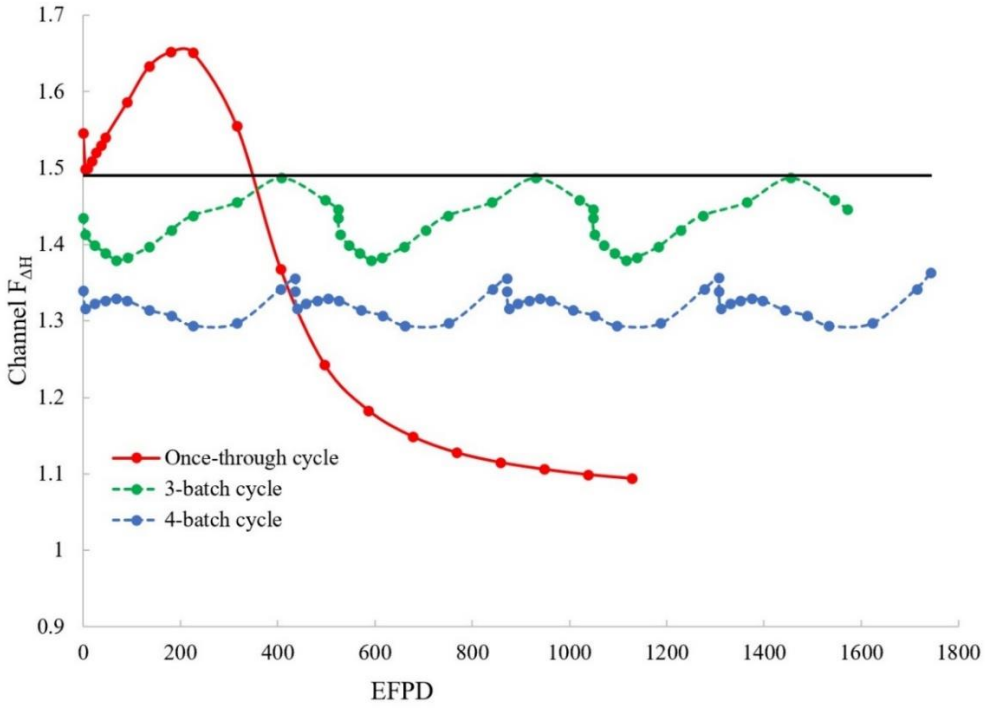

Fig. 5.10 Channel $F_{\Delta H}$ of the SMBWR with various fuel management schemes.

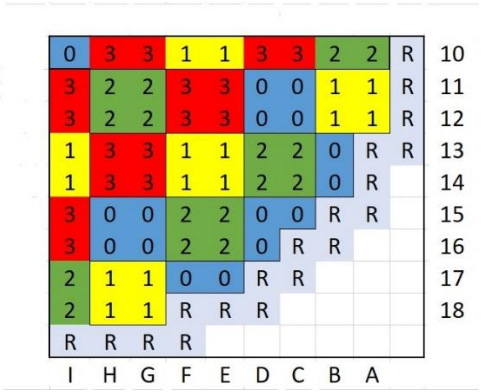

Fig. 5.11 Loading pattern configuration for 4-batch arrangement.

0	1	2	3
C7	A7	C5	E7
C11	A11	C13	E11
C15	E13	G11	I15
E17	E9	A9	G9
G3	G1	E3	G5
G15	G17	E15	G13
K3	K1	M3	K5
K15	K17	M15	K13
M17	M9	Q9	K9
O3	M5	K7	I3
O7	Q7	O5	M7
O11	Q11	O13	M11
O15	M13	K11	O9
Q5	I5	I1	I7
Q13	I13	I17	I11
I9	E5	G7	C9

0	1	2	3
C4	E6	G8	C10
C8	A8	C6	E8
C12	A12	C14	E12
E2	E10	A10	G10
G4	G2	E4	G6
G16	G18	E16	G14
K4	K2	M4	K6
K16	K18	M16	K14
M2	M10	Q10	K10
O4	M6	K8	I4
O8	Q8	O6	M8
O12	Q12	O14	M12
O16	M14	K12	O10
Q6	I6	I2	I8
Q14	I14	I18	I12
I10	E14	G12	I16

0	1	2	3
B6	J6	J2	J8
B14	J14	J18	J12
D4	F6	H8	D10
D8	B8	D6	F8
D12	B12	D14	F12
D16	F14	H12	J16
F2	F10	B10	H10
H4	H2	F4	H6
H16	H18	F16	H14
L4	L2	N4	L6
L16	L18	N16	L14
N2	N10	R10	L10
P4	N6	L8	J4
P8	R8	P6	N8
P12	R12	P14	N12
J10	N14	L12	P10

0	1	2	3
B5	J5	J1	J7
B13	J13	J17	J11
D3	F5	H7	D9
D7	B7	D5	F7
D11	B11	D13	F11
D15	F13	H11	J15
F17	F9	B9	H9
H3	H1	F3	H5
H15	H17	F15	H13
L3	L1	N3	L5
L15	L17	N15	L13
N17	N9	R9	L9
P7	R7	P5	N7
P11	R11	P13	N11
P15	N13	L11	P9
J9	N5	L7	J3

Fig. 5.12 The 4-batch shuffling arrangement for the SMBWR.

Fig. 5.10 shows that both the 3- and 4-batch schemes are able to meet the design criterion for power peaking by having Channel $F_{\Delta H}$ below the specification limit (< 1.5). In terms of the margin to the design limit, it is shown that the 4-batch configuration has a better margin, which might be due to a better shuffling arrangement. The core reactivity feedback is shown in Fig. 5.13. While there is no significant difference in the DC by having a multi-batch configuration, the CVC is becoming more negative with increasing number of batches used, which could partially offset the benefit of requiring fewer control rods.

By comparing the 3- and 4-batch management schemes, it can be observed that the 4-batch scheme offers a more favourable performance compared to the 3-batch scheme as it has lower power peaking, less excess reactivity, and more negative CVC. A stronger negative CVC could be advantageous if some of the excess reactivity is to be controlled by varying the coolant inlet temperature and, as a result, void distribution. It should also be noted that a more negative CVC means the core would require more control rods in order to ensure shutdown margin as reactivity is added between the hot full power and cold zero power shutdown conditions. Although the 4-batch scheme has a shorter cycle duration and thus the reactor would have more

frequent outages throughout its lifetime, the cycle duration is still longer than a year, and therefore should be acceptable. In addition, in a 4-batch scheme the fuel could achieve a higher discharge burnup, and thus, have better fuel utilisation.

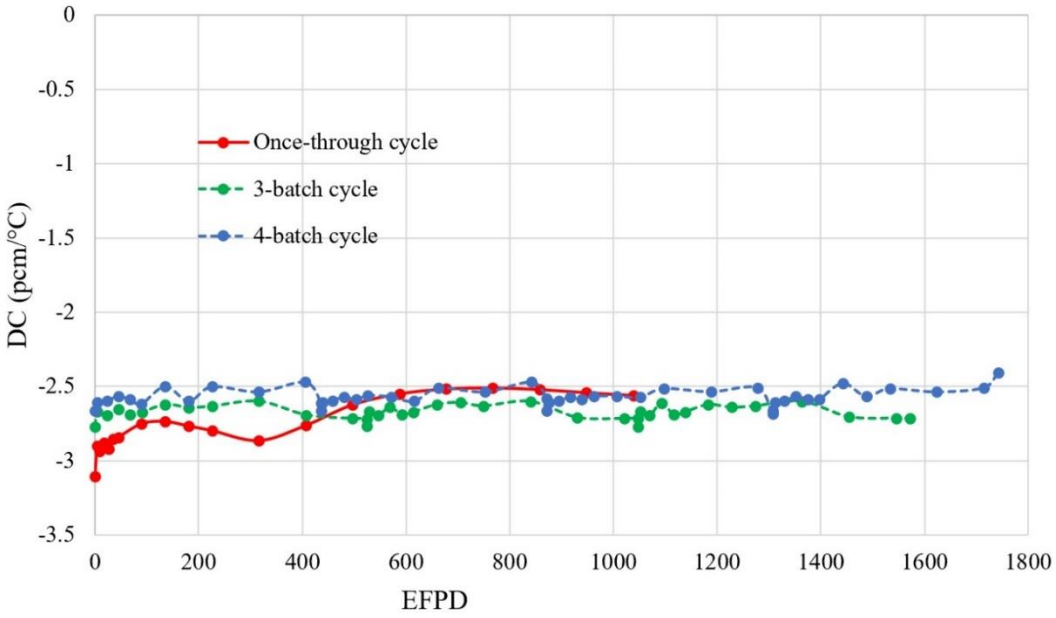

(a)

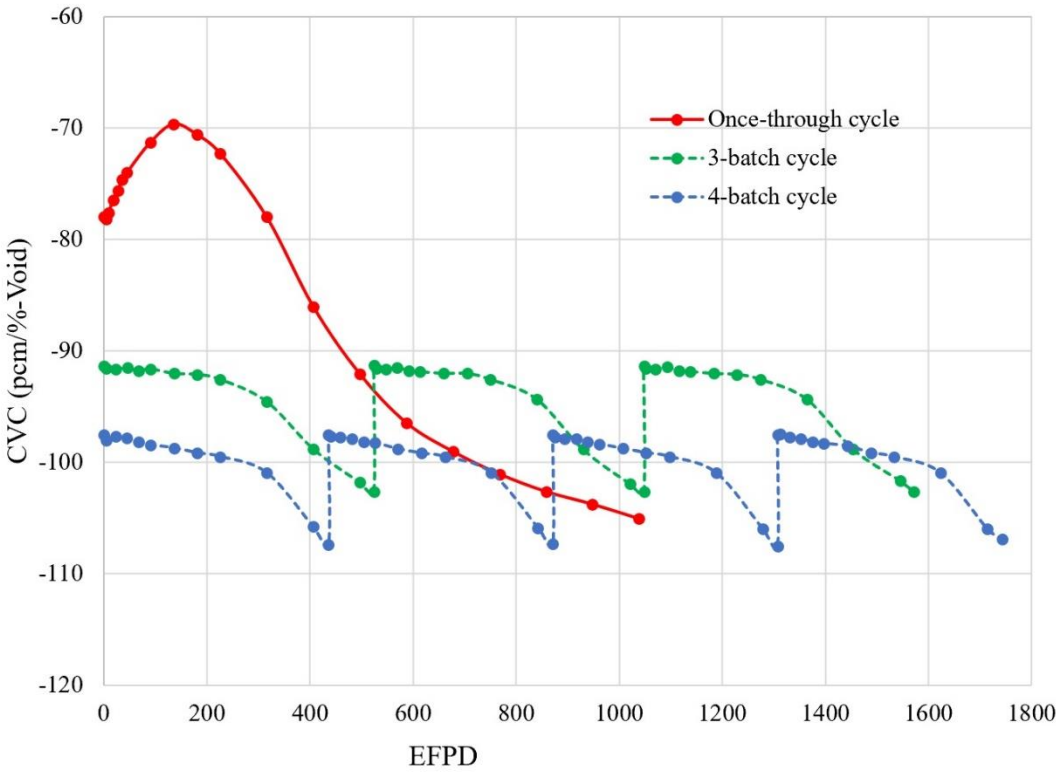

(b)

Fig. 5.13 Reactivity feedbacks of the SMBWR with various fuel management schemes: (a) Doppler Coefficient; (b) Coolant Void Coefficient.

5.4.2 Coolant void variation

Coolant temperature variation can be used to control the reactivity in the SMBWR by leveraging the MTC and CVC to reduce the excess reactivity. It is known that the coolant density changes with temperature, resulting in changes in neutron moderation. In addition, assuming that the linear heat generation is fixed, the increase in core inlet temperature will reduce the inlet subcooling and extend the boiling length inside the core, which also leads to less efficient moderation. Fig. 5.14 shows the reactivity suppression worth when the coolant inlet temperature of the SMBWR with a 4-batch fuel management scheme is increased to 275 and 280 °C. It is shown that increasing the core inlet temperature to 275 °C would reduce excess reactivity by approximately 200 pcm, while increasing it further to 280 °C would give a further reduction of approximately 600 pcm. This coolant temperature reactivity suppression by itself seems insignificant; however, it is still important to understand to what extent the combination of a multi-batch arrangement and coolant temperature variation is able to reduce the core excess reactivity and hence reduce the system dependency on control rods.

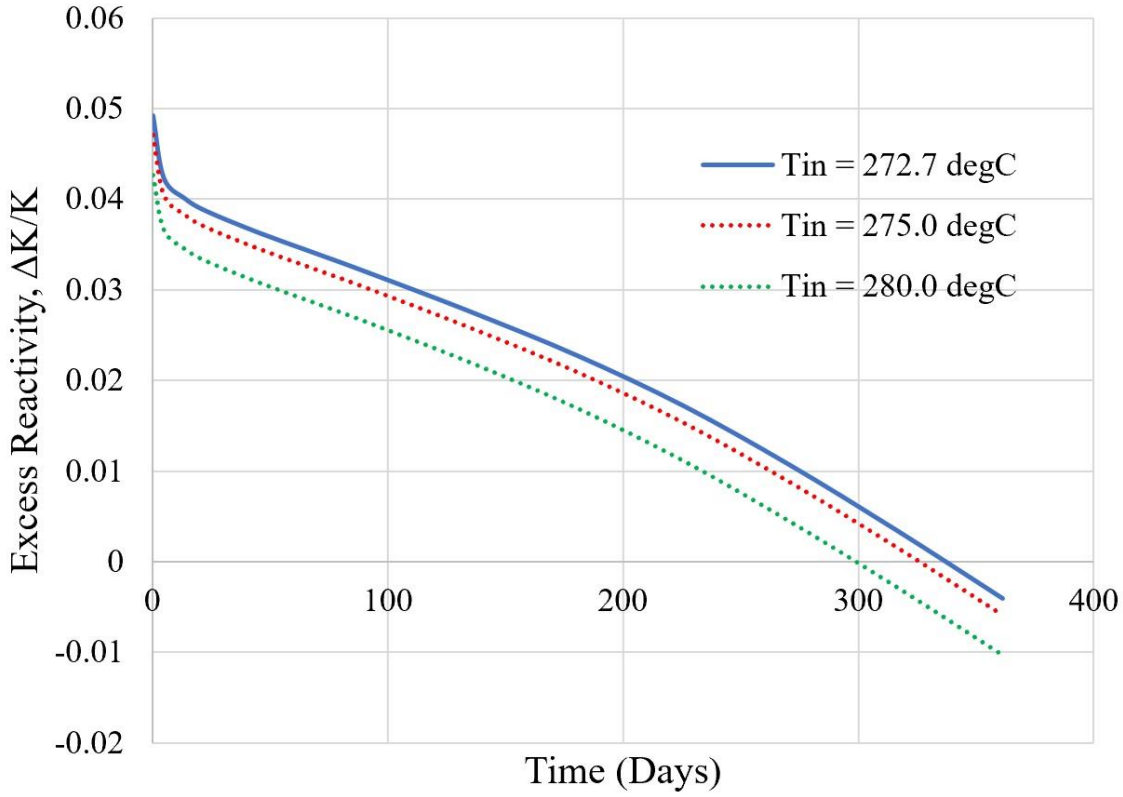

Fig. 5.14 Excess reactivity at various core inlet temperatures.

In order to change the core inlet temperature in a BWR system with natural circulation, the most feasible way is by adjusting the feedwater inlet temperature, without perturbing the reactor coolant inventory. Therefore, it is important to investigate the effect of this feedwater inlet temperature adjustment on the thermodynamic performance of the SMBWR steam cycle. Fig. 5.15 shows that in order to increase the core inlet temperature to 280 °C without changing the mass flow rate inside the core, the feedwater temperature has to be increased to approximately 247 °C. The reactor vessel steam outlet condition would not change as steam exiting the reactor is at saturation conditions. The boiling length is increased as the inlet subcooling temperature is reduced at constant mass flow rate and linear power. Fig. 5.16 shows the relevant power and cycle efficiency, which are affected by this increase in feedwater temperature, while Fig. 5.17 shows how it would affect the core exit quality and steam flow rate exiting the reactor vessel to the superheater.

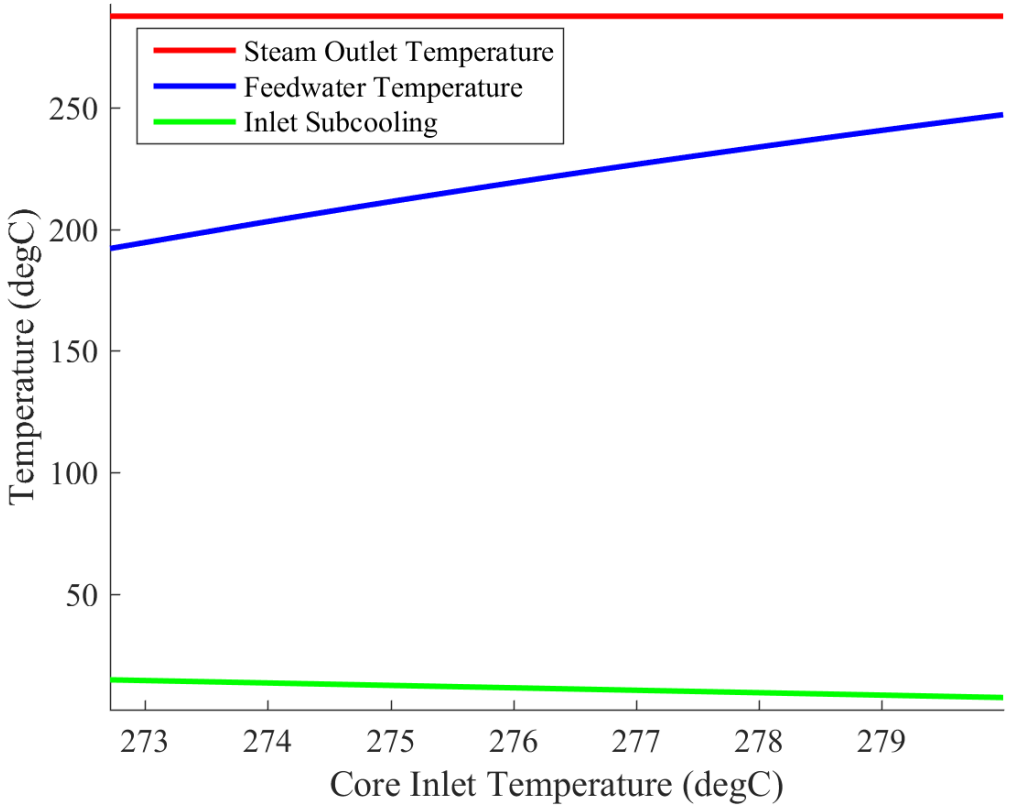

Fig. 5.15 Relevant SMBWR operating temperatures at various core inlet temperatures.

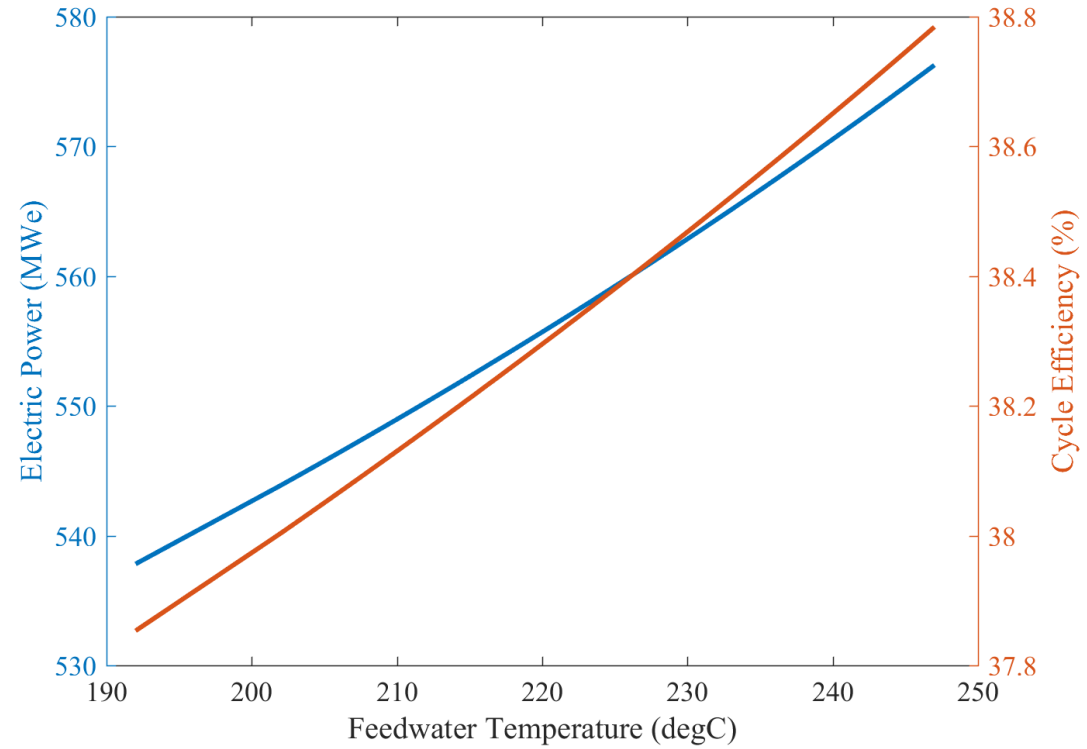

Fig. 5.16 Electric power produced and resulting steam cycle efficiency of the SMBWR at various feedwater temperatures.

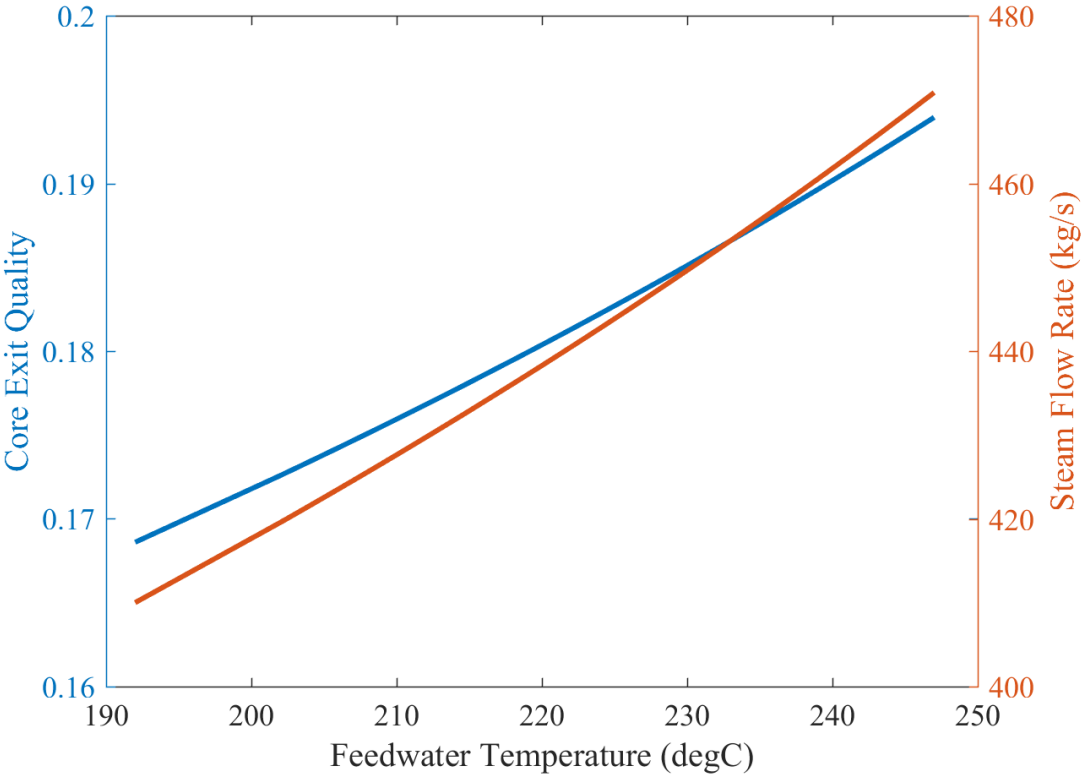

Fig. 5.17 SMBWR core exit quality and steam flow rate at various feedwater temperatures.

It is observed from Fig. 5.16 and Fig. 5.17 that as the feedwater temperature increases, the core exit quality increases and more steam can be taken out from the reactor vessel to the superheater. This phenomenon leads to higher production of electric power and a small increment in cycle thermal efficiency. Although increasing feedwater temperature seems to give some incentive for the SMBWR (reducing excess reactivity and improving cycle thermal efficiency), there is a limit to the extent the feedwater temperature could be increased. A higher feedwater and core inlet temperature would increase the length of the boiling region inside the core. Although it is beneficial to have a longer boiling region in terms of excess reactivity, the MCPR margin becomes smaller as the core inlet temperature approaches the saturation temperature. Another effect that needs to be considered is that, although a higher feedwater temperature means higher cycle thermal efficiency, more external heat is required, as shown in Fig. 5.18. Therefore, if the source of external heat for the SMBWR does not come from a clean energy source, the CO_2 emissions for the hybrid system are going to be increased.

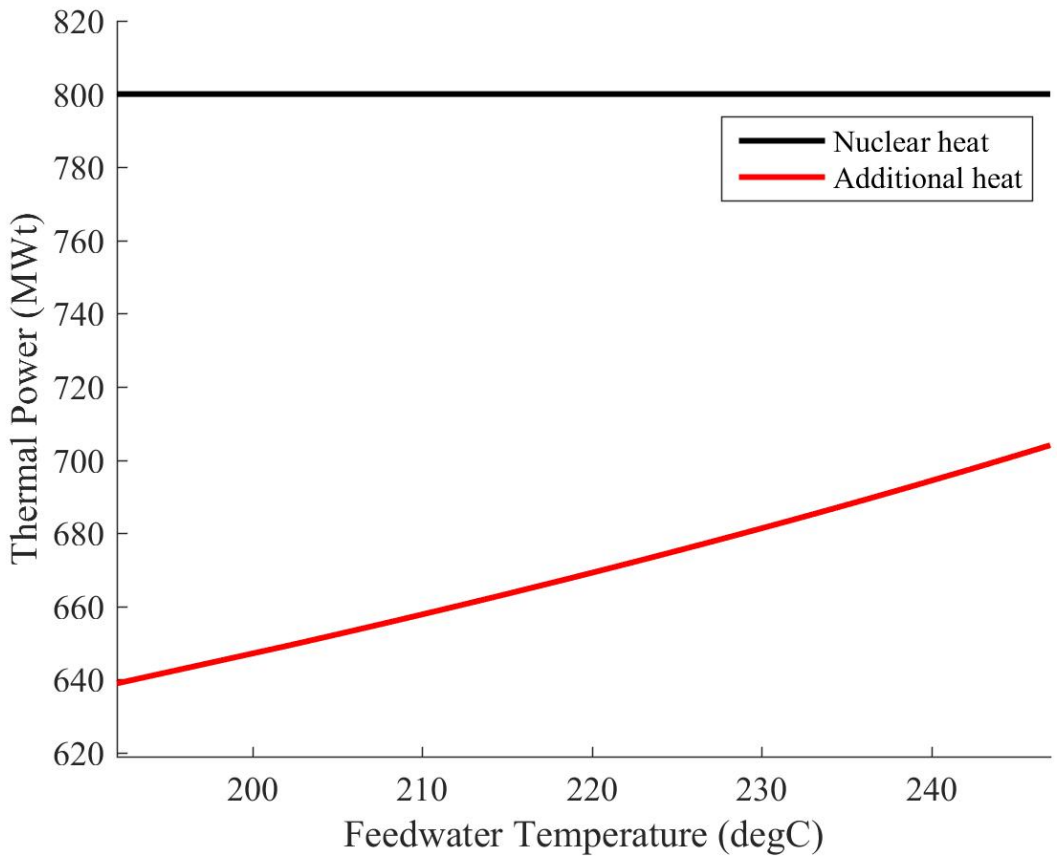

Fig. 5.18 Proportion of heat sources for the SMBWR at various feedwater temperatures.

5.5 Summary of SMBWR Core Design Study

A core design study of the SMBWR was performed which included comparison of three different core geometries, study of the axial fuel loading and its effect on the core neutronics and thermal-hydraulics, and also study of fuel management and its ability to supress the excess reactivity throughout depletion. An investigation of these effects on the neutronic, thermal-hydraulic and thermodynamic performance of the SMBWR has been carried out, and the core design proposed for the SMBWR, which offers a reasonable compromise between the considered effects, is listed in Table 5.4. In addition, axial zoning of fuel enrichment and poison concentration are selected for the SMBWR in order to flatten the axial power distribution. Due to the nature of SMBWRs, which are smaller size BWRs with natural circulation, it is found that partial length fuel rods are not necessarily required in the SMBWR core, which would simplify the fuel assembly design and possibly reduce its manufacturing costs. In order to reduce the reactivity swing in the SMBWR while keeping the power peaking below the safety limit throughout the depletion cycle, the combination of a multi-batch fuel arrangement, coolant temperature variation, and control rods are required.

A comparison of core design and average performance parameters of the SMBWR with the ESBWR **[49]** and ABWR **[54]** are shown in Table 5.5. It can be observed that the SMBWR could achieve a much smaller core pressure drop compared to the ESBWR and ABWR, which is one of the reasons why the SMBWR does not require partial length fuel rods. The core pressure drop is a strong function of mass flow rate and length. The SMBWR and ESBWR could have smaller core pressure losses compared to the ABWR due to their smaller mass flow rate per assembly and shorter core length. The assembly flow rate of the SMBWR is quite similar to that of the ESBWR as both reactors are designed to operate with natural circulation. However, it is shown that the core pressure losses of the SMBWR are approximately a third of that of the ESBWR due to the reasons mentioned above. It can be observed that the total length of fuel rods of the SMBWR are approximately 1 m shorter than the ESBWR. This difference in total length along with differences in the boiling length (as shown in Fig. 5.19) are the major contributors to the difference in the core pressure drop. As discussed earlier, the pressure losses in a 2-phase flow are higher than those of single-phase flow. Fig. 5.19 shows that the ESBWR has a longer boiling length compared to the SMBWR. Besides that, the fact that the SMBWR fuel assembly has only 4 spacer grids is also contributing to the difference in pressure drop, as the total core pressure drop is also proportional to the local pressure losses due to spacers.

Table 5.4 Core and Vessel Design Specification of the SMBWR

Parameter	SMBWR
Thermal power (MWth)	800
Electric power (MWe)	515
Core power density (kW/L)	48.2
Average linear power (kW/m)	12.6
System pressure (MPa)	7.17
Feedwater inlet temp (°C)	192
Active fuel length (m)	2.70
Number of fuel assemblies	256
Minimum required height of chimney (m)	3.58
Estimated vessel diameter (m)	3.94
Estimated vessel height (m)	16.3
Core mass flow rate (kg/s)	2414.3
Core pressure drop (kPa)	50.70
Assembly fuel loading (kgU)	141.08
Void coefficient (pcm/%void)	-98
Core exit quality (%)	17.0

Table 5.5 Comparison of Core Average Parameters of Several BWRs

Parameter	SMBWR	ESBWR	ABWR
Active fuel rod height (m)	2.70	3.05	3.71
Total fuel rod height / FA length (m)	2.92	3.79	4.47
No. of FAs	256	1132	872
No. of spacer grids	4	6	8
Core mass flow rate (kg/s)	2414.3	9583	14500
Core pressure drop (kPa) at 7.1 MPa	50.70	71.8	168.2

Fig. 5.19 shows the core average axial void distributions and Fig. 5.20 shows the core average relative power distribution of the SMBWR at Middle of Cycle (MOC) compared to the reference values of the ESBWR and ABWR. The SMBWR has slightly higher power in the

upper part of the reactor compared to the ESBWR and ABWR because both ESBWR and ABWR fuel assemblies have partial length rods, which is not the case in the SMBWR fuel assembly. It can be observed from Fig. 5.19 and Fig. 5.20 that the suggested SMBWR core design has comparable performance to those of the ESBWR and ABWR.

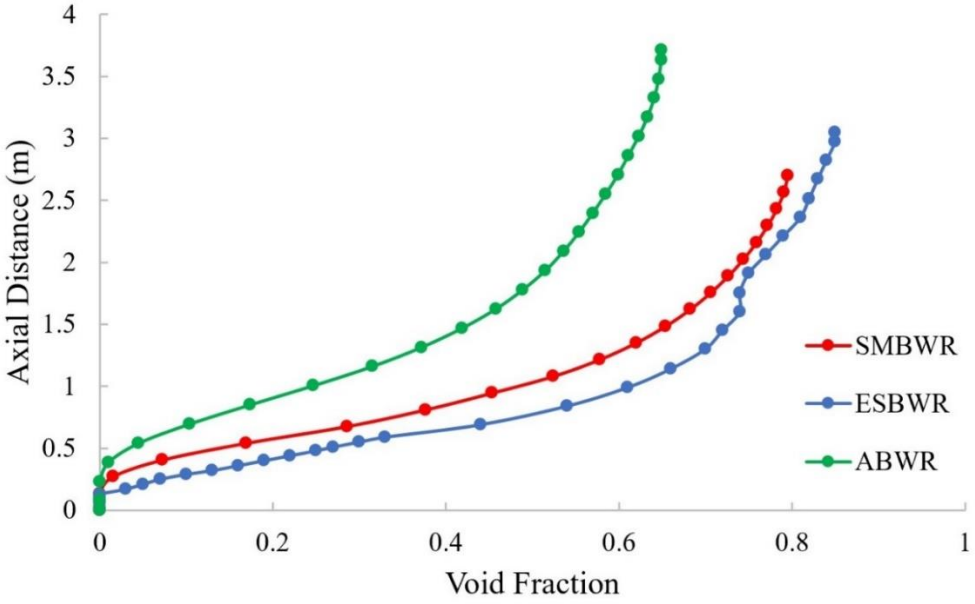

Fig. 5.19 Core average axial void distributions of the SMBWR, ESBWR and ABWR at MOC.

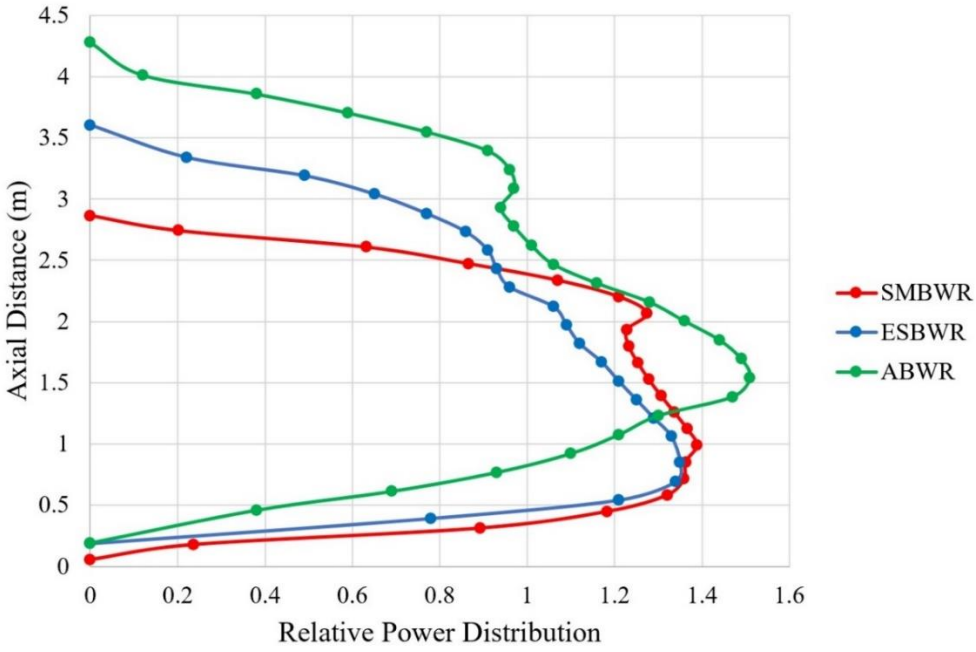

Fig. 5.20 Core average axial power distributions of the SMBWR, ESBWR and ABWR at MOC.

Chapter 6: Implications of SMBWR Hybrid Energy System

This chapter focuses on the implications of having the hybrid energy system of the Small Modular Boiling Water Reactor combined with external superheaters. As mentioned in the previous chapters, the main benefit of having the hybrid system is the capability to adjust the system power to match the load, while maintaining the reactor operation at full power. However, depending on the heat source for the superheater system, the SMBWR emissions rate could be higher than a stand-alone NPP. Therefore, the load-following performance of the SMBWR, the fuel consumption, carbon emission rate, and the overall hybrid system's effect on the economics of the NPP are included as the scope of analysis in this chapter.

6.1 SMBWR Manoeuvring Capability

As mentioned in Chapter 1, since NPPs usually have high capital costs and low operating costs, load-following with nuclear plants is normally undesirable. However, with the increased share of intermittent renewables in the energy mix and the reduction of fossil fuels, the load-following capability of NPP is becoming increasingly important. The main incentive for developing a hybrid SMBWR with external superheaters is therefore to develop a more flexible load-following scheme for the NPP. Having external superheaters allows the SMBWR to adjust its power to some extent while maintaining the reactor operation at full power. By having such power manoeuvring capability, the fixed capital costs of the reactor can be efficiently recovered. In addition, the adjustment of electric power output to meet the demand could be achieved faster. The ramping rate to load-follow in NPP is usually slower than fossil-fuelled power plants because of the thermal inertia and limits on materials in the reactor. The aim of this section is to investigate to what extent the hybrid SMBWR could reduce its load while maintaining the reactor operation at full power.

It is mentioned above that the heat source options for the external superheaters include conventional gas boilers, waste heat from gas turbines and heat stored in molten salt from CSP technology. By having fossil fuel as the external heat source (either from conventional boilers or gas turbines), the SMBWR would have a stable power supply throughout the year. In addition, the waste heat from the economiser would still be relatively high grade and have the potential to be exploited further through a heat network system. In the case of using the heat stored in molten salt from CSP plant, the main benefit is, of course, that the whole system will

become cleaner, practically eliminating CO_2 emissions during the electricity generation process. However, the latter system has to carefully consider the variation in seasonal generation from the CSP system and manage this intermittency issue depending on the local conditions.

A representative case is selected where the SMBWR operates at a reference pressure (approximately 7.17 MPa). It is designed to have two external superheaters (one superheater and one reheater), with the steam cycle configuration following the BOP displayed in Fig. 2.5. The external heat source for these superheaters is assumed to be the waste heat from two units of SGT5-4000F gas turbines. As shown in the specification listed in Table 4.2, the exhaust air enters the superheaters at approximately 599 °C. The outlet temperature of the superheaters is approximately 300 °C in order to allow some temperature difference to assure effective heat transfer to steam produced by the reactor (approximately 287.7 °C at 7.17 MPa). By examining this temperature range of the hot air, it can be observed that the range is similar to the temperature range of molten salts routinely used for energy storage in concentrated solar plants. The molten nitrate salt (60 wt-% $NaNO_3$ and 40 wt-% KNO_3) is known to be a stable mixture and suitable for use as a thermal storage medium within a temperature range of 260 °C to 621 °C **[42]**. Therefore, the hybrid SMBWR could potentially be developed to switch its operation mode to a cleaner heat source, such as a Concentrated Solar Power system. Furthermore, the residual heat from the superheaters still has some potential of further use, such as a heat source in a district heating system or it can be recycled back to the solar plant.

As mentioned briefly in the previous section, one of the possible ways for the SMBWR to load-follow is by having a bypass line with a throttling valve to direct some portion of the steam from the HP turbine inlet directly to the LP turbines. This bypass line is represented by point no. 36 in Fig. 2.5. When the power demanded by the grid is less than 100%, some portion of the exhausted steam from the HP turbine could be bypassed through line 36. The reduction of steam mass flow entering the reheater should be proportional to the load and the heat supplied to the reheater in order to maintain the steam operating condition before entering the LP turbine. By doing this, the load reduction could be achieved by adjusting the heat provided to the reheater and reducing the steam mass flow rate entering the HP turbine and, thus, reducing the work produced by the turbine. With this scheme, the load reduction could be achieved without changing the thermal power and other operating conditions of the reactor such as the feedwater and recirculation flow rates. By using the MATLAB model of the hybrid SMBWR steam cycle, the load-follow capability of the hybrid SMBWR by using bypass line no. 36 was investigated and the results are shown in the following figures.

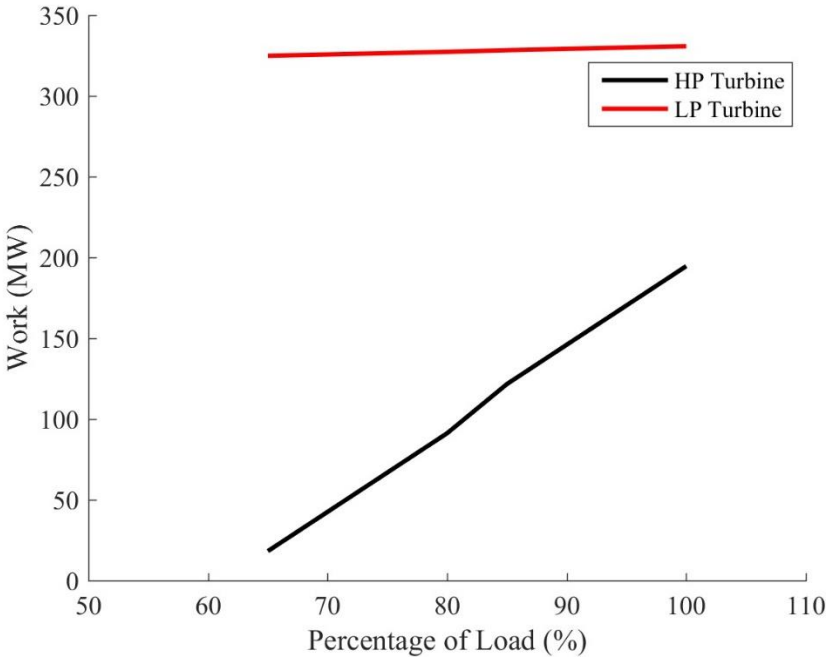

Fig. 6.1 Turbine work of SMBWR at various loads.

The load reduction is achieved by bypassing steam before entering the HP turbine. Thus, both the work from the HP turbine and the reheater heat are affected by this reduction, as shown in Fig. 6.1 and Fig. 6.2. Fig. 6.3 shows that the load reduction is achieved while the reactor power is maintained at 100% and only the externally supplied heat is reduced. There is a limit, however, on how much load reduction could be achieved without reducing reactor power. As the steam exhausted from HP turbine is used to preheat the feedwater before entering the reactor, the HP turbine would require some amount of steam intake all the time and this becomes one of the limiting factors for this load-following scheme. Fig. 6.4 shows the *T*-*s* diagram of the steam cycle at various loads. The points displayed in Fig. 6.4 correspond to the state points specified in Fig. 2.5. The *T*-*s* conditions at every state point in the steam cycle remain constant at various loads. Thus, it can be observed that the load reduction is achieved without changing the steam thermal conditions − only by adjusting the mass flow rate entering the LP turbine. Therefore, the thermal fatigue of the turbine blades due to load-following operation could be minimised. The iteration process to calculate the new steady-state condition when the load changes was done by conserving the superheater operating conditions, and varying the steam mass flow through the reheater, while gradually reducing the load from the full power condition. However, at a certain point, the energy balance iteration would not be able to converge unless the superheater outlet temperature is increased. This small perturbation to superheater conditions in order to help the model reach a convergence is the reason for

several slope changes in the HP turbine line in Fig. 6.1 and the reheater heat line in Fig. 6.2, which also affects the cycle efficiency.

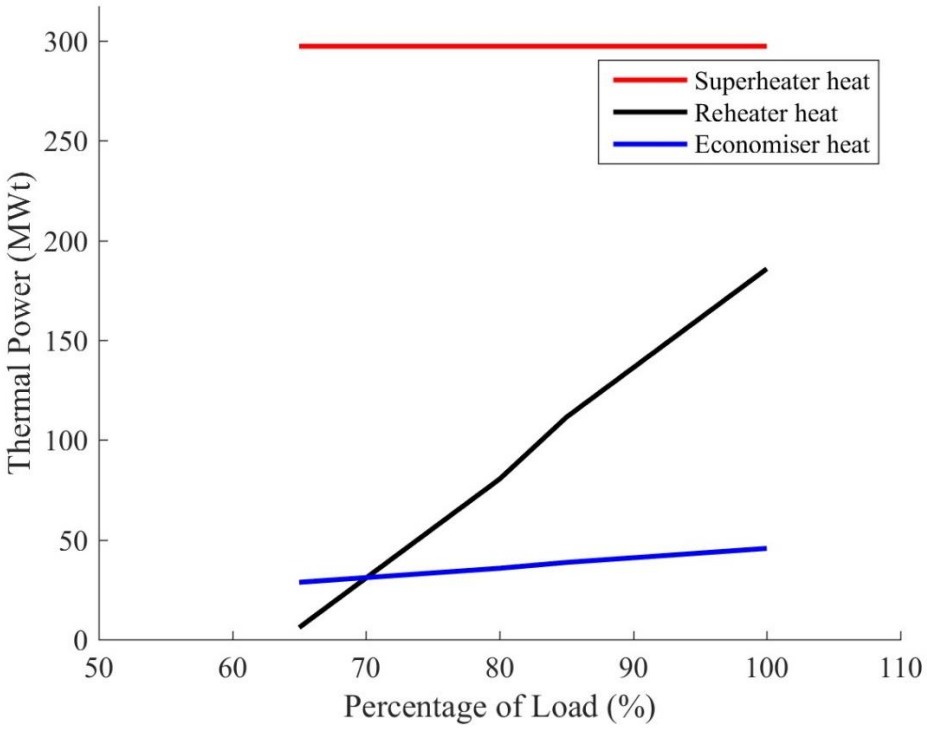

Fig. 6.2 External heat profile of SMBWR at various loads.

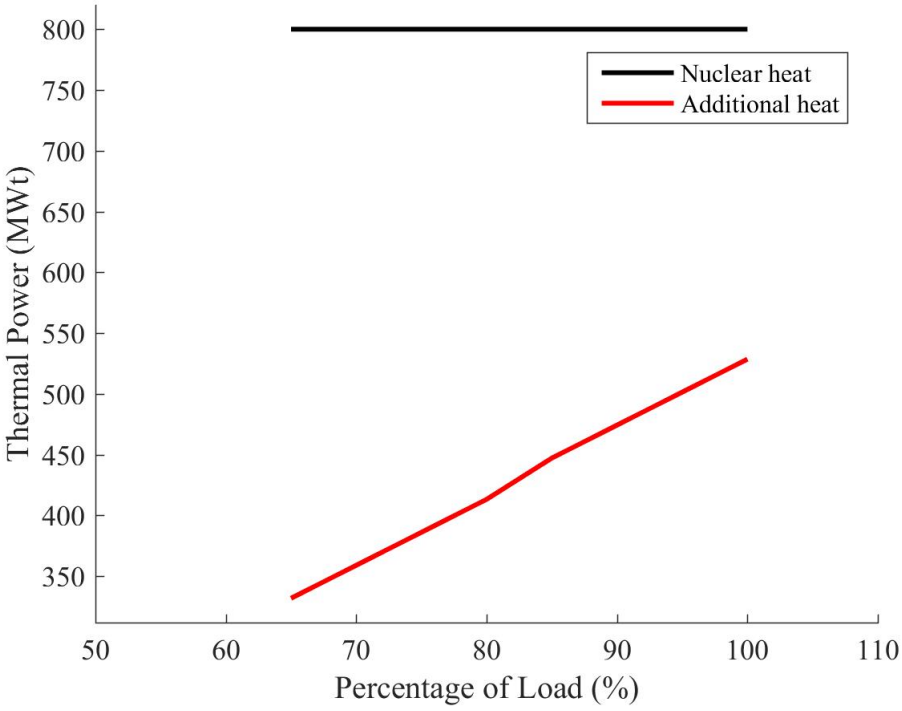

Fig. 6.3 Heat distribution of SMBWR at various loads.

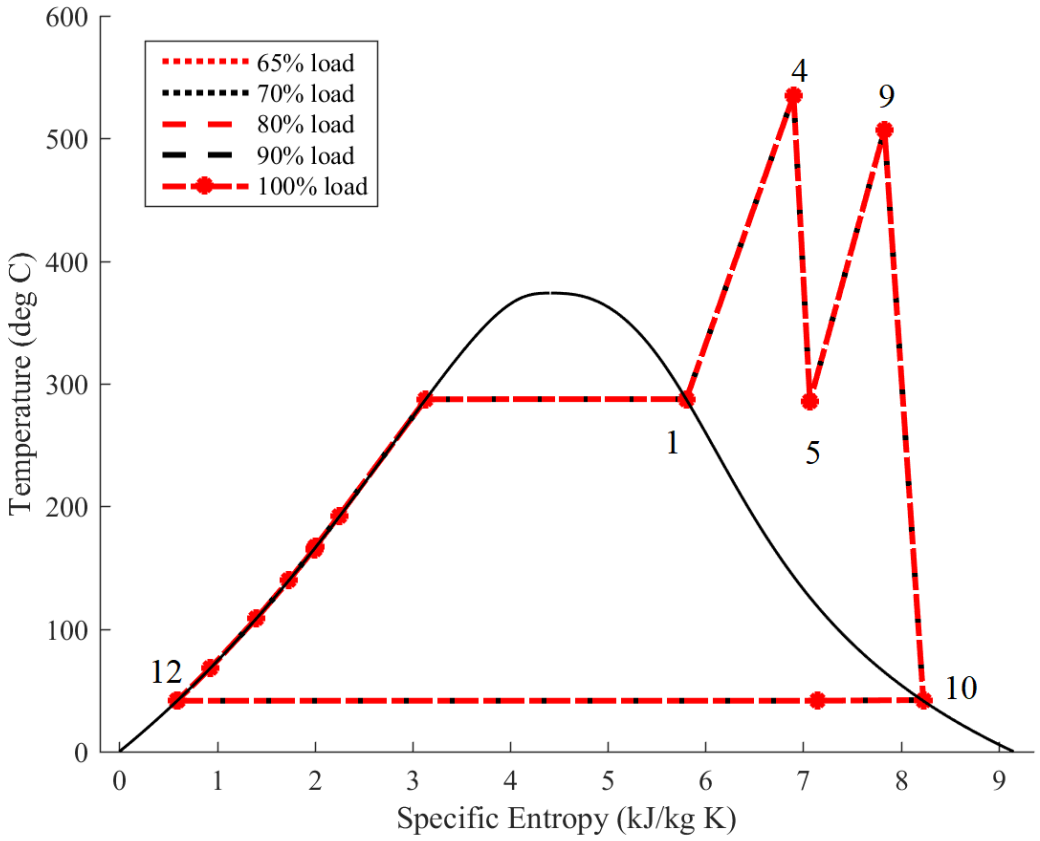

Fig. 6.4 *T-s* diagram of SMBWR at various loads.

In most BWRs, load reduction to about 70% of reactor power is usually possible by reducing the speed of reactor circulation pump, while control rods are used if load reduction below 70% of reactor power is required **[55]**. Varying reactor power by varying the recirculation rate should be easier and faster compared to relying on control rods. The difficulties of using control rods to load-follow could be in maintaining the core power distribution and axial offset. Thus, it would have a slower ramping rate than if the same task is accomplished by relying on the recirculation rate. In the case of a BWR with natural circulation, the elimination of the reactor recirculation pump will force such a system to rely solely on control rods to perform load-following. Although the scope of manoeuvring capability analysis reported in this section includes only steady-state operation, the fact that the SMBWR has an ability to load-follow to some extent without changing the reactor thermal power offers an alternative load-following method for BWR systems with natural circulation.

Another interesting point to be studied is the effect of load reduction on the efficiency of the power conversion cycle. Fig. 6.5 shows that both nuclear thermal efficiency and combined cycle efficiency are reduced when the load is reduced. The thermal efficiency of the hybrid

SMBWR is reduced from approximately 39.2% to about 30% when the load is reduced from 100% to 65%, while the combined cycle efficiency is reduced from about 48.8% at 100% load to 41.3% at 65% load. It should be noted that, although the combined cycle efficiency at 100% load is smaller than the thermal efficiency of CCGT in general, which could be as high as 60%, the heat rejected from the economiser of the representative case of the SMBWR is still at a relatively high temperature (~272 °C). This exhaust temperature is higher than exhaust temperatures common in most of the CCGT plants. Therefore, the cycle efficiency could potentially be increased if one could exploit the remaining heat from this exhaust air for other purposes. There is an option to exploit this heat to provide the heat for the low-pressure feedwater heater. By using the waste heat from the economiser to provide heat for the low-pressure feedwater heater, more steam from the LP turbine, otherwise bled to power the feedwater heating cascade, could be used to produce power, thus, improving the cycle efficiency. However, this option is not investigated further in this thesis as the main objective for the SMBWR BOP design is keeping open the possibility to use stored heat from CSP technology. There is a lower limit of 260 °C for the solar salt operating temperature.

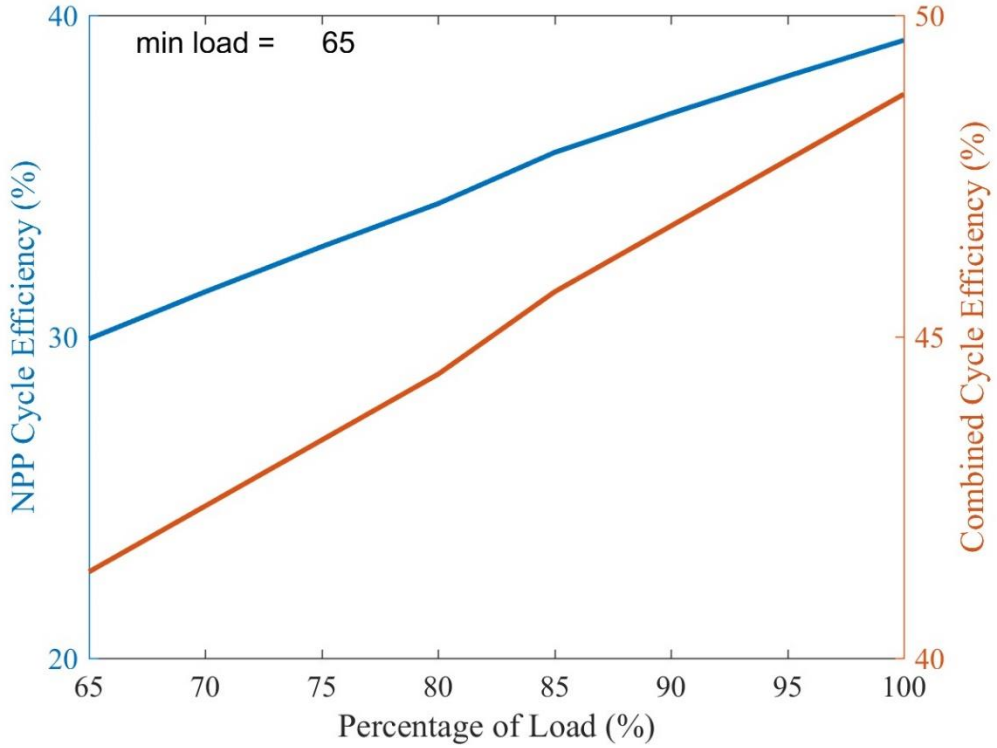

Fig. 6.5 The effect of load reduction on cycle efficiency.

6.2 Fuel Consumption & Emissions Rates

It is expected that, if natural gas is used as the external heat source for the superheater system, the CO_2 emission rate of the SMBWR system would become an issue. Therefore, it is important to quantify and compare SMBWR emissions with both stand-alone gas turbines and combined cycle gas turbines systems. Table 6.1 shows the comparison of the SMBWR with stand-alone gas turbines and CCGT systems. The reference gas turbines used in Table 6.1 are those developed by Siemens **[51]**. The SMBWR type-1 in Table 6.1 are 2 units of SMBWR, with a capacity of 515 MWe each, and use conventional gas boilers for the superheating system. The SMBWR type-2 is a single SMBWR unit combined with 2 units of gas turbines. It can be observed that even though the SMBWR combined with fossil-fuel superheaters would have a higher emission rate compared to a stand-alone NPP, their emission rate would still be considerably smaller compared to a stand-alone gas turbine system or CCGT system. It is also observed that the fuel consumption rate and emission rate is smaller for the SMBWR system which utilises a conventional boiler compared to the one using gas turbines.

Table 6.1 Comparison of SMBWR with Other GT Systems

Parameter	**SMBWR**		**Stand-alone GT**	**CCGT**
	1	**2**		
GT type	N/A	SGT5-4000F	SGT5-8000HL	SGT5-4000F
No. of GT required	0	2	2	2
Total electric power (MWe)	1030	1173	1186	950
Power conversion cycle efficiency (%)	39.2	48.8	42.8	59.7
Fuel consumption rate (Btu/kWh)	3502	4668	7972	5716
Emission rate (gCO_2/kWh)	185.84	247.70	422.99	303.29

It should be noted that the values for the SMBWR displayed in Table 6.1 refer only to the plant operating at 100% capacity (where both the reactor and superheater have maximum power output). If the plant operates below 100% capacity, Case 1, where the external heat is supplied by a conventional gas boiler, would obviously require less external heat supply and,

thus, result in lower fuel consumption and emission rates. There is also a possibility to reduce the gas turbines load of Case 2 along with the nuclear plant load reduction, which would result in a similar reduction in emission rate when the system load is less than 100% capacity.

It is also understandable that in the low-carbon economy, the fact that the SMBWR has a higher emission rate compared to a stand-alone NPP might raise a concern. However, any renewable energy source such as wind or solar as an alternative to nuclear energy is also not entirely emissions free. In the absence of a large scale and economically competitive energy storage option, the intermittency of renewables will normally require a backup generation system. This backup generator can be either a conventional gas power system or diesel generators, both of which would have non-negligible amounts of CO_2 emissions. The hybrid energy system of a wind turbine and a diesel generator or gas turbine can be categorised into low penetration, medium penetration and high penetration. Low penetration systems are defined as systems which have less than 20% average wind power and less than 50% contribution to total generation. Medium penetration systems operate with average wind power contributions between 20% and 50% and instantaneous penetration levels between 50% and 100%, while high penetration systems are defined as systems with average wind power fractions above 50% and instantaneous penetration levels between 100% and 400% **[56]**. Table 6.2 displays the estimated emission rates and fuel consumption of wind power and its backup generation system. In creating Table 6.2 it is assumed that the backup generation system is powered by natural gas with a power conversion efficiency of 40%, and the average wind power penetration for the high, medium and low penetration cases are assumed to be 80%, 40%, and 15%.

Table 6.2 Fuel Consumption and Emission Rates of Wind Turbine Hybrid Energy Systems

Parameter	High Penetration	Medium Penetration	Low Penetration
Average wind power penetration (%)	80	40	15
Fuel consumption rate (Btu/kWh)	1706	5118	7251
Emission rate (gCO_2/kWh)	90.52	271.56	384.71

Table 6.2 shows that the fuel consumption and emission rates of the wind turbine hybrid energy system are very much dependent on the level of average wind power penetration. It is shown that a SMBWR hybrid energy system could consume less fuel and produce less

emissions compared to a wind turbine hybrid energy system at low and medium levels of wind power penetration. Even the hybrid system of a SMBWR and gas turbines, which produces the highest amount of CO_2 emissions compared to the other types of SMBWR hybrid energy system is still able to compete with wind turbine hybrid systems at medium wind power penetration, in terms of its fuel consumption and emission rates. It should be noted that Table 6.2 is created with the assumption that the backup generator for the wind turbine system uses a natural gas boiler. In the case where a diesel generator is used as backup power for the wind turbine hybrid system, the emission rate of the wind turbine hybrid system would be higher compared to the values shown in Table 6.2.

6.3 Economic Benefit of SMBWR Hybrid Energy Systems

Simple economic analysis is performed to highlight the benefits of SMBWR hybrid energy systems. Table 6.3 shows the comparison of component costs which are used to determine the levelised cost of electricity (LCOE) for the SMBWR and some other electricity generation sources. The reference values used for the other power generation technologies listed in Table 6.3 are taken from BEIS estimated values for projects to be commissioned after 2025 **[57]**. While the value reported for the SMBWR accounts for the costs of both NPP and CCGT as reference.

Table 6.3 Levelised Cost Estimates for Specific Power Generation Technologies

Parameter	CCGT	CCGT CHP	OCGT	NPP	Onshore Wind	Solar PV	SMBWR
Pre-Development	0	1	1	7	4	6	4
Construction	6	12	16	66	42	49	36
Fixed O & M	2	4	6	11	10	8	7
Variable O & M	3	5	3	5	5	0	5
Fuel Costs	41	63	60	5	0	0	38
Carbon Costs	30	42	43	0	0	0	24
Decommissioning / Waste	0	0	0	2	0	0	1
Steam Revenue	0	-31	0	0	0	0	-17
LCOE (£/MWh)	82	96	129	96	61	63	96

The estimated value for SMBWR LCOE listed in Table 6.3 uses the representative case of a SMBWR hybrid system combined with 2 SGT5-4000F gas turbines as mentioned above. A weighted average value of the component costs is calculated in proportion to electric output of the NPP and GT, as shown in Eq. (6-1). Since, the waste heat from the economiser is still potentially usable, the component costs of the CCGT with CHP are used in calculating the weighted average values for the SMBWR. Taking the weighted average value to calculate the component costs of the SMBWR hybrid system means that we assume the component costs of a large NPP are equal to those of an SMR. Although this assumption might not be entirely correct, as the economies of scale would make component costs of SMRs higher than those of large reactors, especially for the first of a kind (FOAK) project, one could argue that the costs would be comparable when we consider the saving through standardisation and modularisation **[58]**. It can be seen from Table 6.3 that the SMBWR hybrid system would have higher fuel costs compared to a stand-alone NPP. In addition, carbon costs, which are usually negligible for NPP, are present in the SMBWR hybrid system. Although the fuel costs and carbon costs are relatively high, the hybrid SMBWR could achieve a similar LCOE to the stand-alone NPP, due to its higher thermal cycle efficiency.

$$Comp.Cost_{SMBWR} = \frac{Comp.Cost_{NPP} * Power_{SMBWR} + Comp.Cost_{CCGT-CHP} * Power_{GT}}{Power_{SMBWR} + Power_{GT}} \qquad (6\text{-}1)$$

Compared to CCGT, wind, and solar generation, the LCOE for the SMBWR hybrid system is still higher. For the CCGT, the LCOE is slightly lower than the hybrid SMBWR because the thermal efficiency of the CCGT system is higher than the SMBWR (it can reach as high as 60% at full power). As for wind and solar generation, although their LCOE is considerably below that of the SMBWR, solving the intermittency issue would be a challenge and have associated costs and carbon footprints which are not included in this analysis. At the moment, the only possible solution for the intermittency problem for wind and solar is by having backup generation systems running in-parallel with the renewables, although in the future storing the excess energy in the form of electrical, mechanical or thermal energy could be possible. Both solutions would definitely increase the LCOE of intermittent renewable generation. Thus, it can be concluded that the LCOE of the SMBWR hybrid system can, in principle, compete with solar and wind hybrid systems.

Fig. 6.6 shows the sensitivity of the estimated LCOE of both the stand-alone NPP and the hybrid SMBWR to their capacity factor. It can be seen from Fig. 6.6 that the LCOE of the

SMBWR is less sensitive to the reduction in capacity factor compared to the stand-alone NPP. In order to generate Fig. 6.6, it is assumed that the pre-development costs, construction costs, fixed O & M costs, and decommissioning costs are fixed and independent of the capacity factor, while the rest of the components are varied proportionately to the capacity factor. Fig. 6.6 highlights the economic benefit of a SMBWR hybrid energy system as load-following with such a system would become more economically sensible. In conclusion, it is shown that the SMBWR is able to trade a slight increase in carbon emissions with operational flexibility.

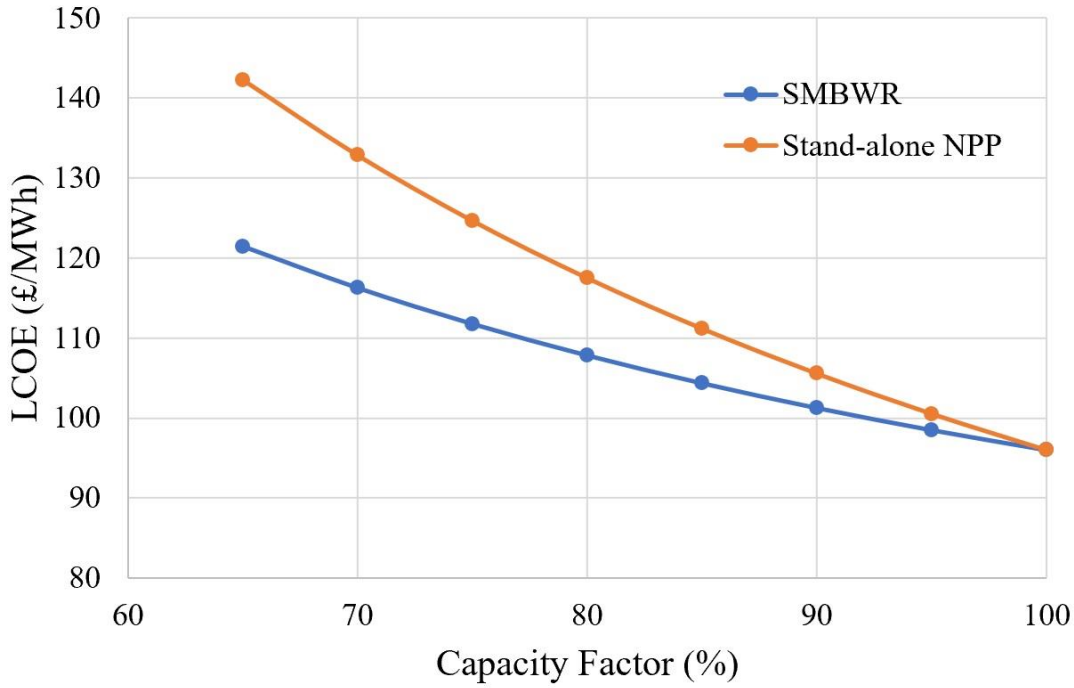

Fig. 6.6 Sensitivity of LCOE of a stand-alone NPP and a hybrid SMBWR to capacity factor.

Chapter 7: Conclusions

7.1 Summary of The Findings

The trade-offs between sustainability, energy security, and affordability need to be considered in order to transform our current energy supply to low-carbon technologies. The path forward lies between two alternatives: reducing the storage costs for the intermittent renewables or developing an affordable and more flexible form of nuclear power. A conceptual design of a hybrid energy system of a Small Modular Boiling Water Reactor combined with external superheaters is proposed in this thesis as one of the possible solutions. This SMBWR has several distinctive design features. First, it is a BWR-type small modular reactor, which offers several potential economic advantages and would be more attractive to developing countries compared to a large reactor. It is designed to adopt natural circulation for coolant recirculation within the reactor pressure vessel. It is easier to develop natural circulation in a BWR compared to a PWR due to the fact that a BWR could rely on a two-phase flow driving head. The last design feature considered is an external steam superheater added at the outlet of SMBWR. The superheater consists of 3 pieces of equipment: a superheater, reheater and economiser. The external heat can be provided by a conventional gas boiler, waste heat from gas turbines, or heat stored in molten salt from Concentrated Solar Power technology. The addition of the superheaters allows the elimination of the Moisture Separator and Reheater and high-pressure feedwater heater from the SMBWR Balance of Plant. In addition, the combination of having both a superheater system and natural circulation allows the SMBWR to eliminate both the steam dryer and recirculation pump, which can potentially reduce the vessel size. Therefore, the objectives of this thesis work are to demonstrate that the concept is practical and achievable and to quantify the hypothesised benefits of the SMBWR with external superheaters.

In order to minimise the development effort and speed up the potential deployment of the SMBWR, many of the reference design parameters set for the SMBWR are taken from the ESBWR design, such as the basic fuel assembly geometry and dimensions of other components inside the vessel. Fig. 2.1 summarises the analytical methods used in this work in order to investigate the performance of the SMBWR. For the neutronics and core analysis, PANTHER is used as a simulation tool using homogenised cross-section libraries prepared in WIMS. For thermal-hydraulics, sub-channel analysis is performed with COBRA-EN to analyse the core

performance, while the natural circulation loop is modelled with MATLAB. In terms of thermodynamics, the BOP of the hybrid system of a SMBWR combined with external superheaters is also modelled in the MATLAB environment.

The investigation on the effect of the SMBWR operating pressure on its performance was carried out with a motivation to quantify the potential for further improvement of power cycle efficiency. The operating pressure values considered in the study have ranged between 6.5 and 10 MPa. The findings showed that increasing the SMBWR operating pressure from 6.5 to 10 MPa has no significant effect on the neutronic performance. In terms of thermal-hydraulics, increasing the SMBWR operating pressure from 6.5 to 10 MPa at a constant primary coolant flow rate and constant core subcooling enthalpy ($\Delta H_{Subcooling}$) would result in a reduction of the recirculation rate and, thus, more steam is delivered to the steam cycle. It is also found that an increase in pressure would reduce the core pressure drop but increase the minimum chimney height required to develop natural circulation. The reason for that is the fact that, at higher pressure, the difference between saturated liquid density and saturated vapour density becomes smaller. Thus, a taller chimney is required at higher pressure in order to overcome the total pressure losses in the loop with buoyancy forces. Most importantly, it is also found that increasing the SMBWR operating pressure from 6.5 to 10 MPa would improve its thermal efficiency slightly by $\Delta\eta$ of about 1.2%. In terms of combined cycle efficiency, the improvement is more substantial if the external heat provided to the superheaters is taken from the waste heat of gas turbines rather than from a gas boiler. However, it should also be noted that using the waste heat of gas turbines would also result in higher CO_2 emissions from the SMBWR hybrid system compared to using a gas boiler as the external heat to superheaters. Based on these findings, there is not enough evidence to support the high-pressure operation of the SMBWR. Therefore, the system pressure for the proposed SMBWR design is kept the same as in conventional BWRs, which is 7.17 MPa.

In order to investigate the trade-offs between neutron leakage (neutronics), the chimney height requirement for natural circulation (thermal-hydraulics) and the dimensions of the core, three different core configurations with different length to diameter ratios are selected for the study. By comparing the three different core geometries, it is found that the configuration with 192 FAs has relatively large variation of reactivity feedbacks throughout depletion cycle and requires a taller chimney to develop natural circulation for its recirculation loop. It is also found that even though the configuration with 368 FAs has the lowest core pressure drop and the most stable reactivity feedbacks throughout the depletion cycle out of the three designs

considered, the diameter of the reactor vessel might be too large for factory fabrication and subsequent transport to site, which is the main idea behind the potential cost savings of SMRs. In addition, this core configuration is not the most neutronically efficient design among the three designs considered with relatively high leakage and short cycle length. Therefore, the final core design for the SMBWR is proposed to have 256 FAs, which gives an approximate length to diameter ratio of 1.01.

Further analysis of the SMBWR fuel assembly suggested that it would be beneficial to have an axial fuel zoning similar to existing BWR practice. Natural uranium is placed at the top and bottom of the assembly to minimise the axial leakage of fast neutrons, the highest fuel enrichment is located in the middle and a higher poison concentration is located at the bottom. However, unlike a conventional BWR fuel design, the SMBWR core has a relatively small pressure drop. Therefore, it would not necessarily require partial length fuel rods, which could be a significant design simplification. In order to help in reducing the excess reactivity, as in large BWRs, in the SMBWR, the core is suggested to have a 4-batch fuel arrangement. Furthermore, it is also found that SMBWR could utilize coolant void variation to reduce excess reactivity to some extent. However, in the absence of the recirculation pumps used in conventional BWRs, the core void fraction could be controlled by feedwater subcooling through variation of power conversion cycle parameters. The design parameters and core performance characteristics for the proposed SMBWR are displayed in Table 7.1.

The investigation on power manoeuvring capability of the SMBWR found that the combined system can reduce its load down to 65% by only reducing the external heat provided to the superheaters, keeping the reactor operation at full rated power. This load reduction could be achieved without perturbing the steam conditions around the cycle but only varying the steam flow rate between different components of the cycle, for example, by bypassing some fraction of the steam before entering the HP turbines and directing it after throttling to the LP turbine. The power conversion cycle efficiency of the SMBWR hybrid system is reduced from approximately 39.2% to about 30% when the load is reduced from 100% to 65%. As expected, the LCOE of SMBWR is less sensitive to changes in the plant capacity factor compared to a stand-alone NPP.

Table 7.1 Proposed Design Specification of SMBWR

Parameter	Value
Thermal power (MWth)	800
Electric power (MWe)	515
Core power density (kW/L)	48.2
System pressure (MPa)	7.17
Feedwater inlet temp (°C)	192
Active fuel length (m)	2.70
Number of fuel assemblies	256
Minimum required height of chimney (m)	3.58
Estimated vessel diameter (m)	3.94
Estimated vessel height (m)	16.3
Core mass flow rate (kg/s)	2414.3
Core pressure drop (kPa)	50.70
Assembly loading (kgU)	141.08
Void coefficient (pcm/%void)	~ - 98
Core exit quality (%)	17.0
Average linear power (kW/m)	12.6
Hydrogen to heavy metal ratio	3.90
Inlet subcooling temperature difference (°C)	14.70
MCPR	1.41
Maximum fuel centreline temperature (°C)	1201.8

7.2 Recommendations for Future Work

The SMBWR design development still requires future work before it can progress to the next, more detailed, design stage. The following list compiles recommendations for future work on the SMBWR development:

- Core Transient and Stability Analysis: The stability of BWR systems is one of the major concerns from the safety and design point of view. It is known that BWR systems can become unstable due to interaction between neutronics and thermal-hydraulics or purely thermal-hydraulic oscillations. Transient performance and stability analysis of the SMBWR core are therefore required to ensure its safe operation.

- Load-Following Transient Analysis: The work on power manoeuvring capability described in this thesis has only covered steady-state operation. Throttling valves have been used extensively in steam Rankine cycles as a means to reduce steam pressure providing confidence that the SMBWR could rely on the bypass line with a throttling valve when a load reduction is required. However, the dynamic response of the hybrid system should be investigated to confirm adequate system response to dynamic changes in power demand.
- Detailed Economic Assessment: The economic analysis presented in Chapter 5 is fairly simple. It was only used to estimate the LCOE of the SMBWR and its sensitivity to the capacity factor of the system. A more thorough economic assessment is required to make the case for SMBWR development, including opportunities to reduce manufacturing, transportation and construction costs by standardisation, modularisation and mass production in factories.

References

[1] Intergovernmental Panel on Climate Change, “Summary for Policymakers, Climate Change 2014: Mitigation of Climate Change,” Contribution of working Group III to the fifth assessment report, IPCC, Cambridge, UK, 2014.

[2] Committee on Climate Change, “Reducing the UK's carbon footprint,” *Technical Report*, CCC, London, UK, April 2013.

[3] Committee on Climate Change, “Net Zero The UK’s contribution to stopping global warming,” Technical Report, CCC, London, UK, May 2019.

[4] Department for Business, Energy & Industrial Strategy, “Updated Energy and Emissions Projections 2017,” Annual Report, London, UK, January 2018.

[5] MIT Energy Initiative, “The Future of Nuclear Energy in a Carbon-Constrained World, An Interdisciplinary MIT Study” Technical Report, MITEI, Cambridge, MA, USA, 2018.

[6] Nuclear Energy Agency, “Technical and Economic Aspects of Load Following with Nuclear Power Plants,” Technical Report on Nuclear Development, OECD-NEA, France, June 2011.

[7] S. M. Bragg-Sitton, R. Boardman, M. Ruth, O. Zinaman, and C. Forsberg, “Rethinking the Future Grid: Integrated Nuclear Renewable Energy Systems,” Proceedings of *The 9th Nuclear Plants Current Issues Symposium: Moving Forward*, Charlotte, NC, USA, December 7-10, 2014.

[8] J. D. Jenkins, “What’s Killing Nuclear Power Power in US Electricity Markets? Drivers of Wholesale Price Declines at Nuclear Generators in the PJM Interconnection,” Working Paper Series MIT Center for Energy and Environmental Policy Research, CEEPR WP 2018-001, MIT CEEPR, Cambridge, MA, USA, January 2018.

[9] F. J. de Sisternes, J. D. Jenkins, and A. Botterud, “The value of energy storage in decarbonizing the electricity sector,” *Applied Energy*, vol. 175, p. 368-379, 2016.

[10] A. F. Wibisono and E. Shwageraus, “Thermodynamic performance of Pressurized Water Reactor power conversion cycle combined with fossil-fuel superheater,” *Energy*, vol. 117, p. 190-197, 2016.

[11] M. A. Darwish, F. M. Al Awadhi, and A. O. Bin Amer, “Combining the nuclear power plant steam cycle with gas turbines,” *Energy*, vol. 35, no. 12, p. 4562–4571, 2010.

[12] A. Zaryankin, M. Lyskov, S. Arianov, and A. Rogalev, “Super powerful steam

superheaters and turbines for hybrid nuclear power plants," *Journal of Power Technologies*, vol. 91, no. 4, p. 191–197, 2011.

[13] ALSTOM, "ARABELLE^{TM} STEAM TURBINE For Nuclear Power Plant," Nuclear Product Solutions, ALSTOM, France, 2012.

[14] Y. Ko and M. S. Kazimi, "Conceptual Design of an Annular-Fueled Superheat Boiling Water Reactor," Advanced Nuclear Power Technology Program, MIT-ANP-TR-130, CANES, MIT, Cambridge, MA, USA, October 2010.

[15] U. S. Atomic Energy Commission - Reactor Engineering Division, Chicago Operations Office, "Small nuclear power plants," Division of Technical Information, USAEC, COO-284 TID-4500, vol. 1, October 1966.

[16] R. L. Loftness, *Nuclear Power Plants: Design, Operating Experience, and Economics*, Van Nostrand, MI, USA, 1964.

[17] P. E. Florido, J. E. Bergallo, and A. Clausse, "Economics of combined nuclear–gas power generation," *Nuclear Engineering and Design*, vol. 195, p. 109–115, 2000.

[18] C. W. Forsberg and J. C. Conklin, "A Nuclear-Fossil Combined-Cycle Power Plant for Base-Load and Peak Electricity," Proceedings of *Transactions-American Nuclear Society Annual Meeting*, ANS, Boston, MA, USA, June 24-28, 2007.

[19] General Electric, "The ESBWR Plant General Description GE Hitachi Nuclear Energy," *Plant Description*, GE Hitachi, Wilmington, NC, USA, 2011.

[20] Y. Kawabata, M. Matsuura, S. Hiruko, and T. Hoshi, "The Plant Feature and Performance of DMS (Double MS: Modular Simplified & Medium Small Reactor)," Proceedings of *the 16th International Conference on Nuclear Engineering*, ICONE16-48949, ASME, Orlando, Florida, USA, May 11-15, 2008.

[21] R. E. Lyons and A. R. M. Roulstone, "Production Learning In A Small Modular Reactor Supply Chain," Proceedings of *the International Congress on Advances in Nuclear Power Plants*, ICAPP 2018, ANS, Charlotte, NC, USA, April 8-11, 2018.

[22] R. P. McDonnell, "Transport Strategy for Small Modular Reactors," MPhil Dissertation, University of Cambridge, Cambridge, UK, 2017.

[23] International Atomic Energy Agency, "Advances in Small Modular Reactor Technology Developments," A Supplement to: IAEA Advanced Reactors Information System (ARIS), Vienna, Austria, September 2014.

[24] K. Shirvan, "Development of Optimized Core Design and Analysis Methods for High Power Density BWRs," PhD Thesis, MIT, Cambridge, MA, USA, 2013.

[25] General Electric, "The ABWR Plant General Description," Plant Description, GE

Energy, Wilmington, NC, USA, 2006.

[26] M. Furuya, “Experimental and Analytical Modeling of Natural Circulation and Forced Circulation BWRs Thermal-Hydraulic, Core-Wide, and Regional Stability Phenomena,” IOS Press, Amsterdam, Netherlands, 2006.

[27] ANSWERS, “WIMS - A Modular Scheme for Neutronics Calculations,” *User Guide for Version 10*, The ANSWERS Software Package, ANSWERS/WIMS/REPORT/014, ANSWERS, UK, Dec, 2015.

[28] A. Morrison, “PANTHER User guide,” Technical report, British Energy, Barnwood, UK, 2003.

[29] D. Basile, R. Chierici, M. Beghi, E. Salina, and E. Brega, “COBRA-EN - an Upgraded Version of COBRA-3C/MIT Code for Thermal-Hydraulic Transient Analysis of Light Water Reactor Fuel Assemblies and Cores,” COBRA-EN User's Manual, 1 September, 1999.

[30] S. Quezada-Garcia, E. Espinosa-Martinez, G. Espinosa-Paredes, and A. Vazquez-Rodriguez, “Power-feedwater temperature operating domain for a BWR driven by natural convection,” *Progress in Nuclear Energy*, vol. 86, p. 110-119, 2016.

[31] N. E. Todreas and M. S. Kazimi, *Nuclear Systems I Thermal-hydraulic Fundamentals*, Taylor & Francis Group, LLC, New York, NY, USA, 1990.

[32] J. N. Reyes, Jr. , “Governing Equation in Two-phase Fluid Natural Circulation Flows,” Annex 6 of *Natural Circulation in Water Cooled Nuclear Power Plants*, IAEA-TECDOC-1474, IAEA, Vienna, Austria, November 2005.

[33] C. F. Colebrook, “Turbulent flow in pipes with particular reference to the transition region between the smooth and rough pipe laws,” *Journal of the Institution of Civil Engineers*, vol. 11, p. 133-156, 1939.

[34] M. Asker, O. E. Turgut, and M. T. Coban, “A review of non iterative friction factor correlations for the calculation of pressure drop in pipes,” *Bitlis Eren Univ Journal of Science & Technology*, vol. 4, no. 1, p. 1-8, 2014.

[35] T. K. Serghides, “Estimate friction factor accurately,” *Chemical Engineering*, vol. 91, p. 63-64, 1984.

[36] A. A. Armand and G. G. Treschev, “Investigation of the Resistance during the Movement of Steam-Water Mixtures in Heated Boiler Pipe at High Pressures,” *Atomic Energy Research Establishment Lib/Trans*, vol. 816, 1959.

[37] C. J. Geankoplis, *Transport Processes and Unit Operations*, Third Edition, Prentice-Hall International, Inc., New Jersey, NJ, USA, 1978.

[38] K. Rehme, “Pressure drop correlations for fuel elements spacers,” *Nuclear Technology*, vol. 17, p. 15-23, 1972.

[39] M. Holmgren, “X Steam Tables, Excel macros, IF-97 Steam Tables,” 2007. [Online]. Available: http://xsteam.sourceforge.net/. [Accessed: 10-Dec-2015].

[40] D. Ion and P. D. Codrut, “Efficiency Assessment of Condensing Steam Turbine,” Proceedings of *Advances in Environment, Ecosystems and Sustainable Tourism*, p. 203-208, 2013.

[41] The International Association for the Properties of Water and Steam, “Revised Release on the IAPWS Industrial Formulation 1997 for the Thermodynamic Properties of Water and Steam,” IAPWS, Lucerne, Switzerland, August 2007.

[42] H. L. Zhang, J. Baeyens, J. Degreve, and G. Caceres, “Concentrated solar power plants: Review and design methodology,” *Renewable and Sustainable Energy Reviews*, vol. 22, p. 466-481, 2013.

[43] A. Al Kindi, “Thermodynamic Analysis of Load-Following Operation of a LWR Combined with a Gas Fired Superheater,” MPhil Thesis, University of Cambridge, Cambridge, UK, 2017.

[44] Westinghouse, “The Westinghouse AP1000 Advanced Nuclear Plant,” *Plant Description*, Westinghouse Electric Co., LLC, USA, 2003.

[45] E. W. Lemmon, R.T. Jacobsen, S. G. Penoncello, and D. G. Friend, “Thermodynamic Properties of Air and Mixtures of Nitrogen, Argon, and Oxygen from 60 to 2000 K at Pressures to 2000 MPa,” *Journal of Physical and Chemical Reference Data*, vol. 29, no. 3, p. 331-385, 2000.

[46] R. Temple, “Generation mPower, B&W mPower^{TM} Program,” IAEA SMR Technical Meeting, Chengdu, China, September 3, 2013.

[47] J. Leppanen, “Serpent - a Continuous-energy Monte Carlo Reactor Physics Burnup Calculation Code,” User's Manual, VTT Technical Research Centre of Finland, June 18, 2015.

[48] Y. Bilodid, D. Kotlyar, E. Shwageraus, E. Fridman, and S. Kliem, “Hybrid microscopic depletion model in nodal code DYN3D,” *Annals of Nuclear Energy*, vol. 92, p. 397-406, 2016.

[49] GE Hitachi Nuclear Energy, “ESBWR Design Control Document Tier 2,” Revision 10, GE-Hitachi Nuclear Energy Americas LLC, April 2014.

[50] General Electric, “GENERAL ELECTRIC BWR THERMAL ANALYSIS BASIS (GETAB): DATA, CORRELATION AND DESIGN APPLICATION,” Technical report, NEDO-10958-A, California, USA, January 1977.

[51] SIEMENS, “We power the world with innovative gas turbines,” *Siemens gas turbines portfolio*, Article-No. PGDG-B10006-05-4A00 Dispo 05400 BR 0418. [Online]. Available: http://www.siemens.com/gasturbines. [Accessed: 21-Nov-2018].

[52] M. Nakamura, “Core Design and Operation of ABWR,” Hitachi ABWR Seminar in Cambridge University, Global Nuclear Fuel – Japan Co., Ltd., Cambridge, UK, March 2017.

[53] U. S. Nuclear Regulatory Commission, “Westinghouse Technology System Manual Section 2.2 Power Distribution Limit,” Rev 0508, Technical Report, 0519 - R304P, USNRC, US, 2008.

[54] GE Nuclear Energy, “ABWR Design Control Document Tier 2,” Rev. 4, GE Nuclear Energy Americas LLC, March 1997.

[55] B. Gjorgiev and M. Čepin, “Nuclear Power Plant Load Following: Problem Definition and Application,” Proceedings of *the International Conference Nuclear Energy for New Europe 2011*, Bovec, Slovenia, September 12-15, 2011.

[56] J. A. Frye, “Performance-Objective Design of a Wind-Diesel Hybrid Energy System for Scott Base, Antartica,” MEng Thesis, University of Canterbury, Canterbury, UK, 2006.

[57] Department for Business, Energy & Industrial Strategy, “Electricity Generation Costs,” Technical Report, London, UK, November 2016.

[58] C. A. Lloyd, A. R. M. Roulstone, and C. Middleton, “The Impact of Modularisation Strategies on Small Modular Reactor Cost,” Proceedings of *the 18th International Congress on Advances in Nuclear Power Plants*, ICAPP 2018, ANS, Charlotte, NC, USA, April 8-11, 2018.

Appendix A: Review of NPPs with Fossil Fuel-fired Superheaters

A.1 The Elk River Reactor

The Elk River Reactor was a natural-circulation, indirect-cycle boiling water reactor with a separate coal-fired superheater. It was owned by US Atomic Energy Commission (AEC) and operated by the Rural Cooperative Power Association (RCPA) of Elk River, Minnesota. The reactor thermal power was 58.2 MWth and the coal-fired superheater was rated at 14.8 MWth. The plant net electrical output was 22.5 MWe **[15]**. The Elk River reactor was only operated from 1962 until 1968 before undergoing decommissioning in the following years. The design features of the Elk River Reactor are shown in Table A.1.

Table A.1 Design Features of The Elk River Reactor **[14]**

Parameter	ERR
Location	Elk River, Minnesota, USA
Owner / Operator	USAEC / RCPA
Type	Indirect cycle BWR, with conventional fuel fired superheater
Reactor thermal power (MWth)	58.2
Superheater power (MWth)	14.8
Electric power (MWe)	22.5
Overall efficiency (%)	30.8
Fuel	(4.3% U^{235}, 0.3% U^{238}, 95.4% Th)O_2
No. of FAs	148
Power density (kW/l)	39.6
Vessel diameter (ft)	7
Vessel height (ft)	25
Turbine steam temperature (°F)	825
Turbine inlet pressure (psig)	620
Mass flow rate (lb/hr)	225,000

A.2 Indian Point Unit 1

Indian Point unit 1 was a pressurized water reactor with a separate oil-fired superheater. It was designed by B&W, owned and operated by Consolidated Edison. The plant was located at Buchanan, New York, USA. The thermal power of the plant was 585 MWth and its superheater was 215 MWth. The net electrical output of the plant was 255 MWe. The reactor started its operation on September 16, 1962 and achieved full power operation on January 29, 1963. Indian Point unit 1 was shut down on October 31, 1974 because the emergency core cooling system did not meet regulatory requirements **[14]**. The design features of Indian Point unit 1 are shown in Table A.2.

Table A.2 Design Features of Indian Point Unit 1 **[16]**

Parameter	**Indian Point unit 1**
Location	Buchanan, New York, USA
Owner / Operator	Consolidated Edison
Type	PWR, with conventional oil-fired superheater
Reactor thermal power (MWth)	585
Superheater power (MWth)	215
Electric power (MWe)	255
Overall efficiency (%)	32.0
Fuel	93% UO_2-ThO_2
No. of FAs	120
Power density (kW/l)	76
Vessel diameter (ft)	9.75
Vessel height (ft)	36.8
Turbine steam temperature (°F)	1000
Turbine inlet pressure (psig)	420
Mass flow rate (lb/hr)	2,200,000

A.3 The Carolinas – Virginia Tube Reactor (CVTR)

The CVTR was a heavy water moderated and cooled pressurized tube reactor, with an oil-fired superheater. It was located at Parr, South Carolina, USA. The plant electrical output was 19 MWe **[14]**. Table A.3 lists the design features of the CVTR.

Table A.3 Design Features of The Carolinas – Virginia Tube Reactor **[16]**

Parameter	CVTR
Location	Parr, South Carolina, USA
Owner / Operator	Carolinas – Virginia Nuclear Power Associates
Type	Pressure tube, heavy water cooled and moderated reactor, with conventional oil-fired superheater
Reactor thermal power (MWth)	65
Electric power (MWe)	19
Overall efficiency (%)	29.2
Fuel	1.5 and 2.0% UO_2
Power density (kW/l)	15
Vessel diameter (ft)	6.9
Vessel height (ft)	8
Turbine steam temperature (°C)	385
Turbine inlet pressure (MPa)	2.75

Appendix B: Review of Two-Phase Flow Models

A wide variety of models are available to represent two-phase flow. A two-phase flow model can either be described as a pseudo single-phase fluid (mixture) or a multifluid flow. In LWR applications, the three-equation Homogeneous Equilibrium Model (HEM) is adequate for predicting the pressure drop in a flow channel under high-pressure steady state conditions. A specified relative velocity or a four-equation mixture model is required to calculate the void distribution due to the vapour tendency to move faster than the liquid, while the two-fluid model (six-equation model) might be best to model two-phase flow under fast transients **[31]**.

B.1 One-Dimensional Two-Fluid Non-Equilibrium Model

In the two-fluid model, three conservation equations are written for each phase (six-equation model). The governing conservation equation in each phase (k) is written as follows **[32]**:

- Mass

$$\frac{\partial}{\partial t}\{\rho_k \alpha_k\} + \frac{\partial}{\partial z}\{\rho_k v_k \alpha_k\} = \Gamma_k \quad \text{(B-1)}$$

- Momentum

$$\frac{\partial}{\partial t}\{\rho_k v_k \alpha_k\} + \frac{\partial}{\partial z}\{\rho_k v_k^2 \alpha_k\} = \{\Gamma_k \vec{v}_{ks} \,.\, \vec{n}_s\} + \sum_{i=1}^{N}\{\vec{F}_{wk} \,.\, \vec{n}_s\}_i - \frac{\partial}{\partial z}\{\rho_k \alpha_k\} + \{\vec{F}_{sk} \,.\, \vec{n}_s\} + \{\rho_k \alpha_k\}\, \vec{g} \,.\, \vec{n}_s \quad \text{(B-2)}$$

- Energy

$$\frac{\partial}{\partial t}\{\rho_k u_k^0 \alpha_k\} + \frac{\partial}{\partial z}\{\rho_k h_k^0 v_k \alpha_k\} = \Gamma_k h_{ks}^0 - \left\{p_k \frac{\partial \alpha_k}{\partial t}\right\} + \sum_{i=1}^{N}\left\{q_k'' \alpha_k \frac{P}{A}\right\}_i - \{\rho_k g v_k \alpha_k\} + \{Q_{sk}\} \quad \text{(B-3)}$$

B.2 Homogeneous Equilibrium Model (HEM)

The HEM is the simplest of the two-phase fluid transport models. The transport equations are derived from the two-phase mixture equations with the assumption that the velocity of the liquid phase and vapour phase are equal (homogeneous) and both phases are at the saturation condition **[32]**. The restrictions imposed in this model are as follows:

- Thermal Equilibrium ($T_l = T_v = T_{sat}$) or Saturated Enthalpies ($h_l = h_f$ and $h_v = h_g$)
- Equal Phase Pressures ($p_l = p_v = p$)

- Equal Velocities ($v_l = v_v = v_m$)

The relevant mixture properties are calculated by Eq. (B-4) to Eq. (B-6).

$$\rho_m = \{\rho_v \alpha + \rho_l (1-\alpha)\} \quad \text{(B-4)}$$

$$v_m = \frac{\{\rho_v v_v \alpha + \rho_l v_l (1-\alpha)\}}{\rho_m} \quad \text{(B-5)}$$

$$h_m = \frac{\{\rho_v h_v \alpha + \rho_l h_l (1-\alpha)\}}{\rho_m} \quad \text{(B-6)}$$

B.3 Drift Flux Model

The Drift Flux model provides a simple method of introducing the relative velocity between fluid phases into the mixture equations. The relative velocity is determined from the drift flux correlation, v_{vj}, as shown in Eq. (B-7). The void fraction can be seen as due to two effects, as shown in Eq. (B-8). The C_o term represents the global effect due to radial nonuniform void and velocity profiles. The $\frac{v_{vj}}{\{j\}}$ term represents the local relative velocity effect. At high total flow rate, the local effect term is negligible, as the relative velocity is negligible, which is valid for a steam-water system. The relation between void fraction and volumetric flow fraction can therefore be represented by Eq. (B-9), where K can be defined by Eq. (B-10) when the local drift is small **[31]**.

$$\{v_v - v_l\} = \frac{v_{vj}}{\{1-\alpha\}} \quad \text{(B-7)}$$

$$\frac{\{\alpha\}}{\{\beta\}} = \frac{1}{C_o + \frac{v_{vj}}{\{j\}}} \quad \text{(B-8)}$$

$$\{\alpha\} = K\{\beta\} \quad \text{(B-9)}$$

$$K = \frac{1}{C_o} = 0.833 + 0.05 \ln\left(\frac{p}{10^5}\right) \quad \text{(B-10)}$$

Appendix C: Steam Operating Conditions

This section provides tables of steam operating conditions at each point of Fig. 2.5, both at various reactor operating pressures and various operating loads. Some of the state points representing the bypass line, which are not used in the respective operating conditions are removed from the relevant tables.

C.1 Steam Condition at Various System Pressures

Table C.1 BOP Steam Conditions of SMBWR at 65 bar

Point	m (kg/s)	p (bar)	T (^{o}C)	h (kJ/kg)	s (kJ/kg K)
1	399.29	64.90	280.86	2779.5	5.85
2	399.29	64.90	280.86	2779.5	5.85
3	399.29	63.90	540.00	3513.7	6.97
4	399.29	63.90	540.00	3513.7	6.97
5	399.29	10.00	300.76	3053.3	7.13
6	383.98	10.00	300.76	3053.3	7.13
7	383.87	10.00	300.76	3053.3	7.13
8	383.87	9.00	500.00	3480.1	7.81
9	383.87	9.00	500.00	3480.1	7.81
10	326.68	0.08	41.51	2570.1	8.21
11	383.87	0.08	41.51	2229.6	7.13
12	383.87	0.08	41.51	173.9	0.59
13	383.87	13.50	41.65	175.6	0.59
14	383.87	12.50	68.02	285.7	0.93
15	383.87	11.50	108.53	455.9	1.40
16	383.87	10.50	139.82	588.9	1.74
17	383.87	9.50	161.14	680.6	1.95
18	399.29	8.50	161.79	683.4	1.96
19	399.29	67.20	162.85	691.4	1.96
20	399.29	66.20	163.01	692.0	1.97
21	399.29	65.20	182.11	775.2	2.15

Contd. BOP Steam Conditions of SMBWR at 65 bar

Point	m (kg/s)	p (bar)	T (°C)	h (kJ/kg)	s (kJ/kg K)
22	19.15	3.60	139.82	588.4	1.74
23	24.04	1.86	296.72	3065.8	7.92
24	43.19	1.36	108.53	455.1	1.40
25	14.01	0.39	148.52	2778.1	8.06
26	57.20	0.29	68.02	284.7	0.93
27	57.20	0.08	41.51	284.7	0.94
28	15.31	10.00	300.76	3053.3	7.13
29	15.31	9.50	177.67	752.9	2.12
31	0.10	10.00	300.76	3053.3	7.13
32	0.10	9.50	177.67	752.9	2.12
33	19.15	4.10	390.86	3254.6	7.86

Table C.2 BOP Steam Conditions of SMBWR at 71.7 bar

Point	m (kg/s)	p (bar)	T (°C)	h (kJ/kg)	s (kJ/kg K)
1	410.39	71.60	287.46	2771.0	5.80
2	410.39	71.60	287.46	2771.0	5.80
3	410.39	70.60	540.00	3507.0	6.92
4	410.39	70.60	540.00	3507.0	6.92
5	410.39	10.00	289.46	3029.1	7.08
6	394.66	10.00	289.46	3029.1	7.08
7	394.30	10.00	289.46	3029.1	7.08
8	394.30	9.00	500.00	3480.1	7.81
9	394.30	9.00	500.00	3480.1	7.81
10	335.55	0.08	41.51	2570.1	8.21
11	394.30	0.08	41.51	2229.6	7.13
12	394.30	0.08	41.51	173.9	0.59
13	394.30	13.50	41.65	175.6	0.59
14	394.30	12.50	68.02	285.7	0.93
15	394.30	11.50	108.53	455.9	1.40
16	394.30	10.50	139.82	588.9	1.74

Contd. BOP Steam Conditions of SMBWR at 71.7 bar

Point	m (kg/s)	p (bar)	T (°C)	h (kJ/kg)	s (kJ/kg K)
17	394.30	9.50	160.93	679.7	1.95
18	410.39	8.50	161.60	682.6	1.96
19	410.39	73.90	162.78	691.5	1.96
20	410.39	72.90	163.25	693.5	1.97
21	410.39	71.90	192.41	821.0	2.25
22	19.67	3.60	139.82	588.4	1.74
23	24.70	1.86	296.72	3065.8	7.92
24	44.36	1.36	108.53	455.1	1.40
25	14.39	0.39	148.52	2778.1	8.06
26	58.75	0.29	68.02	284.7	0.93
27	58.75	0.08	41.51	284.7	0.94
28	15.73	10.00	289.46	3029.1	7.08
29	15.73	9.50	177.67	752.9	2.12
31	0.36	10.00	289.46	3029.1	7.08
32	0.36	9.50	177.67	752.9	2.12
33	19.67	4.10	390.86	3254.6	7.86

Table C.3 BOP Steam Conditions of SMBWR at 80 bar

Point	m (kg/s)	p (bar)	T (°C)	h (kJ/kg)	s (kJ/kg K)
1	424.77	79.90	295.01	2759.3	5.75
2	424.77	79.90	295.01	2759.3	5.75
3	424.77	78.90	540.00	3498.6	6.86
4	424.77	78.90	540.00	3498.6	6.86
5	424.77	10.00	276.98	3002.2	7.04
6	408.48	10.00	276.98	3002.2	7.04
7	408.18	10.00	276.98	3002.2	7.04
8	408.18	9.00	500.00	3480.1	7.81
9	408.18	9.00	500.00	3480.1	7.81
10	347.36	0.08	41.51	2570.1	8.21
11	408.18	0.08	41.51	2229.6	7.13

Contd. BOP Steam Conditions of SMBWR at 80 bar

Point	m (kg/s)	p (bar)	T (°C)	h (kJ/kg)	s (kJ/kg K)
12	408.18	0.08	41.51	173.9	0.59
13	408.18	13.50	41.65	175.6	0.59
14	408.18	12.50	68.02	285.7	0.93
15	408.18	11.50	108.53	455.9	1.40
16	408.18	10.50	139.82	588.9	1.74
17	408.18	9.50	160.67	678.6	1.95
18	424.77	8.50	161.36	681.5	1.96
19	424.77	82.19	162.68	691.5	1.96
20	424.77	81.19	163.06	693.1	1.96
21	424.77	80.19	204.51	875.2	2.36
22	20.36	3.60	139.82	588.4	1.74
23	25.57	1.86	296.72	3065.8	7.92
24	45.92	1.36	108.53	455.1	1.40
25	14.89	0.39	148.52	2778.1	8.06
26	60.82	0.29	68.02	284.7	0.93
27	60.82	0.08	41.51	284.7	0.94
28	16.28	10.00	276.98	3002.2	7.04
29	16.28	9.50	177.67	752.9	2.12
31	0.30	10.00	276.98	3002.2	7.04
32	0.30	9.50	177.67	752.9	2.12
33	20.36	4.10	390.86	3254.6	7.86

Table C.4 BOP Steam Conditions of SMBWR at 100 bar

Point	m (kg/s)	p (bar)	T (°C)	h (kJ/kg)	s (kJ/kg K)
1	463.58	99.90	311.00	2726.2	5.62
2	463.58	99.90	311.00	2726.2	5.62
3	463.58	98.90	540.00	3478.0	6.73
4	463.58	98.90	540.00	3478.0	6.73
5	463.58	10.00	251.99	2947.6	6.93
6	445.80	10.00	251.99	2947.6	6.93

Contd. BOP Steam Conditions of SMBWR at 100 bar

Point	m (kg/s)	p (bar)	T (°C)	h (kJ/kg)	s (kJ/kg K)
7	445.11	10.00	251.99	2947.6	6.93
8	445.11	9.00	500.00	3480.1	7.81
9	445.11	9.00	500.00	3480.1	7.81
10	378.79	0.08	41.51	2570.1	8.21
11	445.11	0.08	41.51	2229.6	7.13
12	445.11	0.08	41.51	173.9	0.59
13	445.11	13.50	41.65	175.6	0.59
14	445.11	12.50	68.02	285.7	0.93
15	445.11	11.50	108.53	455.9	1.40
16	445.11	10.50	139.82	588.9	1.74
17	445.11	9.50	160.19	676.5	1.94
18	463.58	8.50	160.90	679.5	1.95
19	463.58	102.19	162.57	692.2	1.96
20	463.58	101.19	163.34	695.5	1.96
21	463.58	100.19	231.73	999.8	2.61
22	22.20	3.60	139.82	588.4	1.74
23	27.88	1.86	296.72	3065.8	7.92
24	50.08	1.36	108.53	455.1	1.40
25	16.24	0.39	148.52	2778.1	8.06
26	66.32	0.29	68.02	284.7	0.93
27	66.32	0.08	41.51	284.7	0.94
28	17.77	10.00	251.99	2947.6	6.93
29	17.77	9.50	177.67	752.9	2.12
31	0.69	10.00	251.99	2947.6	6.93
32	0.69	9.50	177.67	752.9	2.12
33	22.20	4.10	390.86	3254.6	7.86

C.2 Steam Condition at Various Operating Loads

Table C.5 BOP Steam Conditions of SMBWR at 100% Load

Point	m (kg/s)	p (bar)	T (^{o}C)	h (kJ/kg)	s (kJ/kg K)
1	410.39	71.60	287.46	2771.0	5.80
2	410.39	71.60	287.46	2771.0	5.80
3	410.39	70.60	535.06	3495.2	6.90
4	410.39	70.60	535.06	3495.2	6.90
5	410.39	10.00	285.61	3020.8	7.07
6	391.51	10.00	285.61	3020.8	7.07
7	391.50	10.00	285.61	3020.8	7.07
8	391.50	9.00	506.99	3495.2	7.83
9	391.50	9.00	506.99	3495.2	7.83
10	333.39	0.08	42.07	2577.3	8.23
11	391.50	0.08	41.51	2237.1	7.15
12	391.50	0.08	41.51	173.9	0.59
13	391.50	13.50	41.65	175.6	0.59
14	391.50	12.50	68.02	285.7	0.93
15	391.50	11.50	108.53	455.9	1.40
16	391.50	10.50	139.82	588.9	1.74
17	391.50	9.50	165.19	698.2	1.99
18	410.39	8.50	165.78	700.7	2.00
19	410.39	73.90	166.99	709.7	2.00
20	410.39	72.90	167.02	709.8	2.00
21	410.39	71.90	192.41	821.0	2.25
22	19.43	3.60	139.82	588.4	1.74
23	24.42	1.86	302.23	3076.9	7.93
24	43.85	1.36	108.53	455.1	1.40
25	14.25	0.39	152.76	2786.4	8.07
26	58.10	0.29	68.02	284.7	0.93
27	58.10	0.08	41.51	284.7	0.94
28	18.88	10.00	285.61	3020.8	7.07
29	18.88	9.50	177.67	752.9	2.12

Contd. BOP Steam Conditions of SMBWR at 100% Load

Point	m (kg/s)	p (bar)	T (°C)	h (kJ/kg)	s (kJ/kg K)
30	0.00	9.50	177.67	752.9	2.12
31	0.01	10.00	285.61	3020.8	7.07
32	0.01	9.50	177.67	752.9	2.12
33	19.43	4.10	397.09	3267.6	7.88
34	0.00	71.60	287.46	2771.0	5.80
35	0.00	4.10	158.44	2771.0	6.96
36	0.00	70.60	535.06	3495.2	6.90

Table C.6 BOP Steam Conditions of SMBWR at 80% Load

Point	m (kg/s)	p (bar)	T (°C)	h (kJ/kg)	s (kJ/kg K)
1	410.39	71.60	287.46	2771.0	5.80
2	410.39	71.60	287.46	2771.0	5.80
3	410.39	70.60	535.06	3495.2	6.90
4	192.37	70.60	535.06	3495.2	6.90
5	192.37	10.00	285.61	3020.8	7.07
6	173.49	10.00	285.61	3020.8	7.07
7	169.38	10.00	285.61	3020.8	7.07
8	169.38	9.00	506.99	3495.2	7.83
9	387.41	9.00	506.97	3495.2	7.83
10	329.91	0.08	42.06	2577.3	8.23
11	387.41	0.08	41.51	2237.1	7.15
12	387.41	0.08	41.51	173.9	0.59
13	387.41	13.50	41.65	175.6	0.59
14	387.41	12.50	68.02	285.7	0.93
15	387.41	11.50	108.53	455.9	1.40
16	387.41	10.50	139.82	588.9	1.74
17	387.41	9.50	165.46	699.4	2.00
18	410.39	8.50	166.16	702.4	2.00
19	410.39	73.90	167.37	711.3	2.01

Contd. BOP Steam Conditions of SMBWR at 80% Load

Point	m (kg/s)	p (bar)	T (°C)	h (kJ/kg)	s (kJ/kg K)
20	410.39	72.90	172.61	734.0	2.06
21	410.39	71.90	192.41	821.0	2.25
22	19.23	3.60	139.82	588.4	1.74
23	24.17	1.86	302.22	3076.9	7.93
24	43.40	1.36	108.53	455.1	1.40
25	14.10	0.39	152.75	2786.3	8.07
26	57.50	0.29	68.02	284.7	0.93
27	57.50	0.08	41.51	284.7	0.94
28	18.88	10.00	285.61	3020.8	7.07
29	18.88	9.50	177.67	752.9	2.12
30	0.00	9.50	177.67	752.9	2.12
31	4.11	10.00	285.61	3020.8	7.07
32	4.11	9.50	177.67	752.9	2.12
33	19.23	4.10	397.07	3267.6	7.88
34	0.00	71.60	287.46	2771.0	5.80
35	0.00	4.10	158.44	2771.0	6.96
36	218.02	70.60	535.06	3495.2	6.90

Table C.7 BOP Steam Conditions of SMBWR at 65% Load

Point	m (kg/s)	p (bar)	T (°C)	h (kJ/kg)	s (kJ/kg K)
1	410.39	71.60	287.46	2771.0	5.80
2	410.39	71.60	287.46	2771.0	5.80
3	410.39	70.60	535.06	3495.2	6.90
4	38.47	70.60	535.06	3495.2	6.90
5	38.47	10.00	285.61	3020.8	7.07
6	19.59	10.00	285.61	3020.8	7.07
7	12.60	10.00	285.61	3020.8	7.07
8	12.60	9.00	506.99	3495.2	7.83
9	384.52	9.00	506.95	3495.2	7.83

Contd. BOP Steam Conditions of SMBWR at 65% Load

Point	m (kg/s)	p (bar)	T (°C)	h (kJ/kg)	s (kJ/kg K)
10	327.45	0.08	42.05	2577.3	8.23
11	384.52	0.08	41.51	2237.0	7.15
12	384.52	0.08	41.51	173.9	0.59
13	384.52	13.50	41.65	175.6	0.59
14	384.52	12.50	68.02	285.7	0.93
15	384.52	11.50	108.53	455.9	1.40
16	384.52	10.50	139.82	588.9	1.74
17	384.52	9.50	165.65	700.2	2.00
18	410.39	8.50	166.42	703.5	2.01
19	410.39	73.90	167.63	712.5	2.01
20	410.39	72.90	176.53	751.2	2.10
21	410.39	71.90	192.41	821.0	2.25
22	19.09	3.60	139.82	588.4	1.74
23	23.99	1.86	302.21	3076.9	7.93
24	43.07	1.36	108.53	455.1	1.40
25	14.00	0.39	152.74	2786.3	8.07
26	57.07	0.29	68.02	284.7	0.93
27	57.07	0.08	41.51	284.7	0.94
28	18.88	10.00	285.61	3020.8	7.07
29	18.88	9.50	177.67	752.9	2.12
30	0.00	9.50	177.67	752.9	2.12
31	7.00	10.00	285.61	3020.8	7.07
32	7.00	9.50	177.67	752.9	2.12
33	19.09	4.10	397.06	3267.6	7.88
34	0.00	71.60	287.46	2771.0	5.80
35	0.00	4.10	158.44	2771.0	6.96
36	371.92	70.60	535.06	3495.2	6.90